THE ANALYSIS AND DESIGN OF SOME WINDINGS FOR LINEAR INDUCTION MACHINES

Thesis presented to the University

of London for the award of

the degree of Ph.D.

by

Martin John BALCHIN, B.Sc.(Eng), A.C.G.I.

September, 1975

Department of Electrical Engineering,
Imperial College,
London, S.W.7.

ABSTRACT

Pole-change techniques are potentially useful for the speed control of linear induction motors. A new technique is described that enables parallel connections to be made in linear machine windings. It is shown that the number of switch contacts required for pole-changing using this method is fewer than that required for equivalent series connected windings.

An analysis is presented, and verified experimentally, that gives the currents in any general set of serially connected coil groups energised by independent voltage sources. The coil groups can be arranged to model any machine winding including asymmetric types and those containing parallel paths.

Design techniques for pole-change windings require a knowledge of the harmonic content of the stator mmf wave. A simplified analysis gives this information and an example illustrates the combined use of both models in assessing a particular design.

The poor power factor of high speed linear machines fed at 50 Hz may be improved by incorporating the primary end-windings into the main magnetic circuit of the machine. Difficulties with construction and low air-gap flux-density indicate that this may be accomplished by the use of air-gap windings.

A mathematical model is developed and verified against practical test results to give the complete electrical and mechanical performance of axial-flux linear machines with two-dimensional conductor distribution and air-gap windings. The treatment forms an extension to

the one-dimensional analysis developed for pole-change windings and has the same general features. The model is also suitable for predicting the performance of conventional linear machines and gives improved estimates over those given by the one-dimensional analysis.

The model is used to predict the performance of two equivalent high-speed designs. These results show an improved power factor over a conventional design for an air-gap wound machine with a minimum of coil overhang.

ACKNOWLEDGEMENTS

The Author wishes to express his sincere gratitude to his supervisor Professor J.F. Eastham (who is now with the University of Aberdeen) for providing the inspiration behind, and much encouragement and advice during the course of the work described in this thesis. Thanks are also due to Dr. H.R. Bolton and Professor E.R. Laithwaite (of the Department of Electrical Engineering, Imperial College) for the active interest they maintained in the projects and for many useful discussions.

Many fellow students provided helpful suggestions that improved the work and the assistance given by Mr. D.H. Locke and Dr. D.A. Lowther with some of the experimental work was greatly appreciated.

A great deal of technical assistance was provided by Messrs. P.J. McKeowan and B. Gingall during the construction of the test machines and in setting up and maintaining the experimental apparatus.

The Author also wishes to thank his wife for her continued support and encouragement. Her impeccable typescript has added much to the presentation of this work.

Finally, thanks are due to the Science Research Council for providing financial support during the course of the work.

INDEX

LIST OF PRINCIPAL SYMBOLS

b,B	instantaneous and complex RMS magnetic flux density, T
e,E	instantaneous and complex RMS electric field strength, V/m
F	thrust force, N
h	rotor width, m
h,H	instantaneous and complex RMS magnetic field strength, A/m
i,I	instantaneous and complex RMS coil group current, A
j,J	instantaneous and complex RMS surface current density, A/m
k,K	instantaneous and complex RMS current density, A/m^2
ℓ	depth of winding layer, m
m	transverse harmonic number
n	surface conductor density, conductors/m
N	number of turns/coil
P	power dissipated in layer model, W
P_w	winding pole pitch, m
Q	total number of stator slots
r	longitudinal harmonic number
S	depth of passive layer, m
t	time, s
v	speed, m/s
w	width of stator containing conductors normal to direction of motion, m
z_{in}	layer model input impedance
C_r	longitudinal Fourier series complex conductor amplitude, conductors/m
C_{rm}	double Fourier series complex conductor amplitude, conductors/m

e_T coil group RMS induced emf, V

$2f$ width of stator containing skewed conductors, m

$2k_B P_B$ length of machine section, m

$k_m = \frac{m\pi}{h} =$ transverse wave number

$k_r = \frac{r\pi}{k_B P_B} =$ longitudinal wave number

2β coil pitch, m

2δ width of coil side or slot opening, m

ρ number of coil groups

ω supply angular frequency, rad/s

[A] matrix or vector

T indicates the matrix transpose

* indicates the complex conjugate

Re indicates the complex real part

A subscript of x, y or z indicates the axis along which a component is directed

CHAPTER ONE

GENERAL INTRODUCTION

The induction machine has the advantage over many other forms of electrical machine in that it requires no electrical or mechical contact between its fixed and moving parts. This feature alone has made the rotary form the most popular of industrial drives and is largely responsible for the current interest in linear versions for traction applications.

The topological development of the linear machine may be illustrated by imagining a rotary machine (cut along a radial plane) to be "unrolled". In order to make continuous motion possible either the primary or secondary member must be extended. This gives rise respectively to "short-stator" and "short-rotor" versions of the linear machine. The investigation to be described in the following chapters is concerned with the properties of linear machines intended for medium and high-speed vehicle propulsion. Short-stator machines appear to be the more attractive alternative for this application on the grounds of least expense[1.1].

Linear forms of the induction motor began to appear soon after the invention of the rotary type. A survey published in 1957[1.2] describes a variety of applications that were envisaged for both the "short stator" and "short rotor" versions. These included drives for loom shuttles, drop forging and projectile and vehicle propulsion. Many of these early developments were abandoned on the grounds of expense or lack of suitable materials or technology. Progress was further hindered by the failure to eliminate some of the large unwanted electromagnetic forces and losses that were encountered.

Interest in various forms of the "short stator" linear machine was revived after the Second World War. An ideal application for

induction techniques was found in the pumping of hostile conducting fluids[1.3]. Other variations of the short stator machine appeared in the Russian work on "arch" motors [1.2] and in the evolution of a brushless variable speed induction motor[1.4,1.5]. These developments exposed the basic differences in operation of rotary and linear machines and provided a sound basis from which improved designs could be made. The interest excited by this work has stimulated a great deal of research in many countries and the field of current and proposed applications for linear machines is now almost as great as that of the rotary type.

Energy conversion is performed by a short-stator machine in a similar manner to that of the rotary version. In the case of the linear motor, however, the process is influenced by the discontinuous nature of the primary member. Transient currents are induced in each element of the secondary member as it passes beneath the leading edge of the primary. The presence of these currents is required to maintain the minimum of flux linking each element as it passes the stator edge. Rotor impedance and air-gap inductance govern the decay of the transient currents and as a result, the flux rises to a steady value over a distance that is speed dependent. This phenomenon is known as the "longitudinal edge-effect"[1.5,1.6] and is most pronounced in well coupled machines intended for high speeds.

The slotted structure common in rotary machines is not practicable for the extended rotor of the short-stator machine. A simpler (and therefore cheaper) secondary arrangement can be formed by placing a plain conducting sheet in the machine magnetic circuit. In designs using this configuration the sheet thickness is usually arranged so that secondary leakage is reduced at the expense of an acceptable increase in magnetising reactance.

Use of a plain conductor also allows longitudinal components of rotor current to flow. These reinforce the air-gap flux density at the stator sides at the expense of the flux at the centre. This "transverse edge effect" is most pronounced under primaries that are wide in comparison with the plate overhang and at low speeds[1.7]. Transverse edge effects are of greatest interest to the designers of machines with fluid secondaries. The performance of motors considered in this work is only marginally affected by sideways flux redistribution.

One of the reasons that conventional rotary induction machines have not found popularity in traction applications is that they are basically fixed speed devices. Two schemes are available for removing this limitation. Variable frequency supplies have been proposed[1.1] but these require a great deal of auxiliary equipment. Another alternative is to use multiple or single windings that can be reconnected to give a number of different pole-pitches. The latter technique is known as "pole-changing" and is widely used for rotary machines (an extensive bibliography is given in reference 1.8). Pole-changing only gives a few discrete speed changes but requires a minimum of control apparatus. The essential characteristics of power factor and efficiency on each pole setting compare favourably with those of single speed machines.

Linear machines are inherently unbalanced due to the non-uniform air-gap flux wave. This also makes unworkable many conventional winding designs employing closed paths. As a result, little work appears to have been performed on the application of pole-change windings. Chapter 2 presents a new technique for connecting parallel

paths within a linear machine winding. Using this scheme, many of the advantages of conventional single-speed and pole-change windings may be realised. These include a greater flexibility in matching machines to available supplies and the exploitation of multi-speed windings requiring a minimum number of switch contacts.

In order to predict the performance of machines with windings containing parallel paths, a new analytical approach is necessary. Most linear machine models assume the winding to be adequately represented by a single current sheet of fixed amplitude and wavelength. This model is only applicable to balanced conductor distributions carrying balanced phase currents such as occur in rotary machines. Winding space harmonics are usually neglected although these may have a considerable influence on the terminal characteristics. A complete winding model is developed that considers the harmonic conductor distribution of each series combination of coil groups. Using network techniques the coil groups of the mathematical model are interconnected as they are in the real machine. The induced emf in each harmonic winding is simply related to the winding current by the input impedance of a multi-region mathematical model of the rest of the machine. Predictions of force and flux density are then made after the winding currents have been determined.

In order to minimise the losses associated with longitudinal edge-effects high-speed linear motors are designed with as many poles as is practicable. These long machines only require narrow primary stacks for a given output. Whilst this is advantageous in terms of secondary width and transverse edge-effects, problems arise in the design of stator windings. When conventional winding arrangements

are employed (with coils almost spanning a pole) the end-conductor bulk becomes disproportionately large. As a result of this, linear motors tend to have large primary leakage reactances. In an attempt to reduce this parameter the use of windings employing very short coil pitches is proposed. This leads to a greater harmonic content than is usual. A simplified winding analysis is also presented in Chapter 2 that may be used to indicate the more detrimental harmonics at the initial design stage. The complete machine mathematical model and the simplified version are complementary and are used together in performing a complete winding design.

The problem of primary leakage is also tackled in Chapter 3. A winding is proposed that has as much as possible of the conventional end-conductors included in the main magnetic circuit of the machine. Because of low values of air-gap flux density, the use of thin teeth in linear stators is common. Furthermore, the two-dimensional nature of the proposed windings makes the construction of a slotted stator difficult. It is therefore considered that the adoption of an air-gap winding forms an attractive alternative.

The low leakage property of the proposed windings is only realised in larger machines where the influence of the increased air-gap is less pronounced. Predicted performance comparisons between machines of different types are most reliable when the same analytical model is used for each. To this end, the one-dimensional model used for the pole-change work is extended to two dimensions in Chapter 3. When a winding is not enclosed in slots it is incorrect to use a "thin" current sheet representation. A new winding model is therefore developed to take account of depth effects in air-gap

windings. This model represents real winding distributions as it also incorporates the developments introduced in Chapter 2.

Parts of this work have already been published under joint authorship through the Institution of Electrical Engineers'. The new parallel path windings in Chapter 2 were presented at a conference in 1974[1.9]. A more detailed description of these windings and the full analysis appeared later in a Proceedings paper[1.10]. Much of the material in Chapter 3 is awaiting publication[1.11].

CHAPTER TWO

APPLICATION OF CHANGE-POLE WINDINGS TO LINEAR INDUCTION MACHINES

2.1 Introduction

The speed of the secondary of a cage-type induction motor depends upon the number of poles produced by its primary winding. It therefore follows that if the coils of the primary winding are reconnected to produce a different number of poles then the machine speed will be altered. This method of control has been in use for many years and is known as "pole-changing". Only discrete changes in speed are possible with a pole-change winding but this limitation is quite acceptable since a set of switches is all the control apparatus required and the machine can be designed to operate at optimum efficiency on each speed setting. The speed-change switches may also be used to reconnect the winding to change the effective voltage applied to the machine. These advantages are thought to make pole-change techniques particularly useful for the speed control of linear machines used in transport systems.

A number of new techniques have been described recently for designing two-speed windings for rotary machines[2.1-2.5]. Designs are selected using coil-pitches that are near the pole-pitch of the low speed winding giving high winding factors at the required pole-numbers. When linear machines are considered for traction purposes it is often found that the coil overhang beyond the stator is large when compared with the machine width[2.6]. This leads to the use of shorter coil-pitches and a consequent reduction in the winding factors at the required pole-numbers in comparison with those of sub-harmonics. Large sub-harmonic windings may result in unacceptable modification of the force and current characteristics of the machine and restricts the use of delta connections for the coil groups.

In a linear machine the air-gap flux-density distribution is non-uniform, being low at the rotor entry end and increasing towards the rear of the machine[2.7,2.8]. The degree of non-uniformity is also dependent upon the rotor speed. If a conventional conductor layout is used on the primary, coil-group connections cannot be used that form closed paths within the winding because the unbalanced induced emfs present will drive circulating currents. This implies that only series connected windings are suitable for linear machines. Series connected pole-change windings have the disadvantages of being uneconomical in the number of switch contacts required and inflexible in so far as effective voltage changes are concerned. In a rotary machine, where the air-gap flux is uniformly distributed, these limitations are removed by designing windings that contain parallel connections of coil groups.

In this chapter a simple analysis is employed to give the harmonic winding factors of pole-change windings. These factors are examined to identify those winding harmonics that may be detrimental to the overall machine performance. A novel form of conductor layout is described in which parallel connections are made and a model is developed for predicting the performance of machines with any general stator winding arrangement. The theoretical work is fully supported by a number of practical tests. These show that the new windings have a uniformity of current distribution comparable to that of series windings and also establish the validity of the mathematical model. Finally, an example is included to illustrate the combined use of both machine models as a design aid.

2.2 Conductor distributions and coil-group connections

2.2.1 Consequent-pole windings

In this section, coil group connections and a method for estimating the harmonic winding factors of pole-change windings are given. The connections and analysis are described in terms of the well-known "consequent-pole" arrangement, but the same methods are directly applicable to all two-speed change-pole windings.

The simplest form of change-pole winding is the two-speed consequent-pole arrangement. Figure 2.1 illustrates the electric and magnetic circuits for one phase of a rotary machine using this type of winding. As can be seen, reversal of the current in alternate coils yields a higher pole-number. When a polyphase arrangement of coils is used a rotating wave of flux density is produced in the air-gap. If the secondary member has corresponding electric circuits to those of the primary, a torque is exerted upon it at all speeds up to the rotational speed of the flux wave. The speed of the flux wave is halved when the connections to half the primary winding are reversed resulting in a second torque-speed characteristic. Each primary coil has the same induced emf. The currents drawn from the supply are therefore balanced and parallel connections are possible on either speed setting.

The consequent-pole principle can be directly applied to linear machines. Figure 2.2 shows a layout of electric and magnetic circuits corresponding to those of Figure 2.1. Again, reversal of alternate coils in each phase produces a second pole number and two force-speed characteristics are possible when the secondary electric circuits are completed. In a linear machine secondary circuits are continually being replaced beneath the primary. Currents are induced in each of these

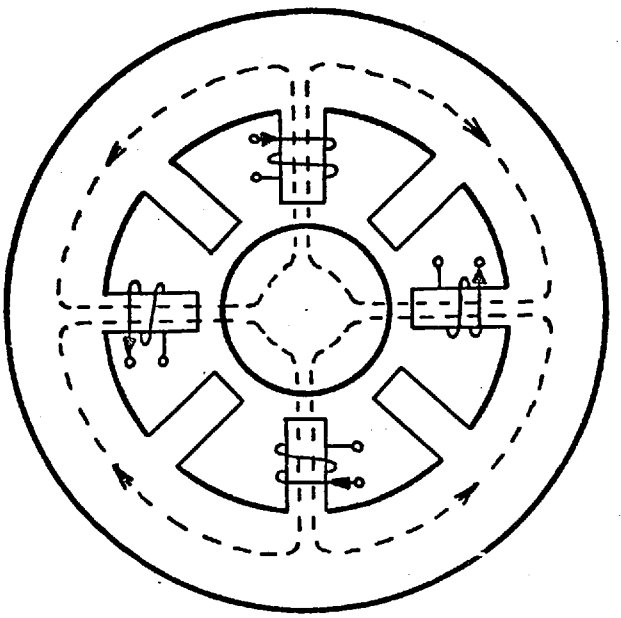

a

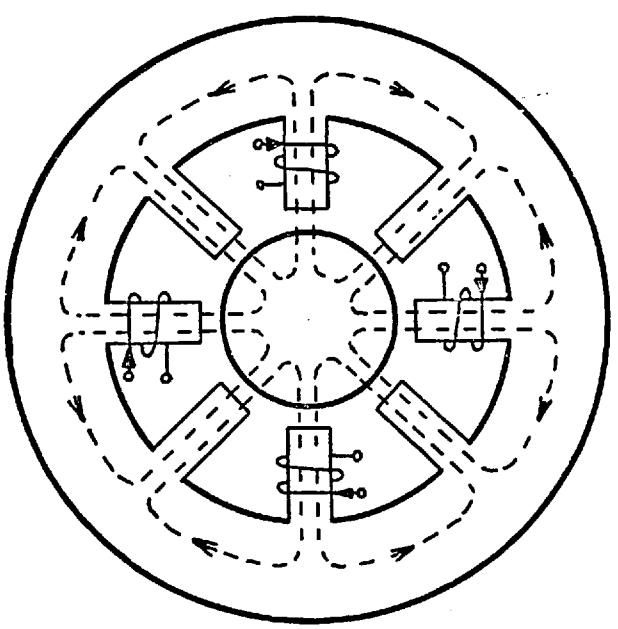

b

Fig. 2.1 Principle of consequent-pole windings for a rotary machine

a) 4-pole connection
b) 8-pole connection

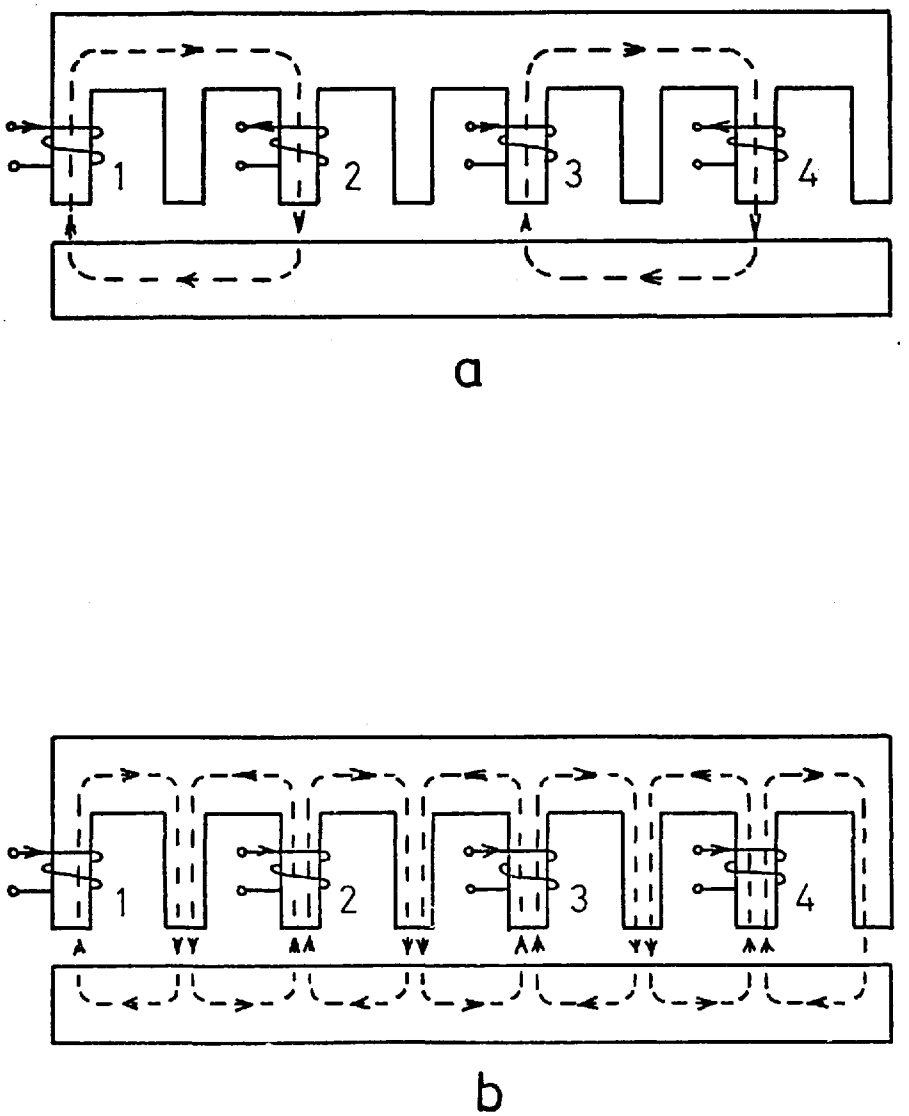

Fig. 2.2 Principle of consequent-pole windings for a linear machine

a) 4-pole connection
b) 8-pole connection

circuits at the rotor entry end in such a direction as to oppose the change of primary flux. This transient current may be large if the rotor speed is high. As the rotor moves on the superimposed transient current decays and the air-gap flux rises to a steady value at a position that is dependent upon the speed[2.7,2.8]. In a linear machine then, the primary coils have different induced emfs, parallel connections are not directly possible and the currents drawn from the supply are not balanced.

2.2.2 Harmonic winding factors

For the sake of clarity, the diagrams of Figures 2.1 and 2.2 show only single coils on each pole. In practice, surface windings with many coils are used producing "phase-bands" of conductors. Figure 2.3a shows the four-pole connection of a conventional consequent-pole winding using double-layer construction with four slots per pole and phase and a coil-pitch of six slots. Reversal of connections to half the winding (indicated by the enclosed groups of conductors in the Figure) gives the eight pole setting. Consequent-pole windings usually employ coils that are fully-pitched for the low speed connection. This gives acceptably high winding factors on each of the principal pole numbers and the force and current characteristics of the machine are found to be virtually uninfluenced by the presence of any sub-harmonic windings.

In linear machines designed for traction applications, it is often found that the coil overhang outside the machine is large when compared with the stator width[2.6]. This gives designs with high stator impedances resulting in poor power factor and efficiency characteristics. The winding overhang can be reduced by using coils with shorter pitches than

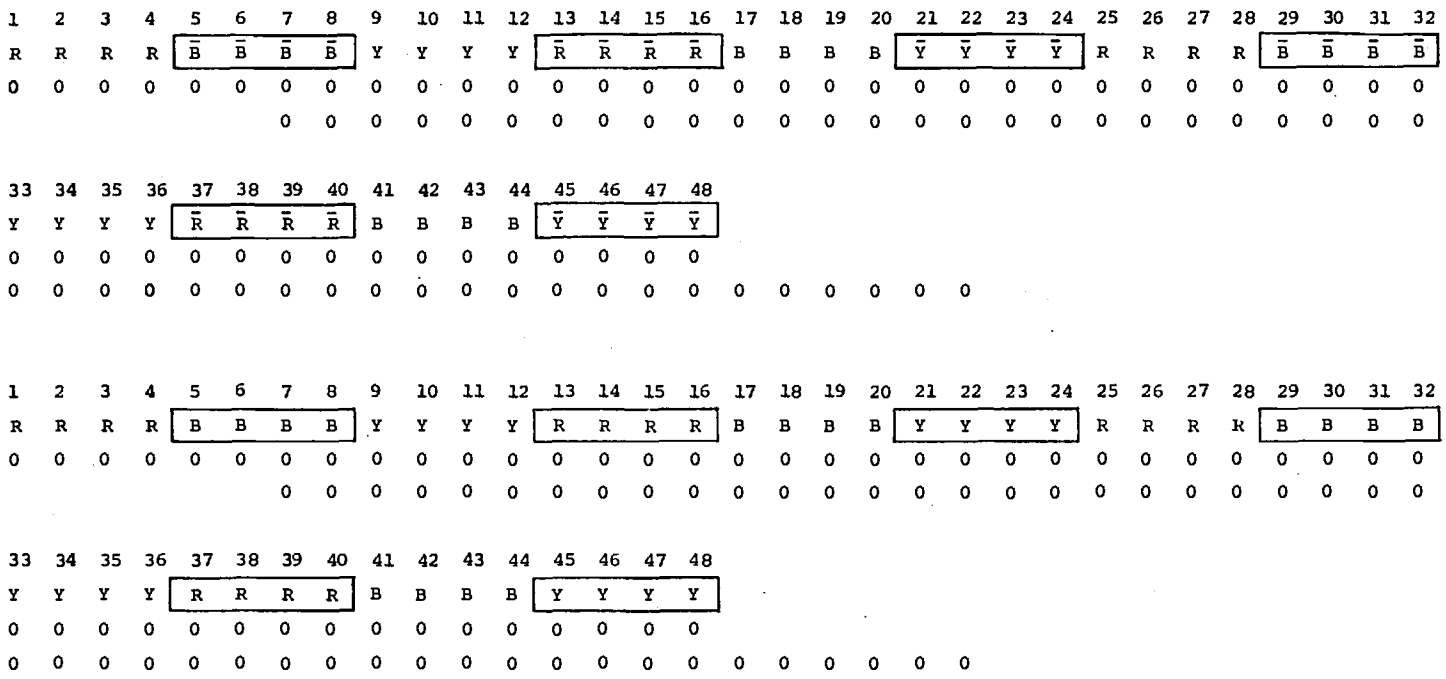

Fig. 2.3. 8 to 4 consequent-pole winding in 48 slots

are conventionally employed, but this introduces larger winding sub-harmonics that may adversely affect the current and force characteristics.

The harmonic content of linear machine windings may be compared at the initial design stage by considering them as double-layer windings taken from rotary machines. A harmonic analysis is performed by first finding the Fourier components of the conductor distribution of each phase as shown in Appendix 2.7.1. Symmetrical component analysis is then used to transform the phase distributions into "forward", "backward" and "zero" sequence sets of series connected windings[2.1]. The distribution of harmonics produced by the top layer is first calculated, the amplitude of each component being the harmonic distribution factor. The bottom layer of conductors is then allowed for by multiplying the harmonic amplitudes of the top layer by a series of factors that depend on the coil span. These factors are the harmonic pitch-factors.

The effects of the sub-harmonic windings on the force-speed characteristic of a principal pole number can be discussed by assuming the machine to be star connected and supplied with constant balanced phase currents. Harmonic flux waves are produced by the phase currents flowing in the sub-harmonic windings. These flux waves travel either with or against the main flux-wave producing their own force-speed curves as shown in Figure 2.4. Forward travelling flux waves with fewer poles than the principal wave give force-speed curves that enhance the required motoring thrust at all speeds. When the harmonic wave has more poles, the force produced only augments that due to the principal winding up to the harmonic synchronous speed. Beyond this speed the harmonic force is negative and may cause a depression in the main force-

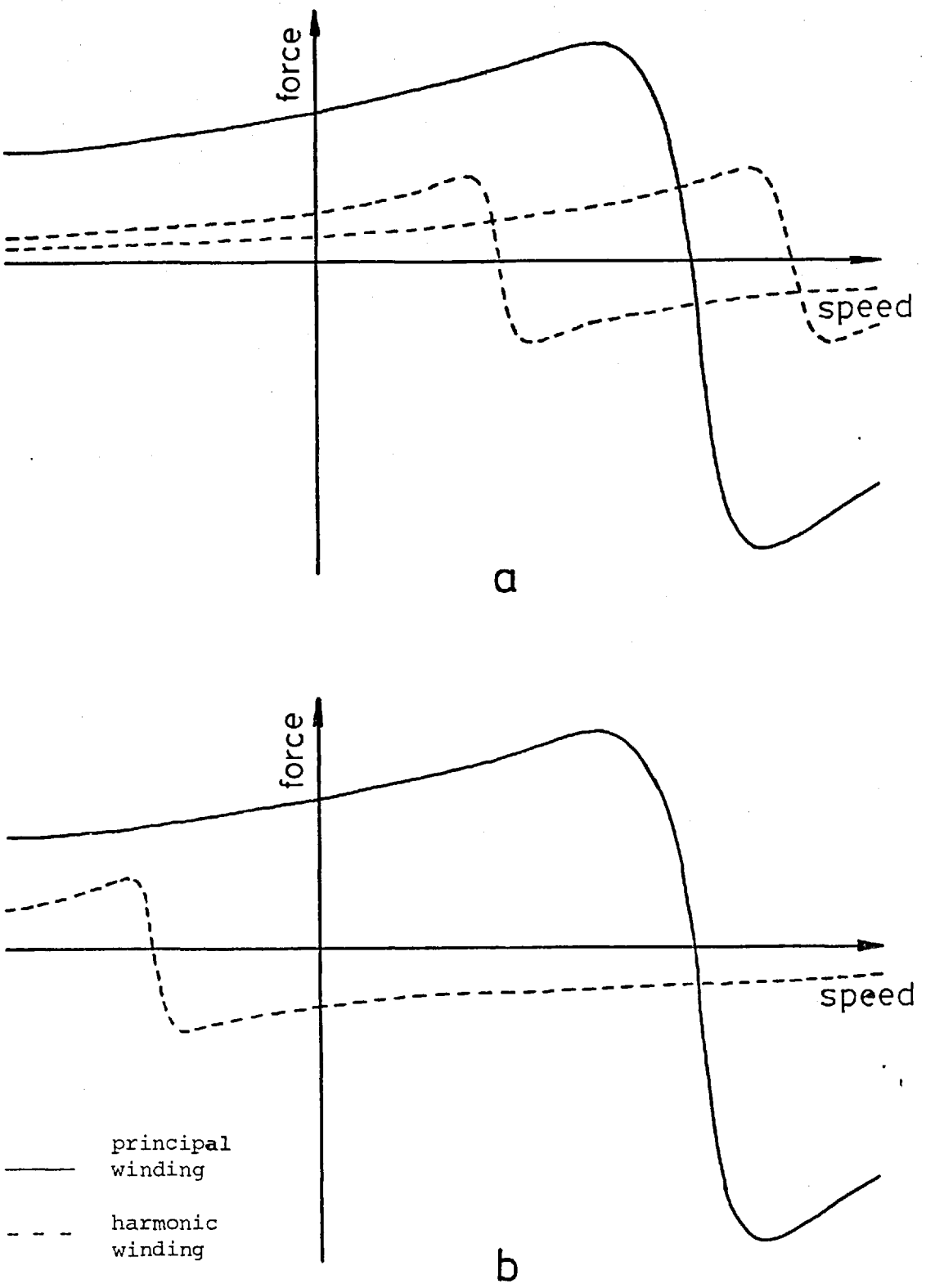

Fig. 2.4 Effect of subharmonic windings on induction machine force-speed characteristics

a) forward travelling fields
b) backward travelling fields

speed characteristic. If the corresponding load curve cuts this depression, then the machine may never attain its full design speed. Backward travelling waves of any speed detract from the main force at all speeds. This effect is greatest at standstill thus affecting the starting force of the machine.

The magnetising reactance of a linear machine is usually low when compared with that of the rotary type. This reactance decreases still further in inverse proportion to the square of the number of harmonic winding poles. As a result, most of the harmonic forces produced are small but the effects produced by those fields with pole numbers close to that of the principal may still be appreciable.

Induction machines are more usually fed from a balanced constant voltage supply. Under these conditions the phase currents fall as the machine speed rises so reducing the peak amplitude of harmonic force-speed curves produced by windings with pole numbers close to that of the principal winding. This improvement in mechanical performance is offset by the action of induced emfs in the harmonic sequence windings. The super-position of forward and backward harmonic induced emfs of the same pole number in each phase causes an unbalance in currents drawn from the supply. Zero-sequence emfs, being all in phase, simply cancel when the stator is star-connected with no neutral line. When the primary is delta connected, these co-phasal voltages drive a circulating current that may be large if the stator impedance is low.

The foregoing discussion may be illustrated by the results of a winding analysis of the consequent pole arrangement of Figure 2.3. The distribution factors of Table 2.1a show that the consequent-pole winding is balanced on a rotary machine because each harmonic pole

4-pole setting

Poles	k_{df}	k_{db}	k_{dz}
[4]	0.958	-	-
12	-	-	0.653
20	-	0.205	-
28	0.158	-	-
36	-	-	0.271
44	-	0.126	-
52	0.126	-	-

8-pole setting

Poles	k_{df}	k_{db}	k_{dz}
[8]	-	0.837	-
16	0.433	-	-
32	-	0.250	-
40	0.224	-	-
56	-	0.224	-

a) distribution factors

4-pole setting

Coil Pitch (slots)	4			5			6		
Poles	k_{wf}	k_{wb}	k_{wz}	k_{wf}	k_{wb}	k_{wz}	k_{wf}	k_{wb}	k_{wz}
[4]	0.479	-	-	0.583	-	-	0.677	-	-
12	-	-	0.653	-	-	0.604	-	-	0.462
20	-	0.103	-	-	0.027	-	-	0.145	-
28	0.079	-	-	0.156	-	-	0.111	-	-
36	-	-	0.271	-	-	0.104	-	-	0.191
44	-	0.063	-	-	0.100	-	-	0.089	-
52	0.063	-	-	0.100	-	-	0.089	-	-

8-pole setting

Coil Pitch (slots)	4			5			6		
Poles	k_{wf}	k_{wb}	k_{wz}	k_{wf}	k_{wb}	k_{wz}	k_{wf}	k_{wb}	k_{wz}
[8]	-	0.725	-	-	0.808	-	-	0.837	-
16	0.375	-	-	0.217	-	-	-	-	-
32	-	0.217	-	-	0.217	-	-	-	-
40	0.194	-	-	0.058	-	-	0.224	-	-
56	-	0.194	-	-	-	-	-	0.224	-

b) winding factors

Table 2.1. Distribution and winding factors for the winding of Fig.2.3

number has no corresponding opposite or zero sequence components. On the four pole setting, the usual fifth, seventh and eleventh harmonics appear together with the "triplen" zero sequence components. Both even and odd harmonic components are present on the eight-pole setting with the principal distribution factor appearing in the "backwards" column. This reversal of the winding phase sequence when alternate coil groups are reconnected means that the supply phase sequence must also be reversed in order to maintain thrust in the required direction. The harmonics close to both eight and four poles produce forces that may affect the machine starting performance. Also, the large zero-sequence component may make delta connection on four poles impossible. Large harmonic distribution factors can be reduced by arranging the coil pitch so that the pitch-factor attenuates them with respect to the principal. Tables 2.1b show that with a pitch of six slots (i.e. full pitch on eight poles) the close-in harmonic winding factors are considerably reduced. If shorter pitched coils are used the harmonic content again becomes appreciable.

2.2.3 Series connections

The air-gap flux in a rotary machine is uniformly distributed. In a linear machine relative movement between the primary and secondary members causes a distortion of the flux wave in the direction of motion that increases with speed. The non-uniform nature of the air-gap flux means that different emfs are induced in similar coil groups on a linear stator. When sets of coils with different induced emfs are parallel connected, circulating currents flow in the winding that are limited only by the coil group impedances. If a conventional winding layout is employed, coil groups must be series connected in each phase to remove any closed paths.

The connections to half the coils in a two-speed winding must be reversed in order to change the number of poles. In Figure 2.5, twelve contacts are required for a series-star connection on each setting. Closing the contacts marked S_1 gives one pole number and S_2 the other. The coils r_1, r_2, y_1 etc. are used to indicate series combinations of half of the coils in a phase. In terms of the consequent pole winding of Figure 2.3 r_1 would represent coils 1, 2, 3, 4, 25, 26, 27 and 28 and r_2 the coils 13, 14, 15, 16, 37, 38, 39 and 40.

A common specification met with in machine design is that of the available supply voltage and current. The machine impedance must be adjusted to draw the required current for particular output characteristics from a given voltage source. Parallel connection is used in some rotary machine designs to set the basic current level. In a linear machine with a conventional conductor layout only series connections are possible. Impedance adjustment may also be viewed as altering the effective voltage applied to the machine. Star to delta switching provides a method of voltage changing but the closed path formed may allow the passage of currents due to unbalanced phase emfs or harmonic zero-sequence windings. When a star to delta connection is combined with reversal of half the winding a considerable number of switches is required. Figure 2.6 shows an arrangement requiring seventeen contacts. The contacts marked S_3 or S_4 can be closed to give a star or delta connection on either speed setting.

A more usual switching requirement is that of a change of voltage with a change of pole number. In Figure 2.7 the S_1 contacts are closed to provide a star connection at one pole number. Closure of the S_2 contacts gives a delta connection at the second pole number. The control

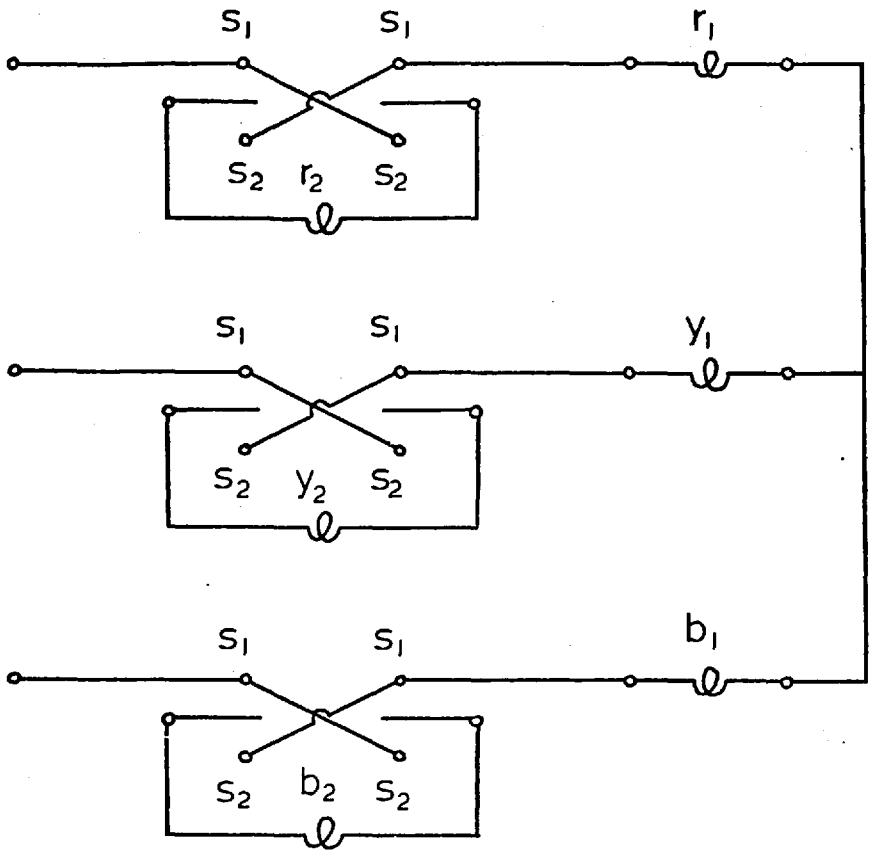

Fig. 2.5 Switching arrangement for a basic series star-series star connection

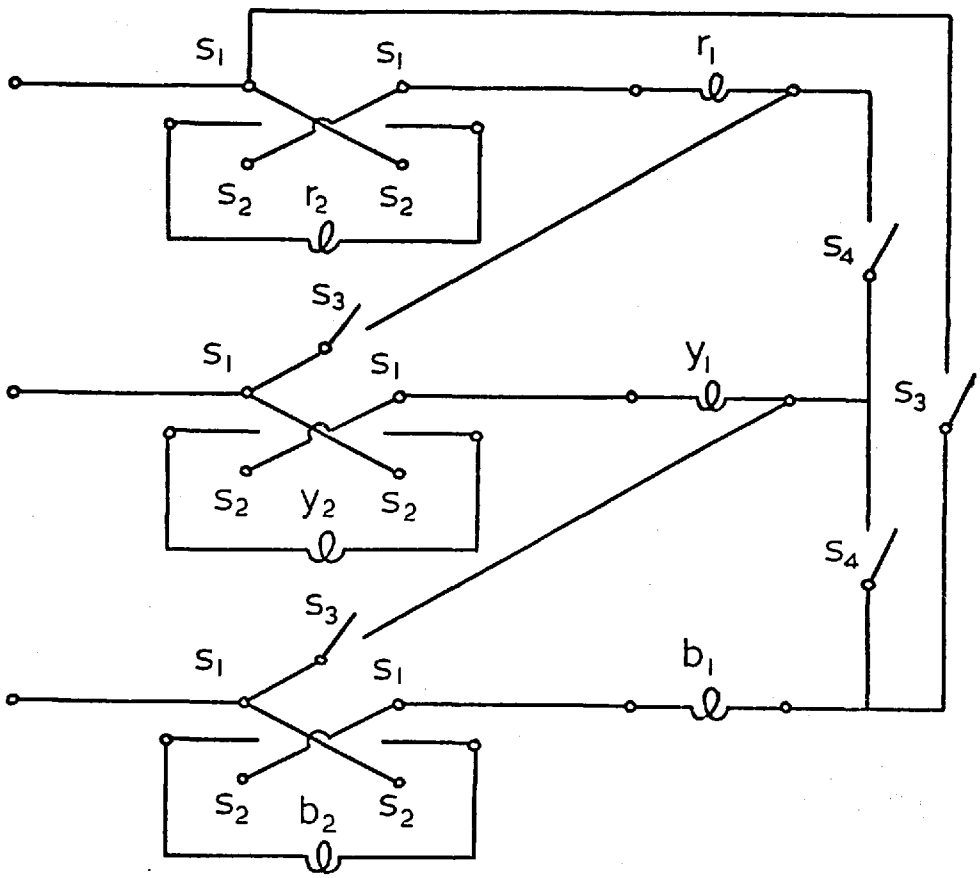

Fig. 2.6 Switching arrangement for series star or series delta connections on each speed setting

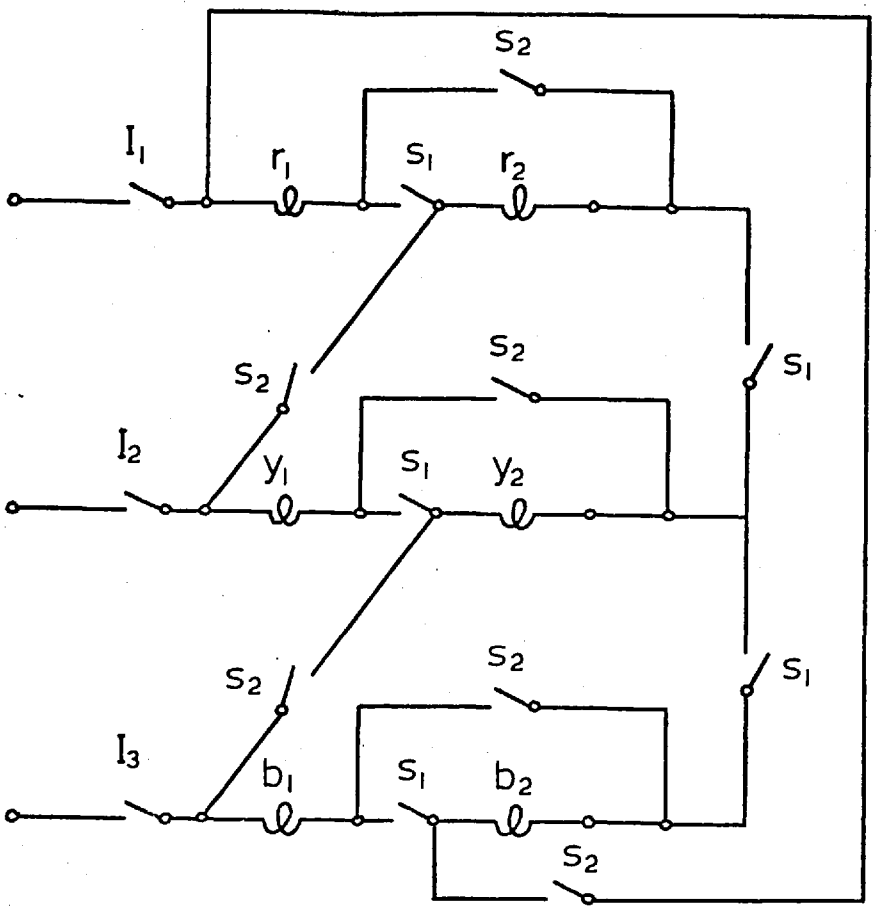

Fig. 2.7 Switching arrangement for a series star-series delta connection

function is provided with eleven switch contacts but three more (marked I in the Figure) are required to enable the machine to be isolated from the supply.

2.2.4 Parallel connections

In series connected windings the only allowable method of voltage changing is star to delta switching. The considerable number of switch contacts required is reduced and extra design flexibility introduced for rotating machines by using parallel connected coil groups. A novel "double winding" technique is now described that allows parallel connections to be made in linear machine windings in spite of the non-uniform nature of the air-gap flux.

The principle of the double winding technique can be explained by referring again to the single phase diagram of Figure 2.2. Each coil in this Figure is replaced by a pair of coils in Figure 2.8. Two groups of coils are formed in the four-pole case that have the same induced emf. These two coil groups can be parallel connected to form a phase winding as shown in Figure 2.8(b). A pair of coil groups can also be formed that have the same emf induced by an eight-pole flux wave as Figure 2.8(d) shows. The same basic phase winding is formed on each pole setting giving two parallel paths and a reversal of the current in half of the coils.

The new parallel phase groups of Figure 2.8 may be formed using surface windings with a large number of coils. An obvious method of construction would be the "four-layer" technique in which two separate windings are placed in the same slots. The usefulness of this method is limited by the different slot leakage reactance seen by each winding.

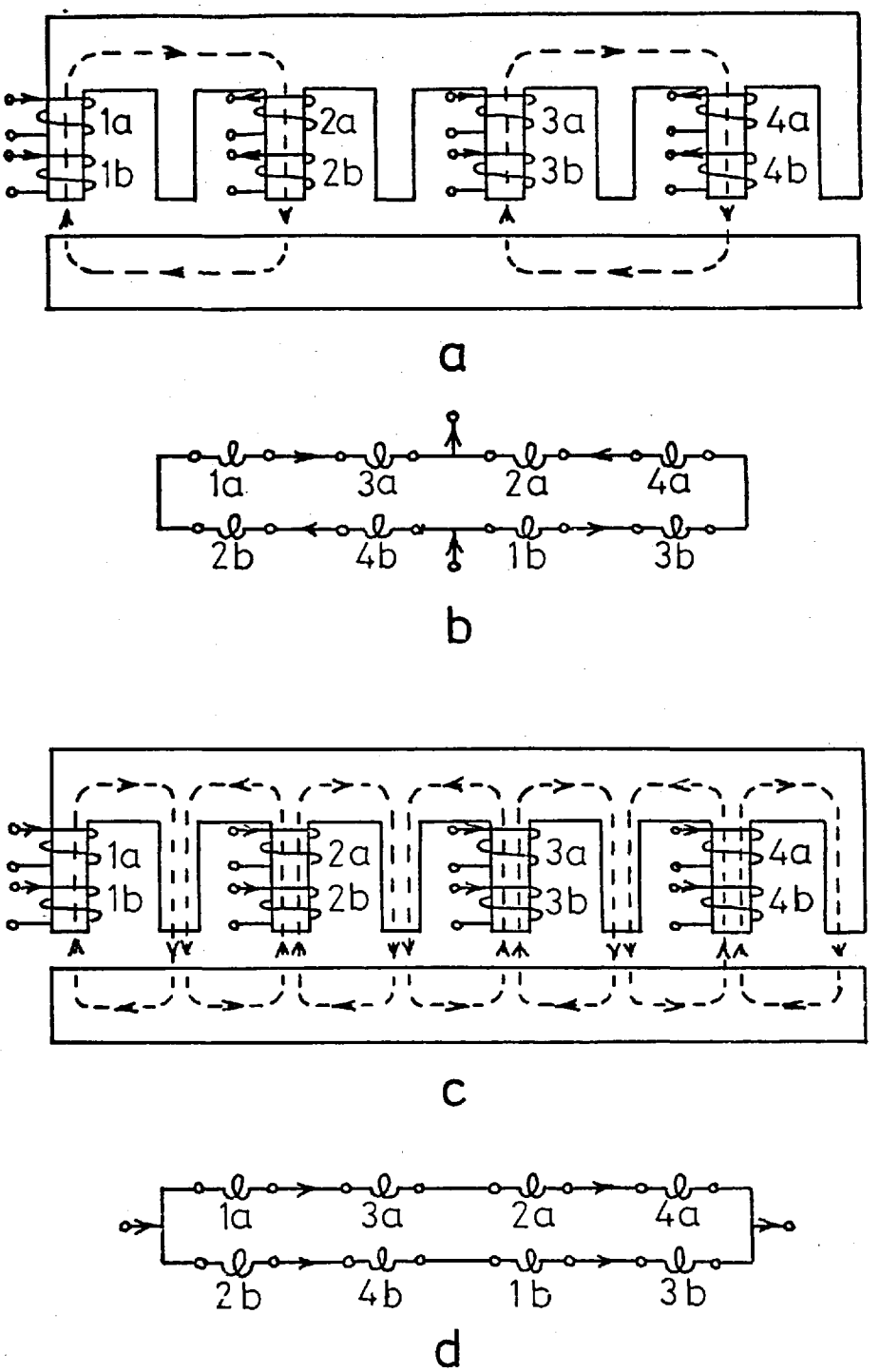

Fig. 2.8 Principle of parallel connected pole-change windings for a linear machine

a) 4-pole setting
b) coil group connections for 4 poles
c) 8-pole setting
d) coil group connections for 8 poles

A direct application for the parallel phase group exists in machines such as the "U-core" transverse flux motor of reference 2.9 where there are two distinct windings that see the same flux distribution. Provided that the stator accommodates an even number of coils, four layer construction can be avoided by connecting the two windings one slot pitch apart. The coil groups formed in this way will have different induced emfs but parallel connection may be possible if the flux density changes are small enough over a slot pitch. It may also be necessary to employ a combination of both the "four-layer" and "two-layer" techniques when fractional slot windings are used or the number of individual coils is odd. The small difference in induced emfs between the parallel paths may be further reduced by placing one group in the even numbered slots in one repeatable section of the winding, and in odd numbered slots in the following section.

A complete three-phase winding using parallel phase groups is shown in Figure 2.9. The two pole settings are formed by closing either the contacts marked S_1 or those marked S_2. For each pole setting the winding is star connected and is directly comparable with the series arrangement of Figure 2.5. The star connection using series phase groups requires twelve switch contacts. This is two more than are required when parallel groups are employed. Figure 2.10 shows an arrangement that provides star connection on one pole setting and delta connection on the other. In this case eleven switch contacts are required compared with the fourteen shown in Figure 2.7.

The change-pole arrangements in this section have been described in terms of the consequent-pole winding. Similar methods can be directly applied to all two-speed windings.

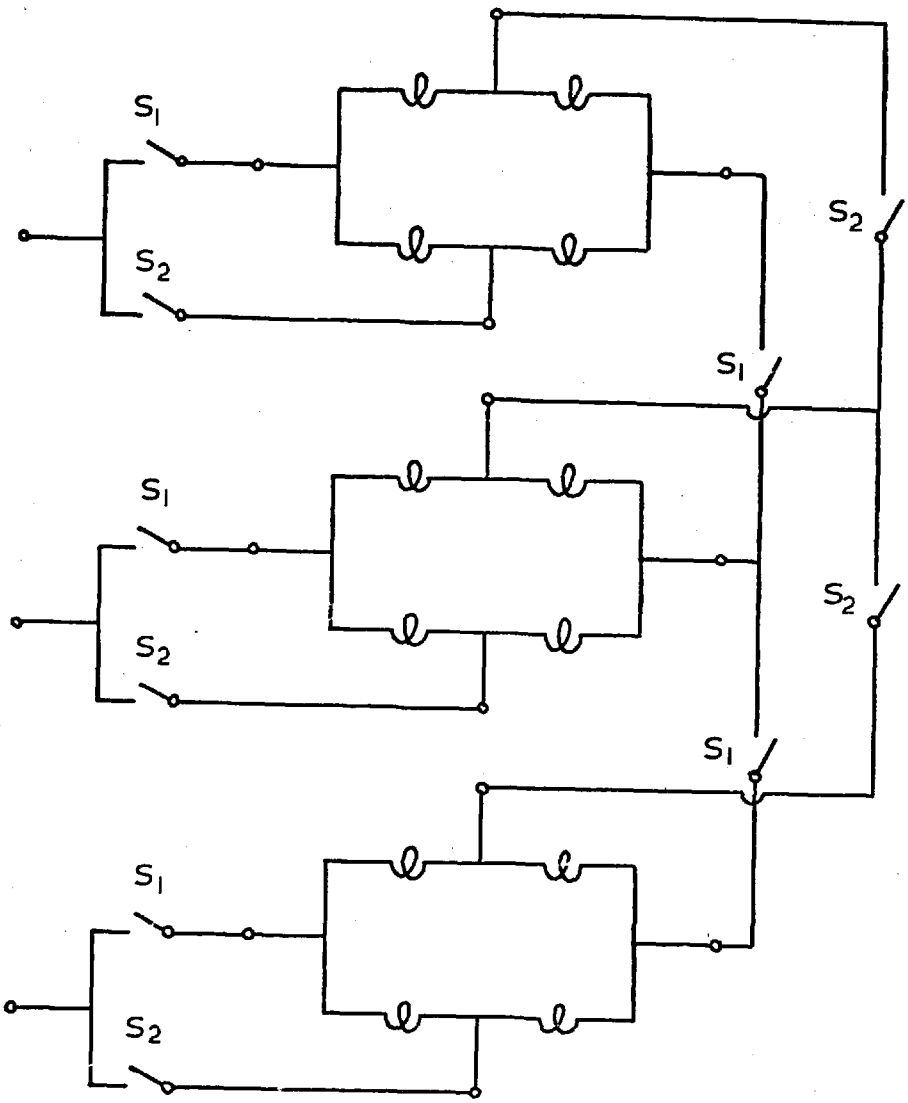

Fig. 2.9 Star-star connection using parallel groups

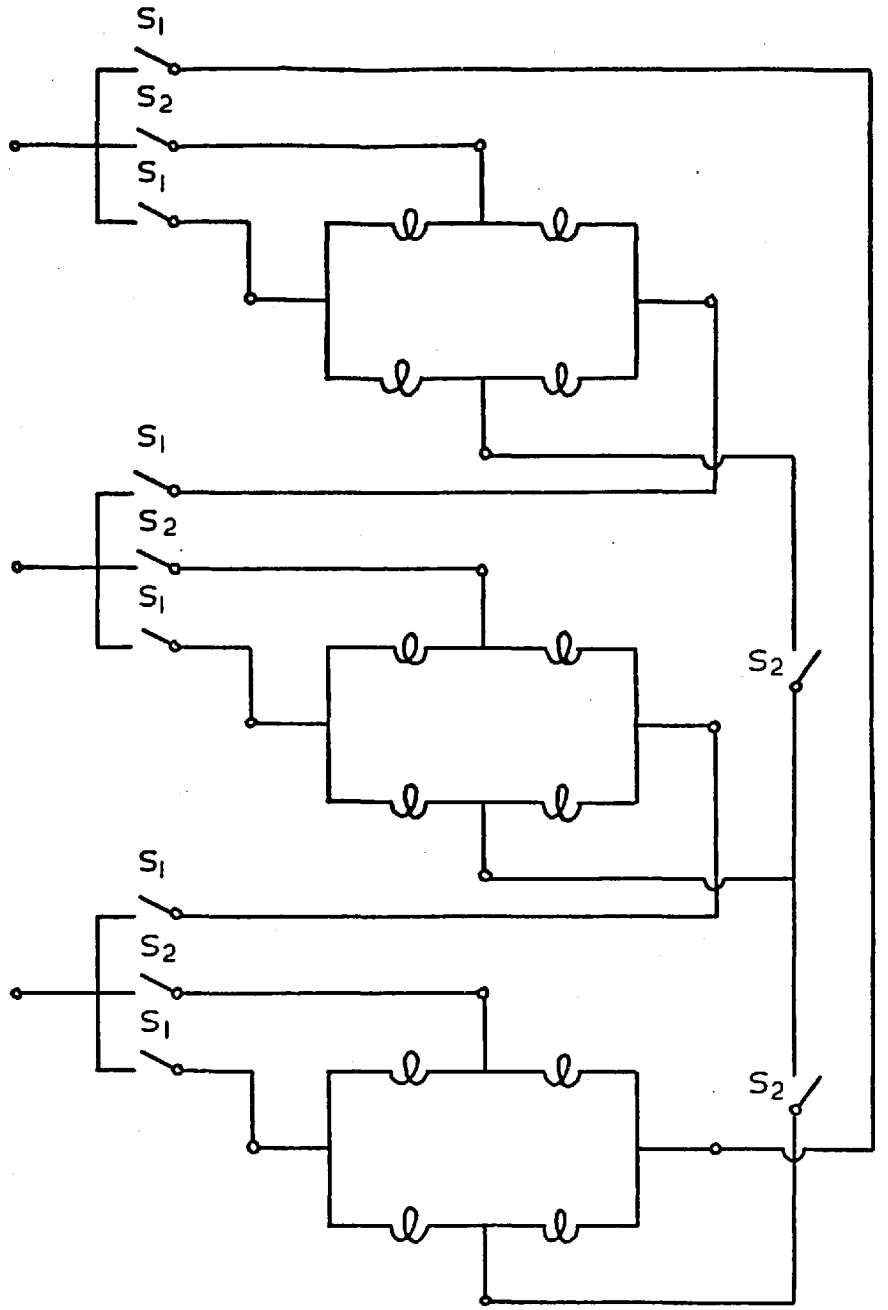

Fig. 2.10 Star-delta connection using parallel groups

2.3 Prediction of machine performance

2.3.1 Introduction

In the previous section the application of some pole-change windings to linear machines was described. A consequence of the shorter coil pitches required was an increase in harmonic content. The flexibility of the windings was considerably increased by using parallel and delta connections. Because of the non-uniform nature of the air-gap flux, any closed paths within a winding may allow the passage of circulating currents. The purpose of this section is to present a model for linear machines that allows the presence of circulating currents and the effects of winding harmonics to be predicted.

A one-dimensional multi-layer model is employed for the machine regions[2.10,2.12] using the boundary matching technique[2.11]. This model has the advantage of including thickness effects in a direction normal to the secondary surface whilst keeping to a minimum the amount of algebra required. Excitation for the model is provided by a thin current sheet representing the stator windings. In all previous linear machine models the magnitude of the current density in the excitation sheet has been estimated assuming a series star connected winding with balanced phase currents. No assumptions are made about winding connections or balance in the new model. The currents flowing in separate coil groups are calculated for any winding connection or distribution. These currents are then used for the calculation of forces and flux densities.

2.3.2 A model for the machine regions and calculation of thrust and flux density

In the absence of long sections of track, the testing of many linear machines has been performed on static rigs. A static test rig usually consists of a section of the proposed track attached to the surface of a rotatable drum or disc. The machine stator is curved in the appropriate direction and held above the track member leaving a uniform air-gap. This facility provides a realistic simulation of actual operating conditions if the circumference is sufficiently large to allow rotor currents to decay before re-entry beneath the stator.

A multi-layer model corresponding to a linear machine test rig is shown in Figure 2.11. The section (of length $2\,k_B P_B$) in the Figure corresponds to the rig circumference and is repeated at periodic intervals as indicated[2.13,2.14]. Machine windings are represented in the model by current sheets whose periodic repetition allows them to be expressed in Fourier Series form. Each layer in Figure 2.11 is of infinite extent in the x/y plane, of uniform thickness in the z-direction and possesses constant permeability and resistivity.

Appendix 2.7.2 gives the solution of Maxwell's Equations for the layer of Figure 2.12(a) and its representation by the equivalent circuit[2.11] of Figure 2.12(b). The circuit sections corresponding to each layer are connected in cascade on either side of a current source representing one harmonic of the current distribution produced by the machine windings. If the rth forward travelling current sheet with complex RMS amplitude J_{Fr} A/m sees a layer model input impedance of $Z_{in\ Fr}$ Ω, then the power input is $|J_{Fr}|^2\ \mathrm{Re}[Z_{in\ Fr}]$ W/m^2. The part of the layer model corresponding to the test rig is a section of stator of

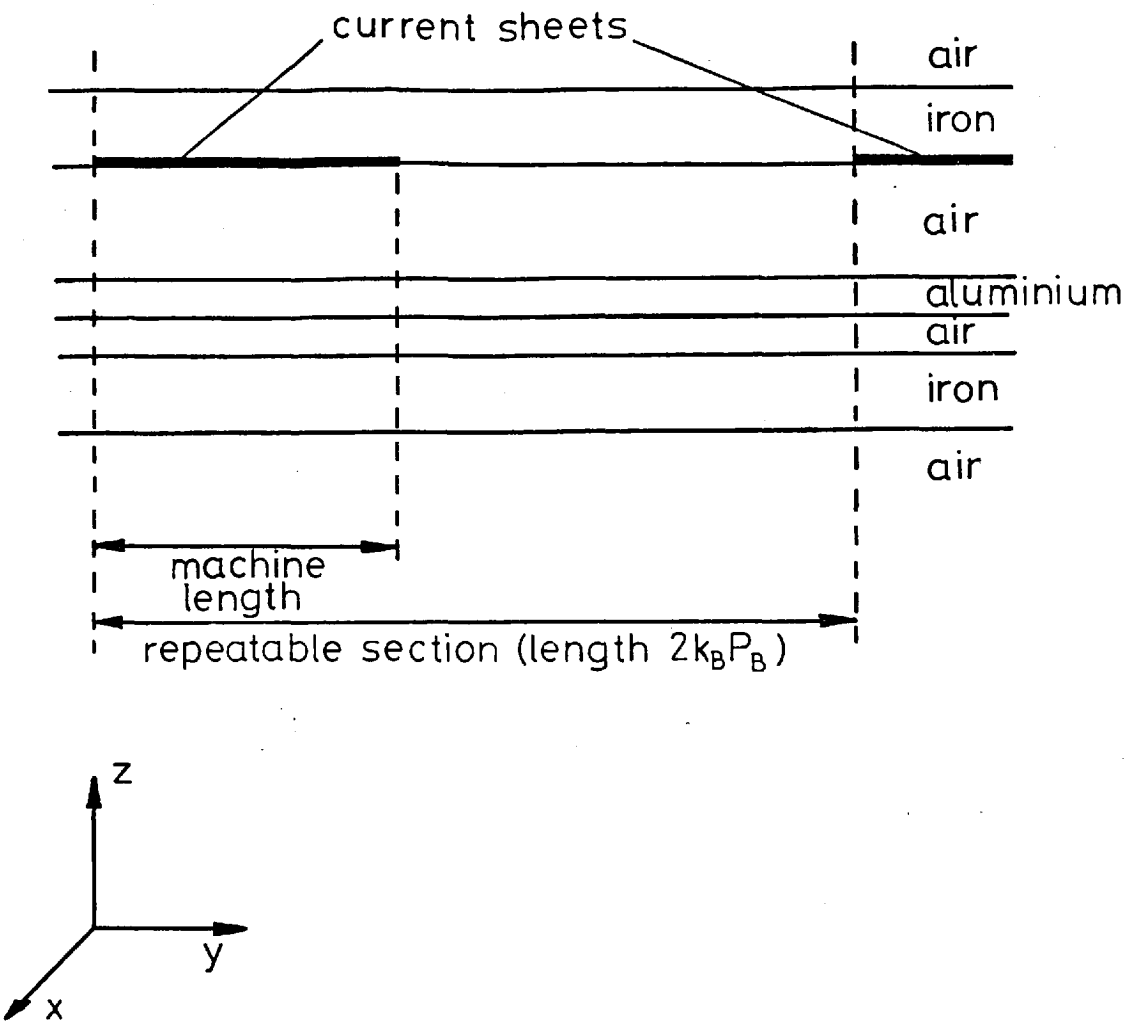

Fig. 2.11 Linear machine mathematical model

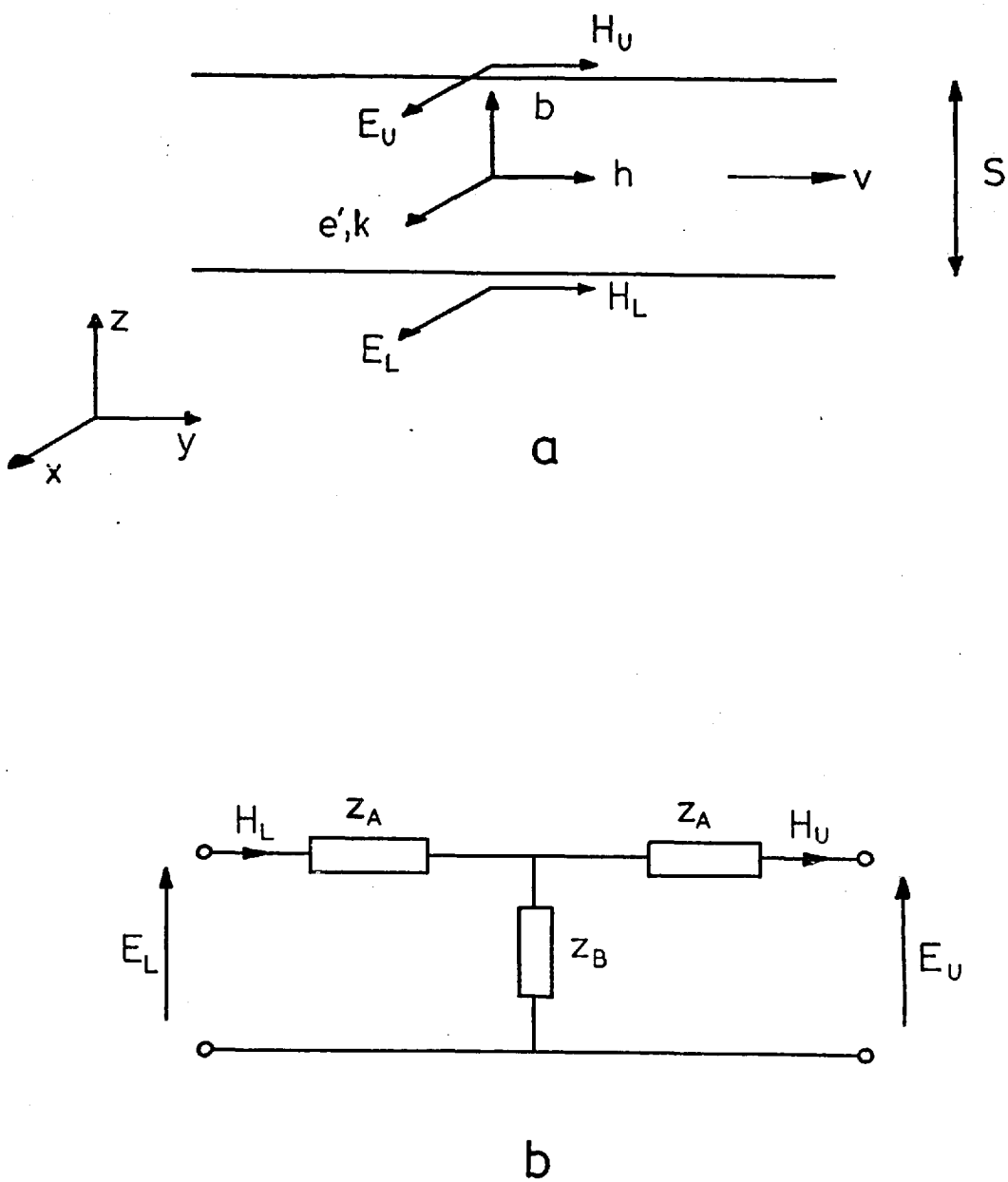

Fig. 2.12 Mathematical model for a single layer

a) field components
b) network representation

width w in the x-direction and length $2\,k_B P_B$ in the y-direction so that the power inputs for forward and backward travelling fields of the same order are given by

$$\begin{aligned} P_{in\ Fr} &= 2\,k_B P_B w\,|J_{Fr}|^2\,\mathrm{Re}[Z_{in\ Fr}] \\ P_{in\ Br} &= 2\,k_B P_B w\,|J_{Br}|^2\,\mathrm{Re}[Z_{in\ Br}] \end{aligned} \qquad (2.1)$$

If it is assumed that all the power loss in the model occurs only in the moving layers, then the power inputs of equation (2.1) may be directly related to the mechanical force produced. The synchronous speed of the rth harmonic waves is

$$v_{sr} = \frac{\omega}{k_r} \qquad (2.2)$$

so that the force produced in the y-direction is

$$F_r = \frac{P_{in\ Fr} - P_{in\ Br}}{v_{sr}} \qquad (2.3)$$

After substitution of equations (2.1) and (2.2) in (2.3) and the effects of all harmonics are considered, the total thrust force on the secondary is given by

$$F = \sum_{r=1}^{\infty} \frac{2\,k_B P_B w k_r}{\omega} \left\{ |J_{Fr}|^2\,\mathrm{Re}[Z_{in\ Fr}] - |J_{Br}|^2\,\mathrm{Re}[Z_{in\ Br}] \right\} \qquad (2.4)$$

The rth forward harmonic distribution of electric field strength on the rotor surface at coordinate y" is

$$e''_{Fr} = \sqrt{2}\,E''_{Fr}\,e^{j(\omega t - k_r y'')} \qquad (2.5)$$

where the complex amplitude E''_{Fr} is given at the appropriate junction in the layer model. A corresponding distribution of flux-density is given by

$$b''_{Fr} = \sqrt{2}\, B''_{Fr}\, e^{j(\omega t - k_r y'')}$$

$$\text{where} \quad B''_{Fr} = -\frac{E''_{Fr}}{v_{sr}} \tag{2.6}$$

When all forward and backward harmonic components are considered, the total flux density at coordinate y" is given, using equations (2.5), (2.6) and (2.2), as

$$b = \sqrt{2}\, B\, e^{j\omega t}$$

$$\text{where} \quad B = \sum_{r=1}^{\infty} -\frac{k_r}{\omega} \{E''_{Fr}\, e^{-jk_r y''} - E''_{Br}\, e^{jk_r y''}\} \tag{2.7}$$

2.3.3 A model for the machine windings and calculation of primary currents

The primary winding is assumed to lie in a uniformly slotted iron core. Currents in each coil side of a slotted winding can be replaced by "strips" of current in the slot openings[2.15,2.16]. This substitution leaves the air-gap flux virtually unaltered and provides a suitable excitation for the layer model. In the following analysis (based on that in references 2.3 and 2.17) it is found more convenient to begin by considering a surface distribution of conductors. The separate coils forming the conductor distribution are assumed to be series connected in a number of groups. At the winding surface the current density is related to the electric field strength by the input impedance of the layer model. Knowledge of the electric field distribution allows the emf induced in each coil group to be found. The separate coil groups are considered as network branches consisting of series connected voltage sources, self-impedances and the induced voltages. Application of the connection matrix technique[2.18] completes

the analysis allowing the coil group currents to be found when the supply voltages are given. This model is very suitable for computer use in that the connection matrix removes the need to set up new electric circuit equations each time a different coil group connection is required.

Figure 2.13 shows the sth slot in a linear machine primary. This stator has a total of Q slots including any that may be half-filled at the ends. The slot shown contains N conductors of the νth coil group (i.e. $N_{s\nu}$ conductors), giving a surface density of conductors at the slot openings of $N_{s\nu}/2\delta$ conductors/m. By a process similar to that used in Appendix 2.7.1, this conductor density may be resolved into a Fourier distribution with an rth harmonic amplitude of

$$C'_{r\nu} = \frac{\sin(k_r\delta)}{(k_r\delta)} \frac{N_s}{2\, k_B P_B} e^{-jk_r y_{s\nu}} \qquad (2.8)$$

A similar distribution may be obtained for each slot that contains conductors of the νth winding. The resultant distribution is given by the sum of the individual distributions as

$$C_{r\nu} = \frac{\sin(k_r\delta)}{(k_r\delta)} \sum_{s=1}^{\infty} \frac{N_{s\nu}}{2\, k_B P_B} e^{-jk_r y_{s\nu}} \qquad (2.9)$$

The corresponding Fourier Series for the winding is

$$n_\nu = \sum_{r=1}^{\infty} (C^*_{r\nu}\, e^{-jk_r y} + C_{r\nu}\, e^{jk_r y}) \qquad (2.10)$$

which assumes that $C_{o\nu} = 0$ since the machine is coil wound.

If a current $i_\nu = \sqrt{2}\, I_\nu\, e^{j\omega t}$ flows in the coil group, then the instantaneous surface current density is:

$$n_\nu i_\nu = \sqrt{2} \sum_{r=1}^{\infty} \{J_{Fr\nu}\, e^{j(\omega t - k_r y)} + J_{Br\nu}\, e^{j(\omega t + k_r y)}\} \qquad (2.11)$$

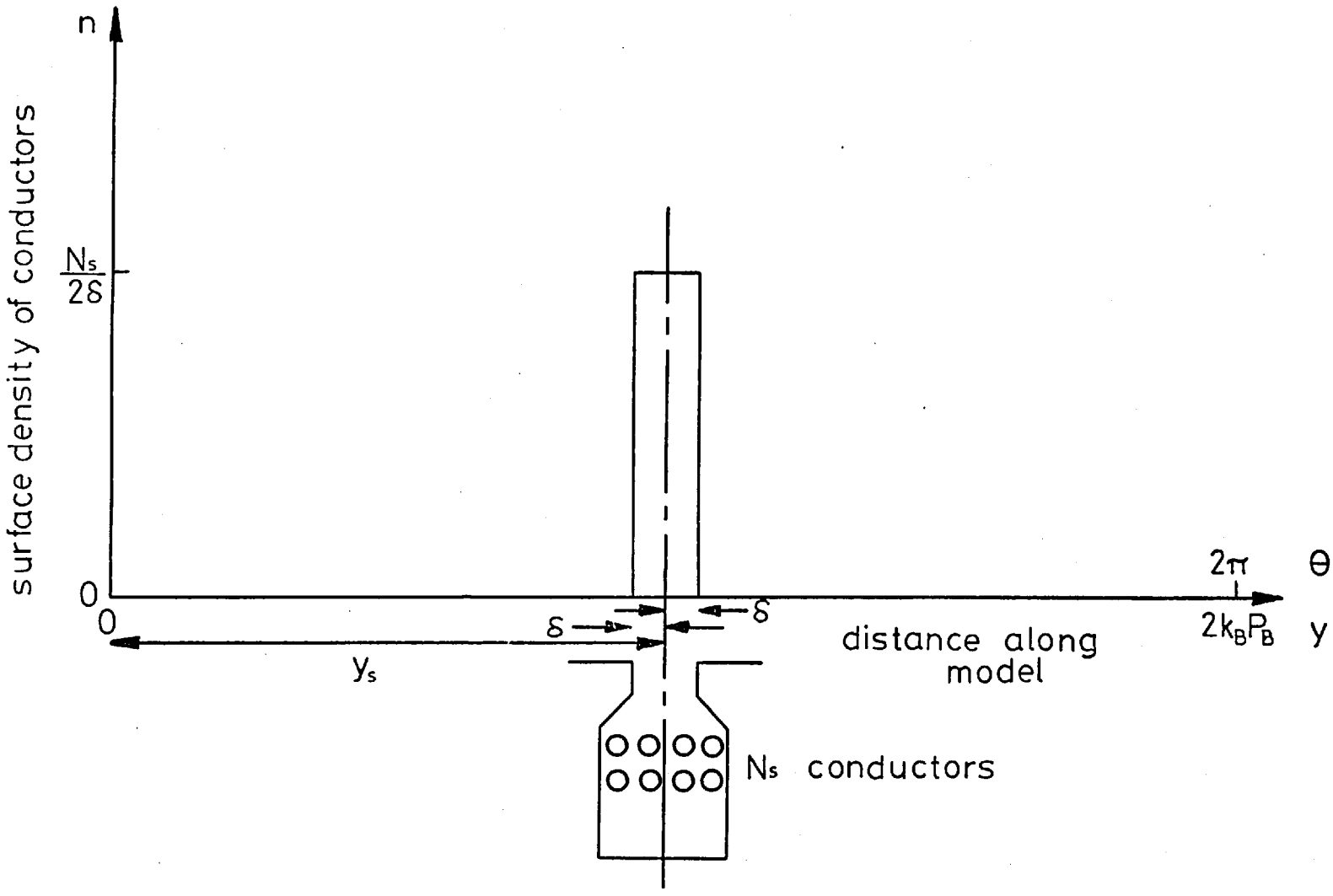

Fig. 2.13 Surface density of conductors produced by a single coil side

where the amplitudes of the forward and backwards travelling waves of current density are

$$\begin{aligned} J_{Fr\nu} &= C^*_{r\nu}\, I_\nu \\ J_{Br\nu} &= C_{r\nu}\, I_\nu \end{aligned} \qquad (2.12)$$

The total RMS current density due to ρ coil groups may be expressed as the product of two vectors of length ρ, i.e.

$$\begin{aligned} J_{Fr} &= [C^*_r]^T [I] \\ J_{Br} &= [C_r]^T [I] \end{aligned} \qquad (2.13)$$

When these currents flow in the layer model, they excite corresponding electric fields

$$\begin{aligned} E_{Fr} &= -Z_{in\ Fr}\, J_{Fr} \\ E_{Br} &= -Z_{in\ Br}\, J_{Br} \end{aligned} \qquad (2.14)$$

Appendix 2.7.3 shows how the instantaneous form of equation (2.14) may be related to the induced emf in a coil group. For the rth harmonic acting on the νth coil group, the induced emf is

$$e_{T\nu r} = 2\, k_B P_B w \left\{C_{r\nu}\, E_{Fr} + C^*_{r\nu}\, E_{Br}\right\} \qquad (2.15)$$

When all the coil groups are considered, $e_{T\nu r}$ becomes a column vector of length ρ so that

$$[e_{Tr}] = 2\, k_B P_B w \left\{[C_r]\, E_{Fr} + [C^*_r]\, E_{Br}\right\} \qquad (2.16)$$

The total induced emf in each coil group is now found by substituting for E_r and J_r from (2.14) and (2.13) and summing over all the harmonics, hence

$$[e_T] = -2\, k_B P_B w \sum_{r=1}^{\infty} \left\{[C_r]\, Z_{in\ Fr}\, [C^*_r]^T + [C^*_r]\, Z_{in\ Br}\, [C_r]^T\right\} [I] \qquad (2.17)$$

Now the windings may be considered as ρ separate network elements as shown in Figure 2.14, each having a self impedance z_ν and an independent voltage source e_ν. For all the windings then:

$$[e] + [e_T] + [E] = [z][I] \qquad (2.18)$$

The connection matrix technique[2.18] can now be used to link the windings together as shown in Appendix 2.7.4 so that each current may be found, given the applied voltages, i.e.

$$[I] = [S]\{[S]^T([Z] + 2\, k_B P_B w \sum_{r=1}^{\infty} \{[C_r] Z_{in\ Fr} [C_r^*]^T + [C_r^*]\ Z_{in\ Br}\ [C_r]^T\})[S]\}^{-1}[S]^T[e] \qquad (2.19)$$

2.3.4 Practical aspects of the model

It will be appreciated that the model of Figure 2.11 is not truly representative of a linear machine test rig. A number of approximations are required to enable finite dimensions to be taken into account and the evaluation of material constants.

In a real machine all current paths are closed at finite distances. Secondary circuits are usually completed by extending the conducting regions beyond the stator in the x-direction. A complete circuit places a restriction on the secondary currents and introduces extra resistance not accounted for by the layer model. The increase in resistance may be estimated by scaling the bulk resistivity used for the secondary regions with an appropriate Russell and Norsworthy factor[2.19].

Some difficulties also arise in the choice of material constants for the ferrous regions in the model. It was assumed that iron parts were worked below saturation and that a constant value of permeability

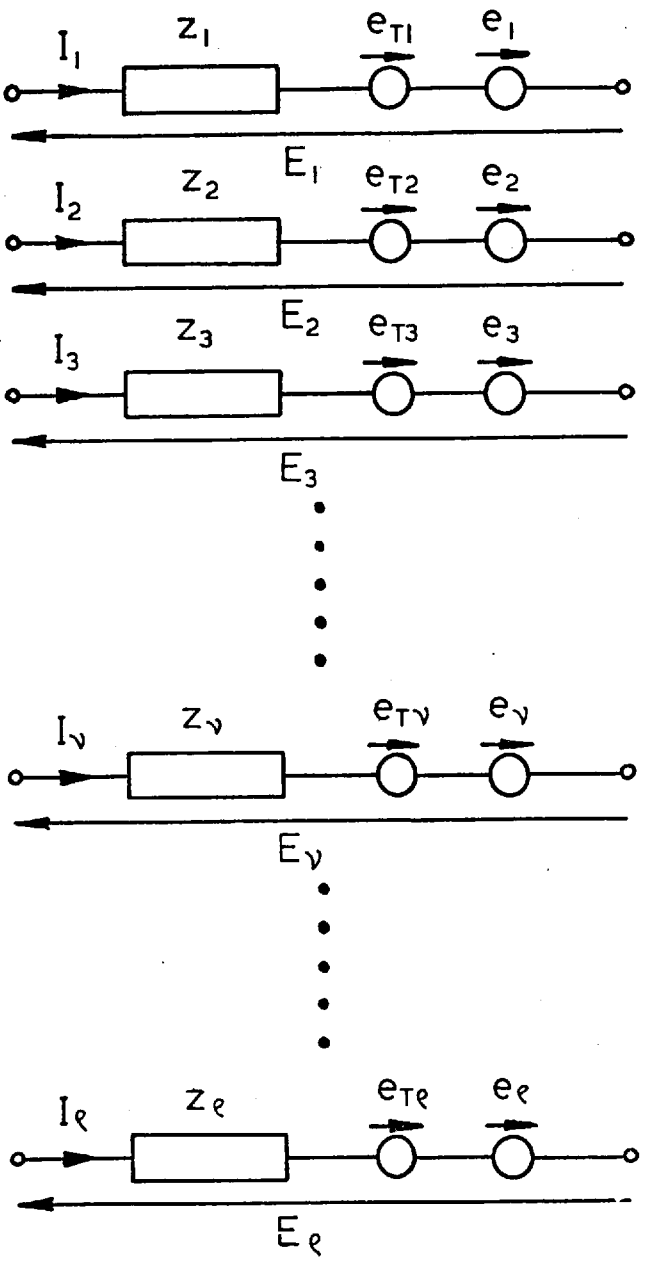

Fig. 2.14 Winding network elements

was appropriate. Magnetic circuits are designed so that the effects of unwanted eddy currents are minimised. In order to remove core currents and also make the thrust calculation possible a very high resistivity value was used for laminated regions. The eddy current problem in unlaminated steel is extremely complex because of "depth of penetration" and local saturation effects that increase with frequency. It is envisaged that unlaminated steel will only be used in track members where it will be faced by a highly conductive layer. At low rotor speeds the reaction of the conducting plate keeps the flux low. When the machine is running the flux-density increases but the rotor frequency is low allowing the flux to penetrate well into the secondary core. Under these conditions, it was thought that the use of constant values for resistivity and permeability for solid steel was realistic.

A real linear machine has a primary of limited length. It is therefore necessary to apply a correction to the thrust calculated from the model[2.20,2.7]. Induction machines are usually designed so that the air-gap is small in comparison with the winding pole-pitch. This forces most of the air-gap flux to enter the rotor in a direction normal to its surface. Magnetic energy is stored in the machine air gap at an approximate density of $B^2/2\mu_o$ J/m^3 where B is the RMS magnitude of the flux density normal to the rotor surface. At the exit end of the excitation in Figure 2.11, the removal of energy by the rotor amounts to a steady power loss of $\frac{B_{ex}^2}{2\mu_o} wg_i v$ W where g_i is the total air-gap and B_{ex} is the normal flux density at the exit end. This loss is supplied by the electrical input to the machine. The finite length of the stator in a real machine causes a modification of the field distributions beyond the exit edge. When the stator iron is removed, the effective

air-gap is increased to P_w/π[2.7,2.20] and the loss to $\frac{B_{ex}^2}{2\mu_o} wv \frac{P_w}{\pi}$. The excess loss over that given by the model must be supplied from the rotor. Removal of rotor power results in a retarding force of

$$F_{ret} = \frac{B_{ex}^2 w g_i v}{2\mu_o v_s} \left(\frac{P_w}{\pi} - g_i\right) \qquad (2.20)$$

which must be subtracted from the predicted force given by the model.

The network branch representing each primary coil group includes a self impedance. This is used to take account of winding resistance and slot and end turn leakage reactance. Estimation of coil group resistance is straight forward when the usual geometric and material parameters are known. Leakage reactances were evaluated by a number of formulae that are frequently employed. The most consistent results were given using the method described by Liwshitz-Garik[2.21] and this was used throughout the work. Winding self-impedance calculations are based on a balanced arrangement assuming sinusoidal waves with the winding pole-pitch. The values of impedance given are "per-phase" and these were appropriately scaled to apply to individual windings. Use of this method was considered realistic since the final machine design strives to achieve balance.

The length of the model of Figure 2.11 in the y-direction must be made consistent with the infinite nature of a linear machine secondary. All fields must decay substantially to zero within the repeatable section for the model to be truly representative. The distance required beyond the exit-edge may be estimated by assuming that the fields decay with the same time constant that governs the decay of transient rotor currents under the stator. In the solutions to the problem, represented by equations (2.19), (2.4) and (2.7), a summation over an infinite number

of harmonics is indicated. Practical calculations only allow the effects of a finite number of harmonics to be evaluated. A close approximation to the required solution is found by increasing the number of harmonics considered until only small variations are apparent.

2.4 Experimental verification of winding performance and the prediction technique

2.4.1 A machine with low secondary resistance

Figure 2.15(a) shows a general view of the rotating disc apparatus used to test the pole-change machines described in this section. The outer annulus of the disc simulates the moving parts of the secondary member of a linear machine and was 2.135 m in diameter overall. Stationary members were mounted on "L" brackets within the bearing pedestal, as Figure 2.15(B) shows. A clamping ring was provided on the central part of the disc to allow secondary members of different materials and sizes to be fitted.

The stator constructed for this series of tests is shown in Figure 2.16 and had the following dimensions:

Mean core length	1.46 m
Core width	15.9 cm
Overall core depth	12.0 cm
Slot type	open
Number of slots	54
Slot width	1.43 cm
Slot depth	3.81 cm
Number of coils	48
Coil pitch	6 slots
Turns/coil	12

Each coil end was taken separately to a terminal board. This enabled different winding arrangements to be connected with ease.

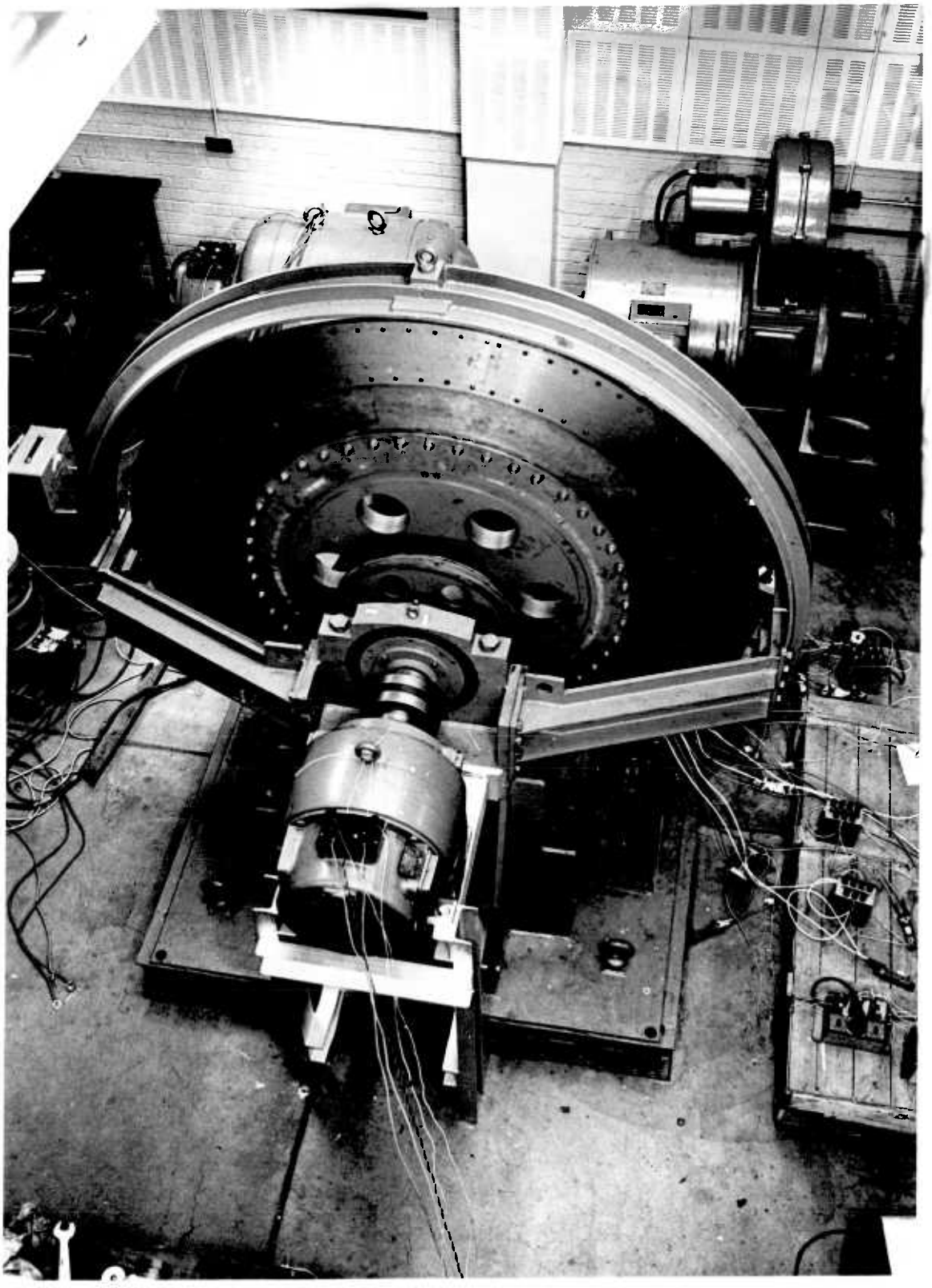

Fig.2.15.a. Linear machine test apparatus

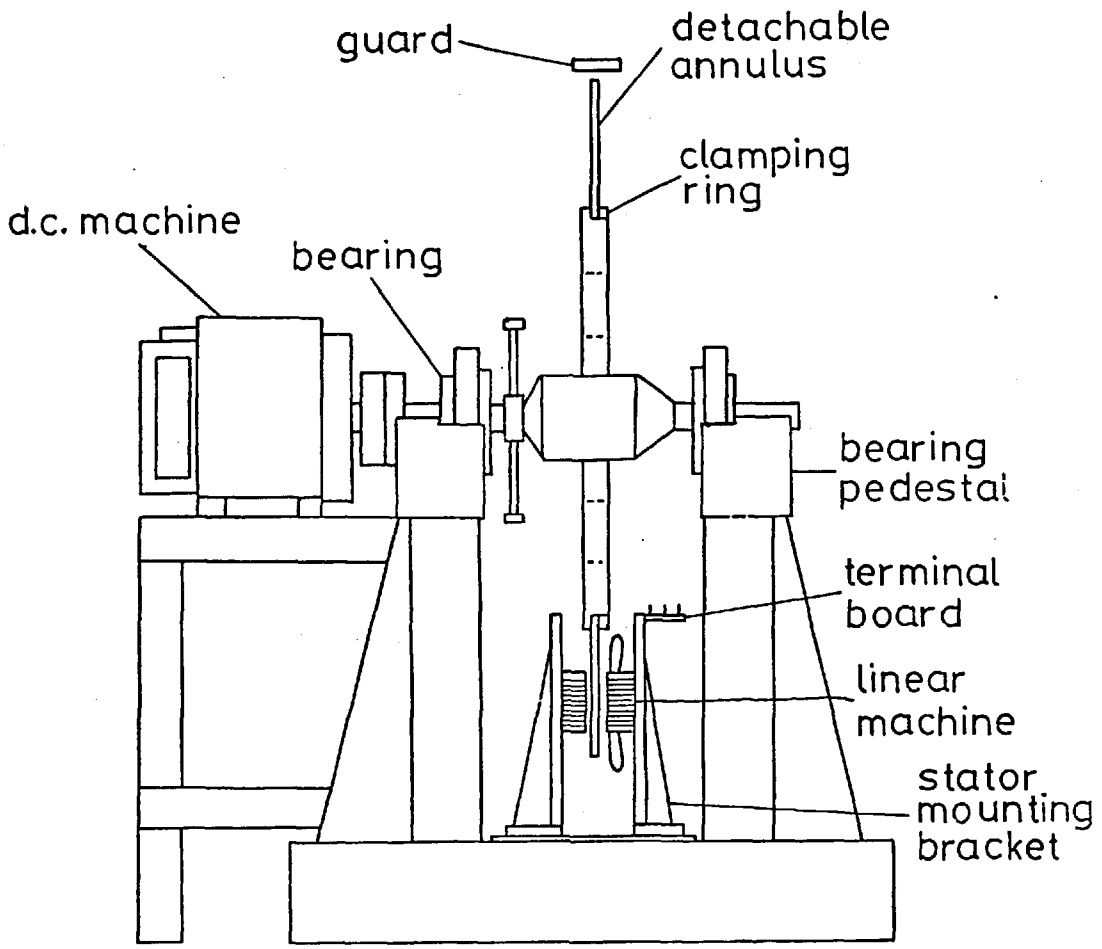

Fig. 2.15b Detailed view of test apparatus showing position of linear machine

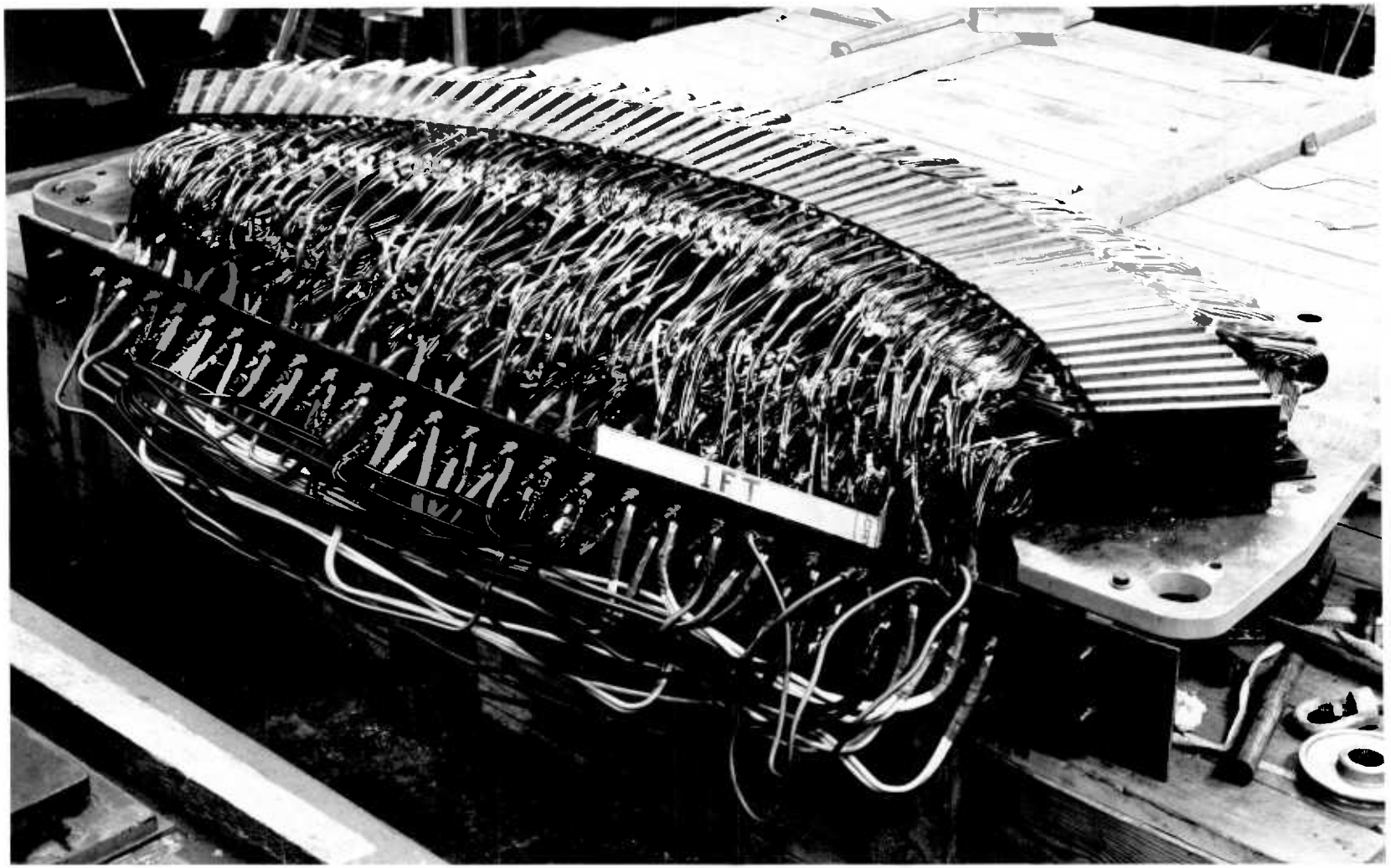

Fig.2.16.Stator of test machine

In order to provide a rigorous test for the layer model of Section 2.3.2, two different secondary members were constructed. The first of these consisted of a plain aluminium annulus, 2 cm thick, giving an effective secondary width of 39.3 cm. An unwound laminated block with the same dimensions as the stator was fitted behind the disc to complete the machine magnetic circuit. This arrangement required two air-gaps to allow for disc clearance. The winding chosen for these tests was the eight to four consequent-pole type illustrated in Figure 2.3. Coil groups were connected according to the double winding principle discussed in Section 2.2.4 and the resulting winding is shown in Fig. 2.17.

Current and force characteristics, obtained with a supply of 50 V phase at 50 Hz, for both pole settings are compared with the mathematical model predictions in Figures 2.18 and 2.19. The overall agreement is generally good with the model predicting both phase current and parallel path unbalance. Force predictions at peak thrust tended to be optimistic.

2.4.2 A machine with solid iron in the secondary

In a linear motor driven transport system, an item of major expense will be that of the track member. Recent proposals for economic track construction include the use of solid iron to complete the machine magnetic circuit.

In order to test a similar configuration, the disc apparatus was furnished with an outer annulus of unlaminated mild steel 2 cm thick. The steel was faced with a layer of aluminium 1.6 mm thick to give an effective secondary width of 22.9 cm. Tests were performed

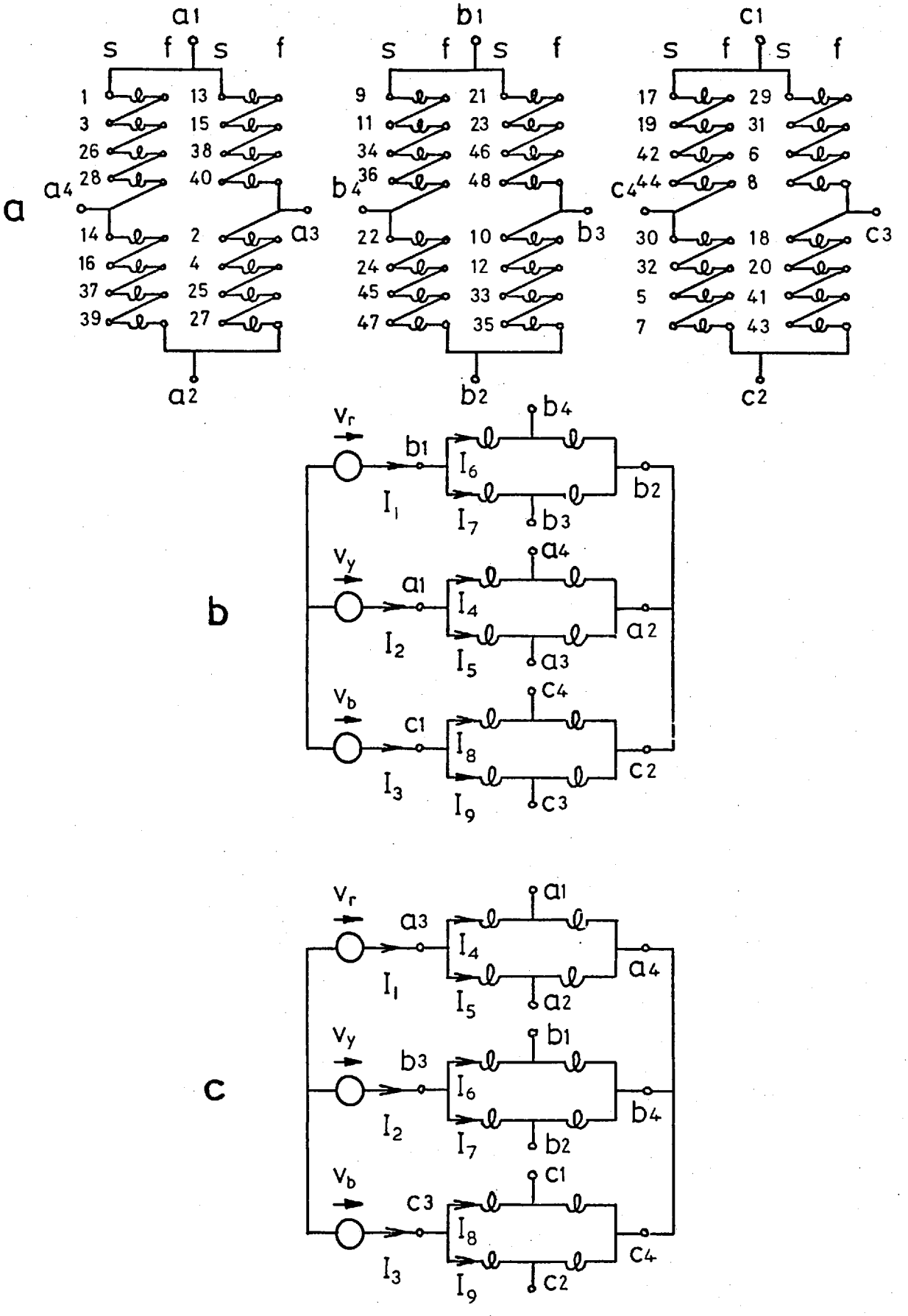

Fig. 2.17 Parallel connections for the experimental machine

a) coil groups
b) 8-pole connection
c) 4-pole connection

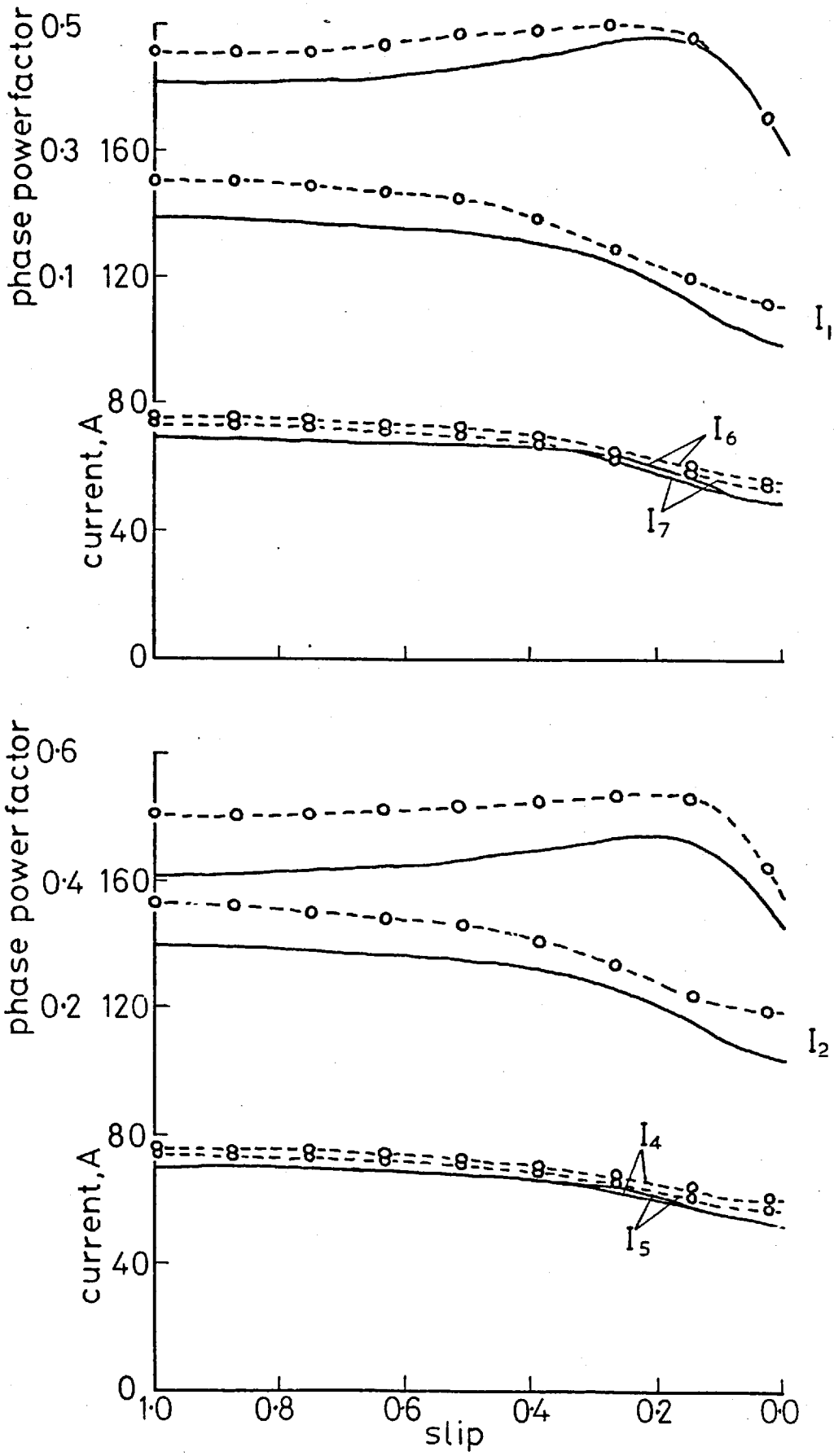

Fig. 2.18a Comparison of results for the 8-pole setting with low resistance secondary

——— calculated
- o - measured

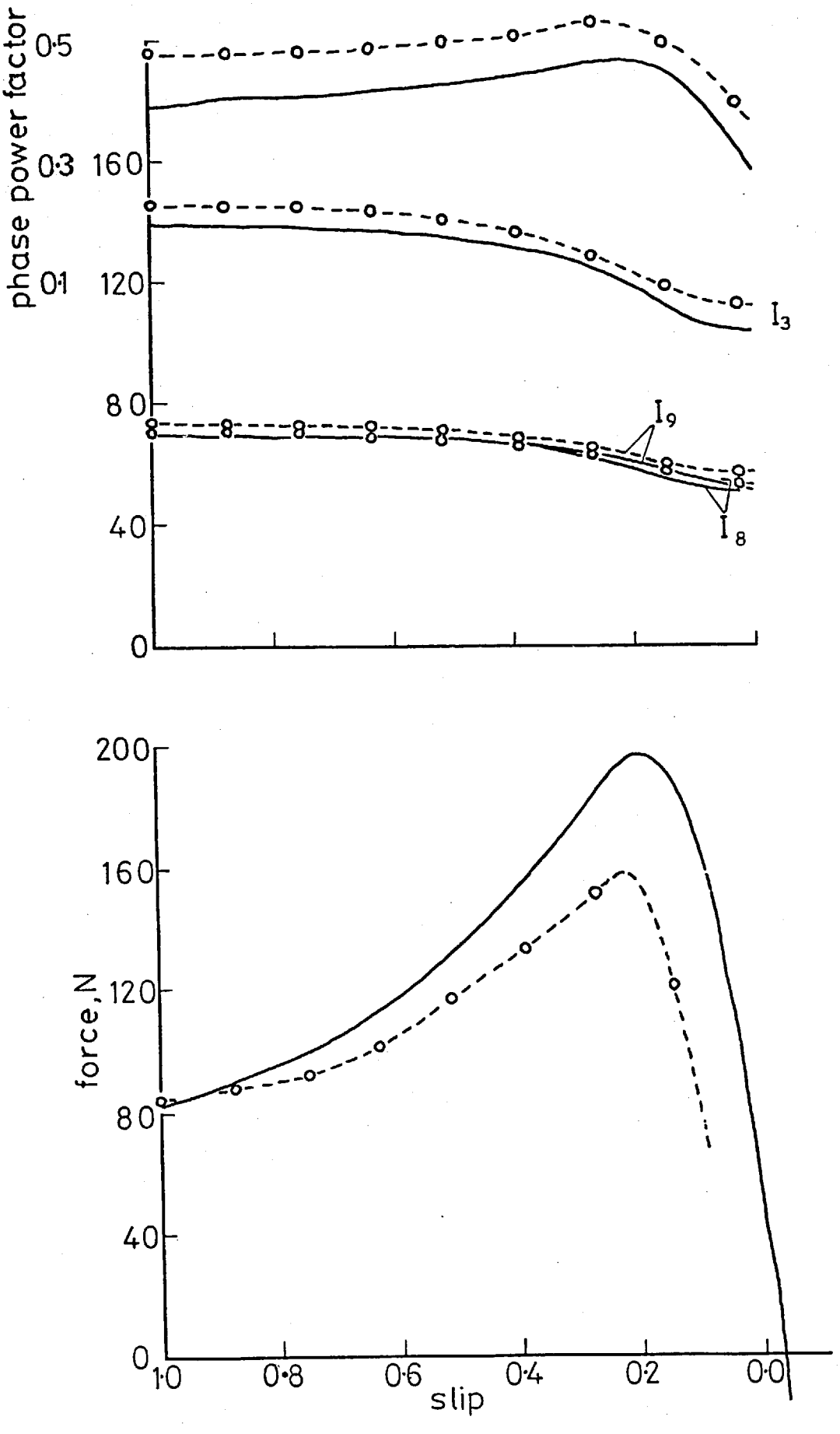

Fig. 2.18b Comparison of results for the 8-pole setting with low resistance secondary

——— calculated

- o - measured

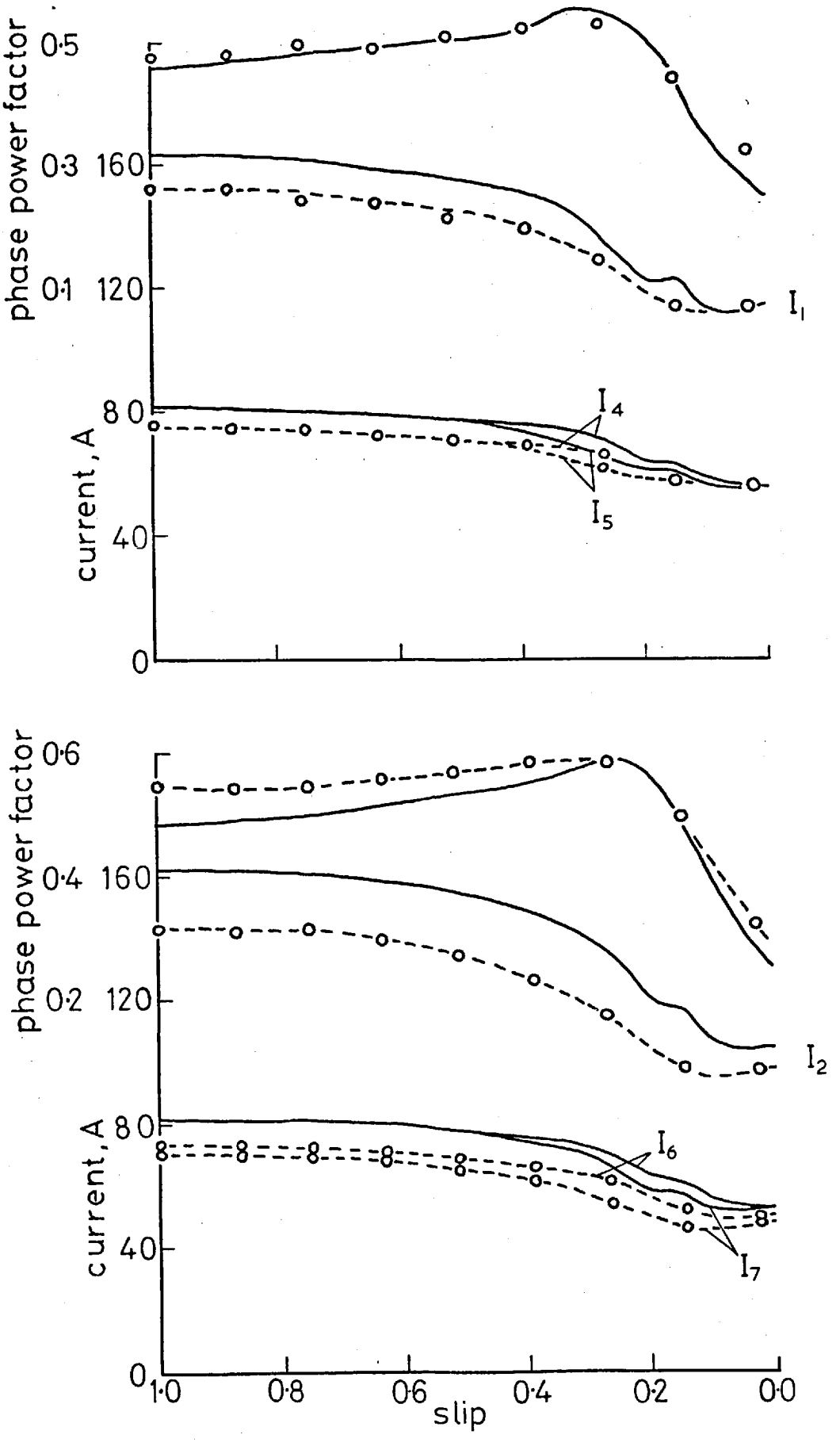

Fig. 2.19a Comparison of results for the 4-pole setting with low resistance secondary

——— calculated

- o - measured

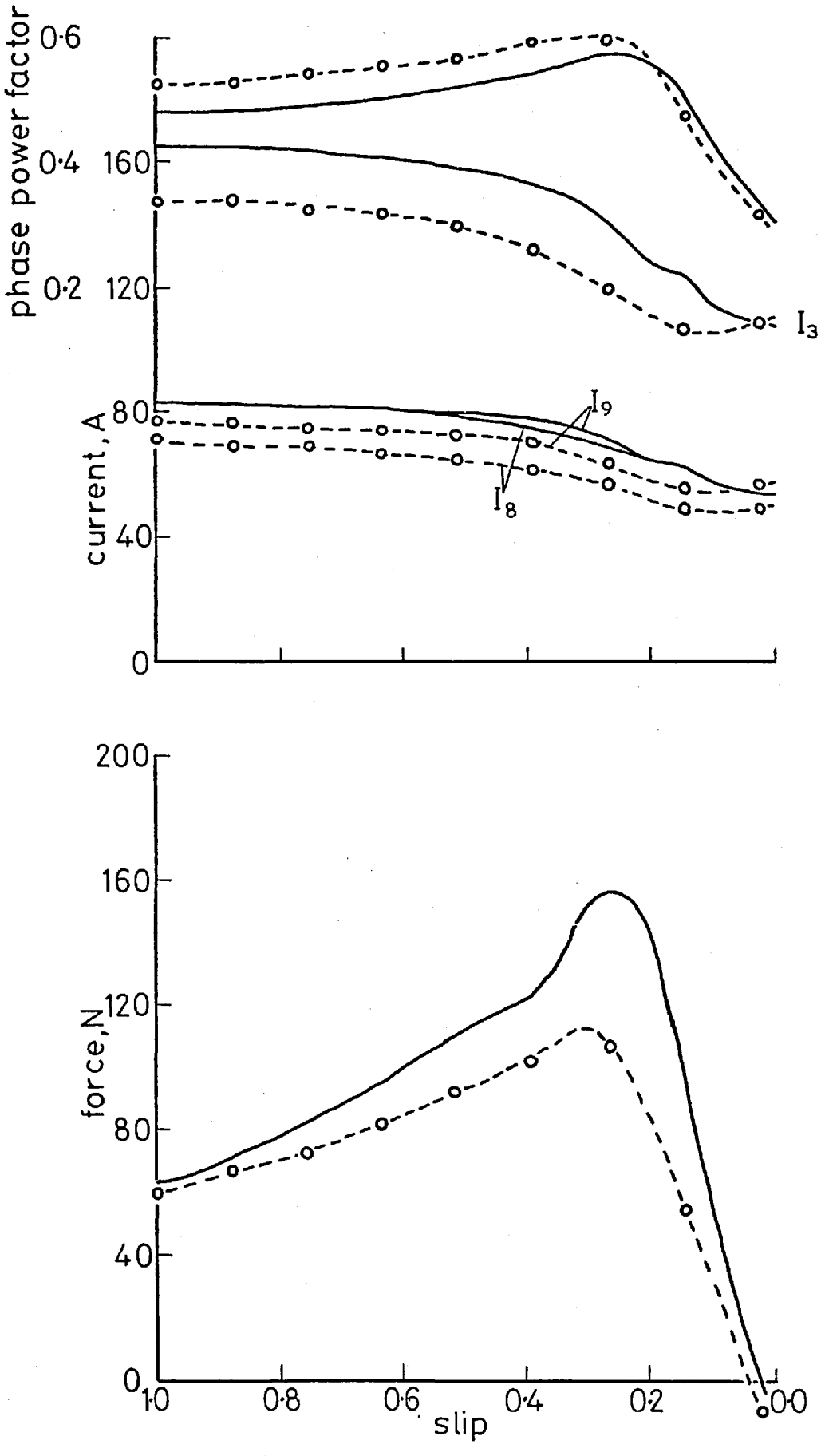

Fig. 2.19b Comparison of results for the 4-pole setting with low resistance secondary

——— calculated

- o - measured

at 50 V phase and 50 Hz using the parallel connected stator described in the previous section. Predicted and measured terminal characteristics for both pole settings are shown in Figures 2.20 and 2.21. Again, balance between phase and parallel path currents was acceptable over the full speed range but peak forces were overestimated.

During this series of tests it was decided to examine the degree of air-gap flux distortion tending to produce unbalance between the parallel paths. A number of search coils were attached to an arc-shaped former fixed in the machine air-gap. The coils were positioned to just clear the aluminium surface of the disc. Curves of flux density for both pole-settings at slips of 1.0 and 0.2 are shown in Figures 2.22 and 2.23. These figures show considerable flux distortion at 0.2 slip on the four-pole setting. The model gives closer estimates of flux density at higher speeds because solid iron penetration and transverse edge effects decrease with slip frequency.

The tests described above were repeated with the stator reconnected to form the eight to four-pole series winding of Figure 2.24. These results (with the same supply conditions) are shown on the corresponding curves for the parallel connected winding and indicate that the use of parallel groups incurs no loss of performance.

2.5 A design example

2.5.1 Step phase-modulated windings

In Section 2.2 the application of consequent-pole two-speed windings to linear machines was discussed. A simple method for estimating the degree of unbalance within the winding was also given. The complete mathematical model of Section 2.3 allowed the winding

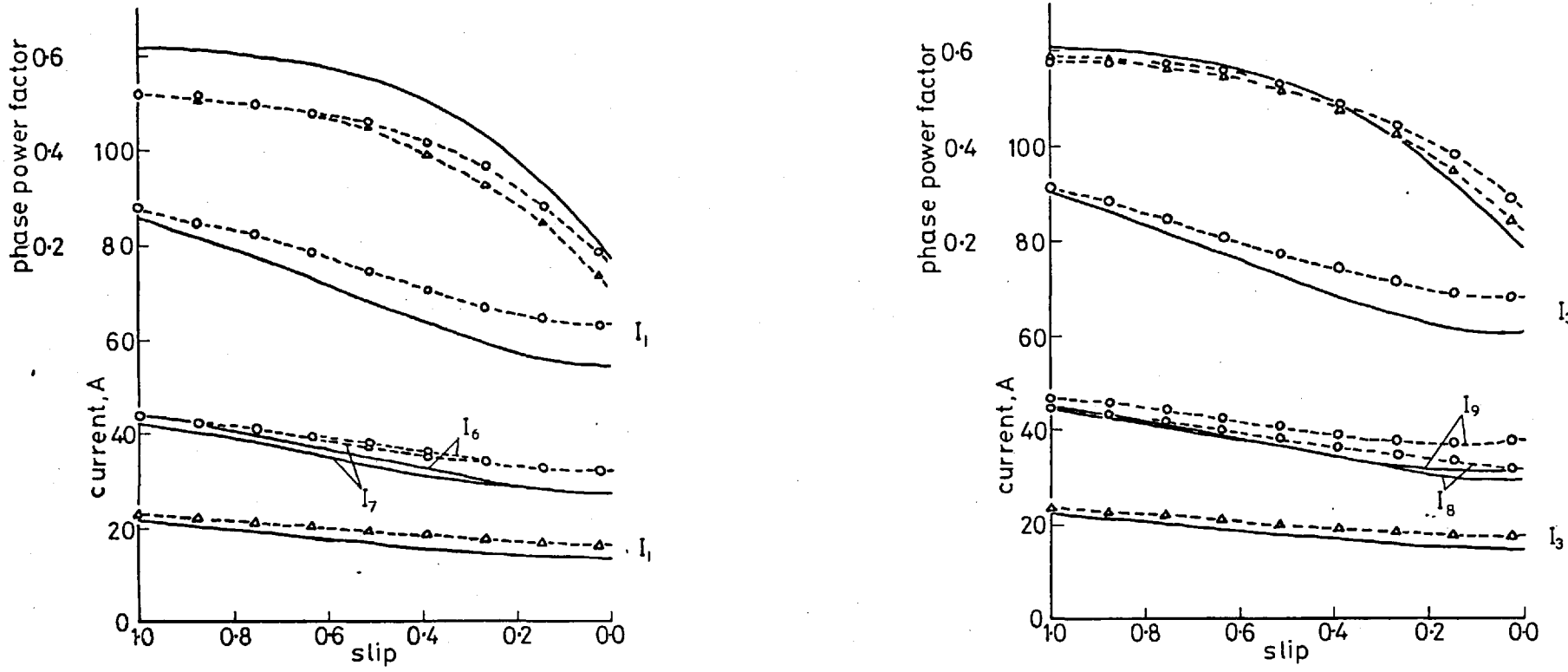

Fig. 2.20.a. Comparison of results for the 8-pole setting with solid iron in the secondary

——— calculated
---o--- measured (parallel)
---Δ--- measured (series)

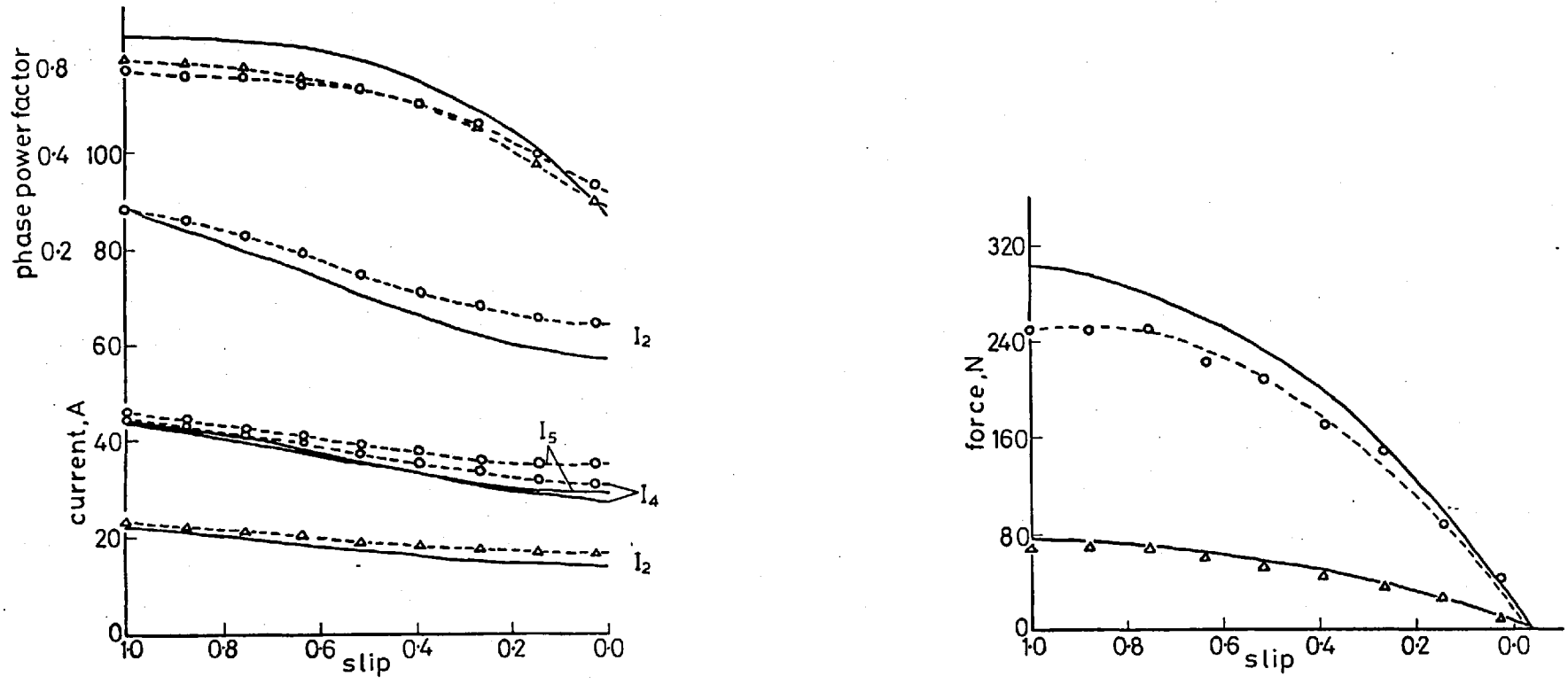

Fig. 2.20.b. Comparison of results for the 8-pole setting with solid iron in the secondary

——— calculated
---o--- measured (parallel)
---Δ--- measured (series)

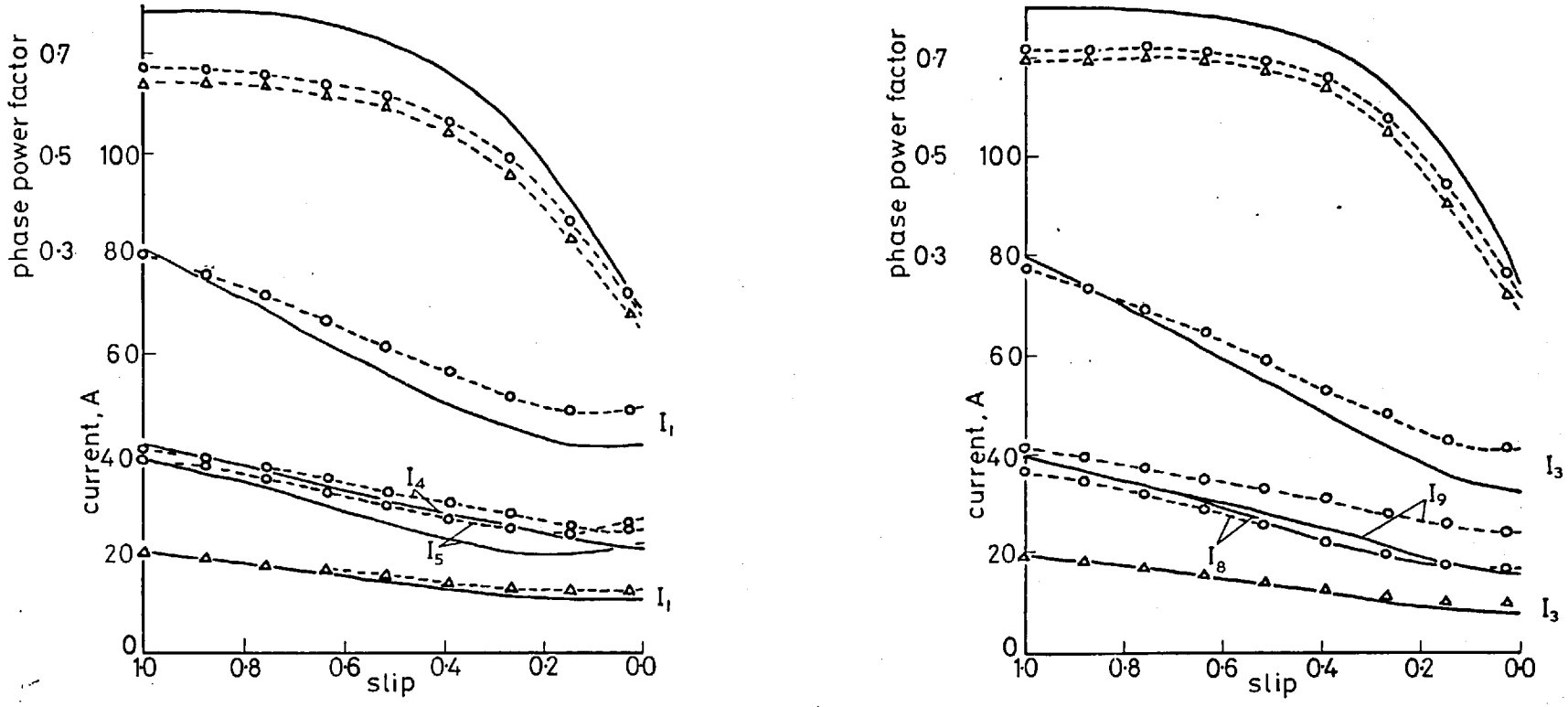

Fig. 2.21.a. Comparison of results for the 4-pole setting with solid iron in the secondary

——— calculated
---o--- measured (parallel)
---Δ--- measured (series)

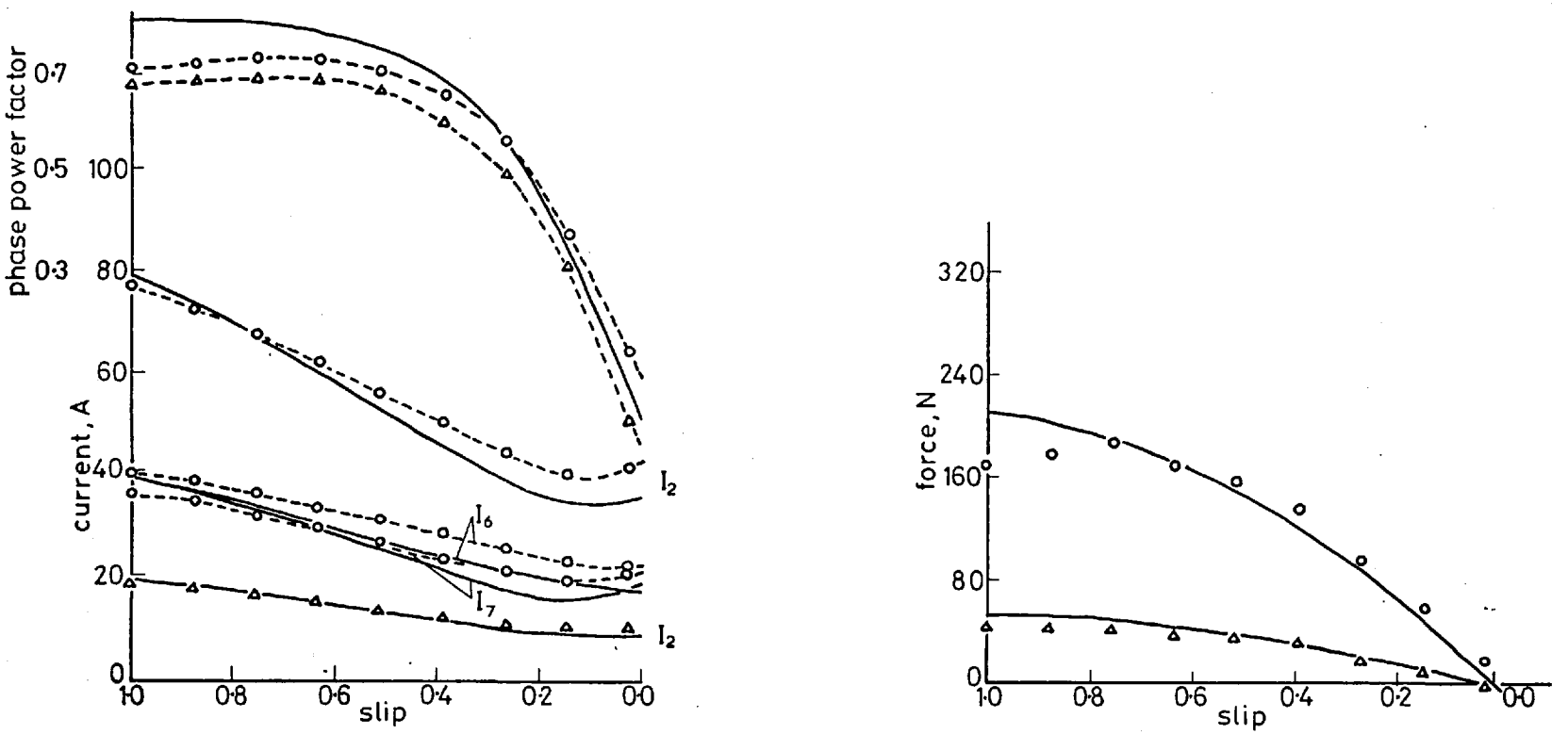

Fig. 2.21.b. Comparison of results for the 4-pole setting with solid iron in the secondary

——— calculated
---o--- measured (parallel)
---Δ---measured (series)

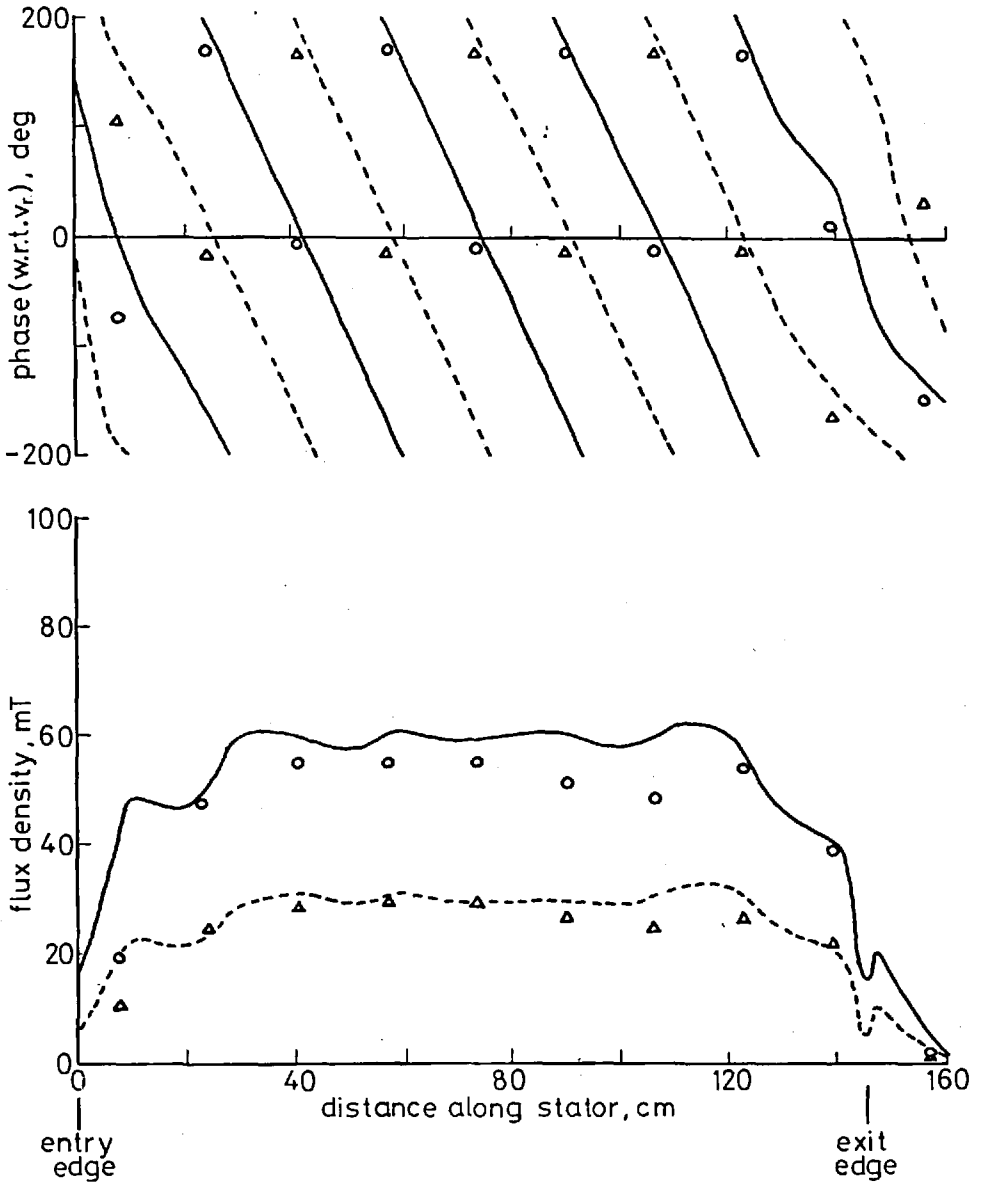

Fig. 2.22.a. Flux density on the 8-pole setting at 1·0 slip with solid iron in the secondary

——— calculated } parallel
o o o measured }

------- calculated } series
Δ Δ Δ measured }

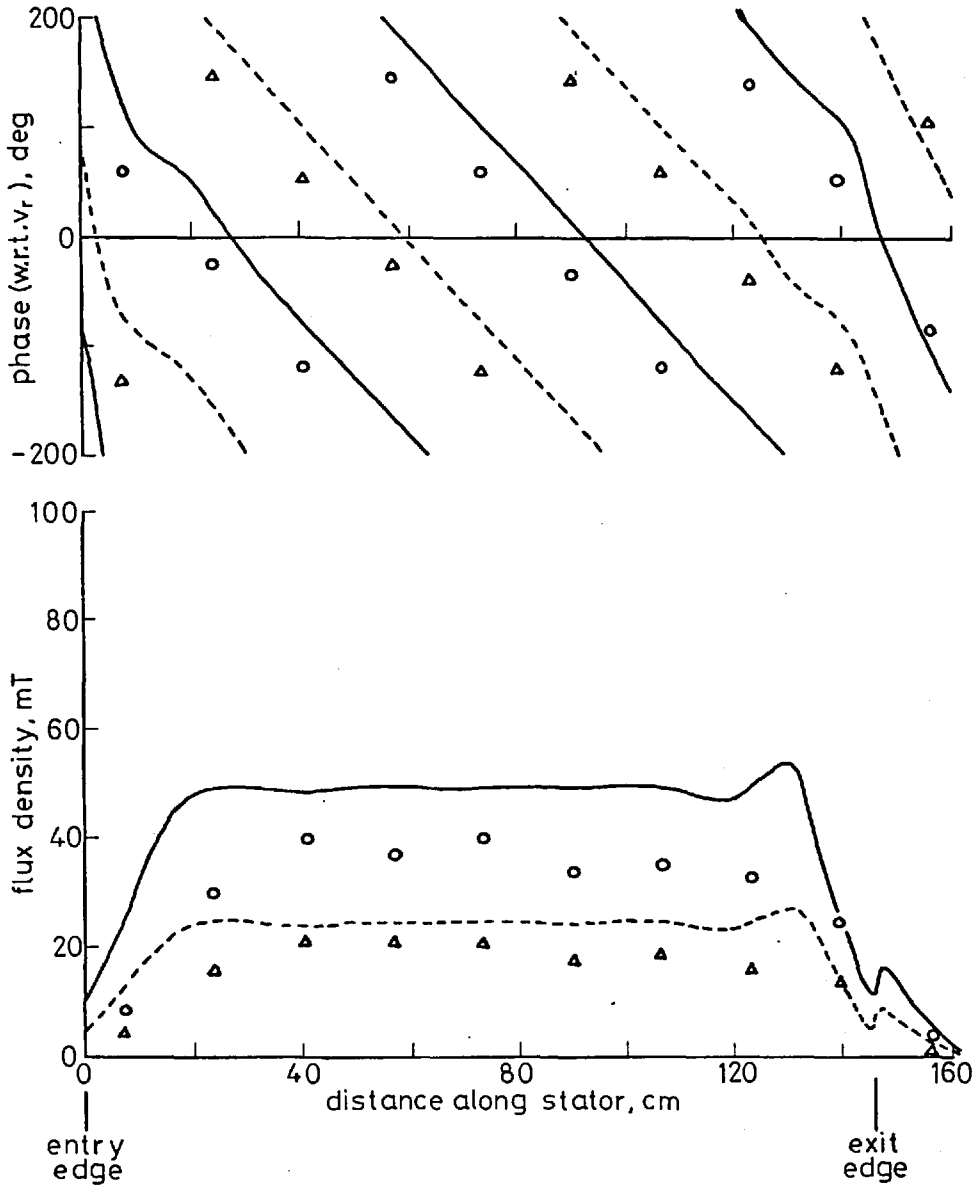

Fig. 2.22.b. Flux density on the 4-pole setting at 1·0 slip with solid iron in the secondary .

——— calculated } parallel
o o o measured }

------ calculated } series
Δ Δ Δ measured }

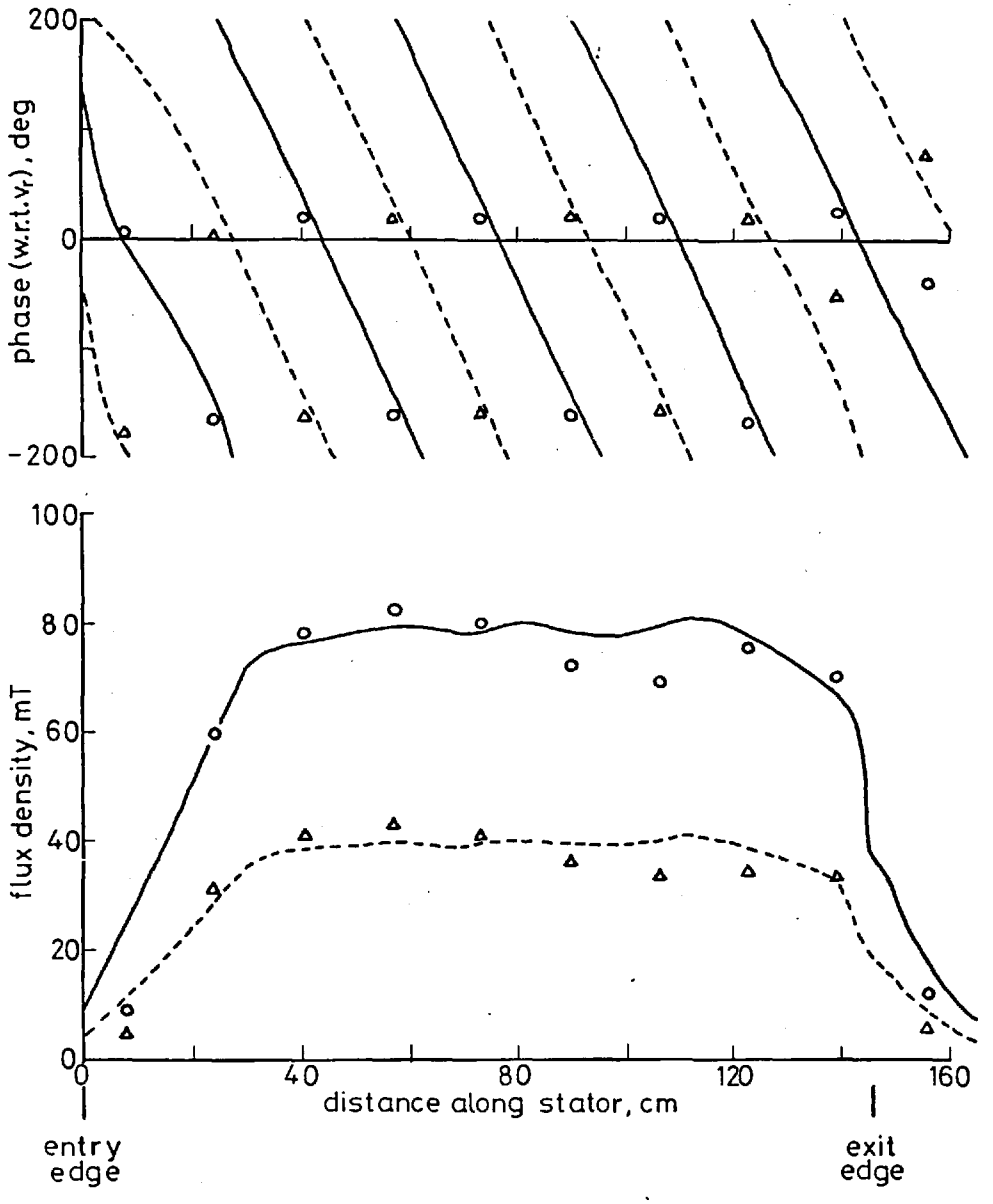

Fig. 2.23.a. Flux density on the 8-pole setting at 0·2 slip with solid iron in the secondary

——— o o o calculated / measured } parallel

- - - - - - △ △ △ calculated / measured } series

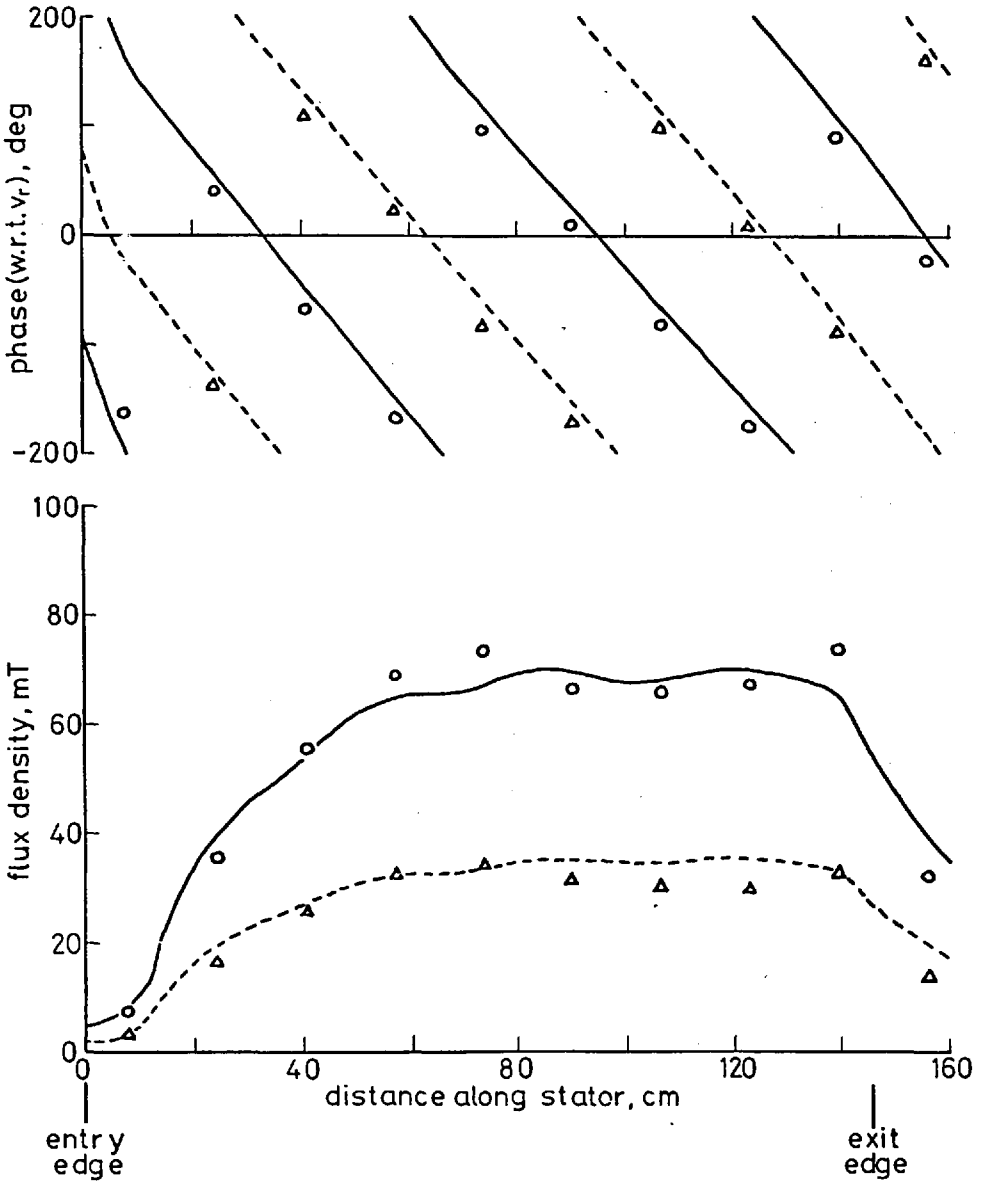

Fig. 2.23.b. Flux density on the 4-pole setting at 0·2 slip with solid iron in the secondary

——— calculated } parallel
o o o measured }

------ calculated } series
Δ Δ Δ measured }

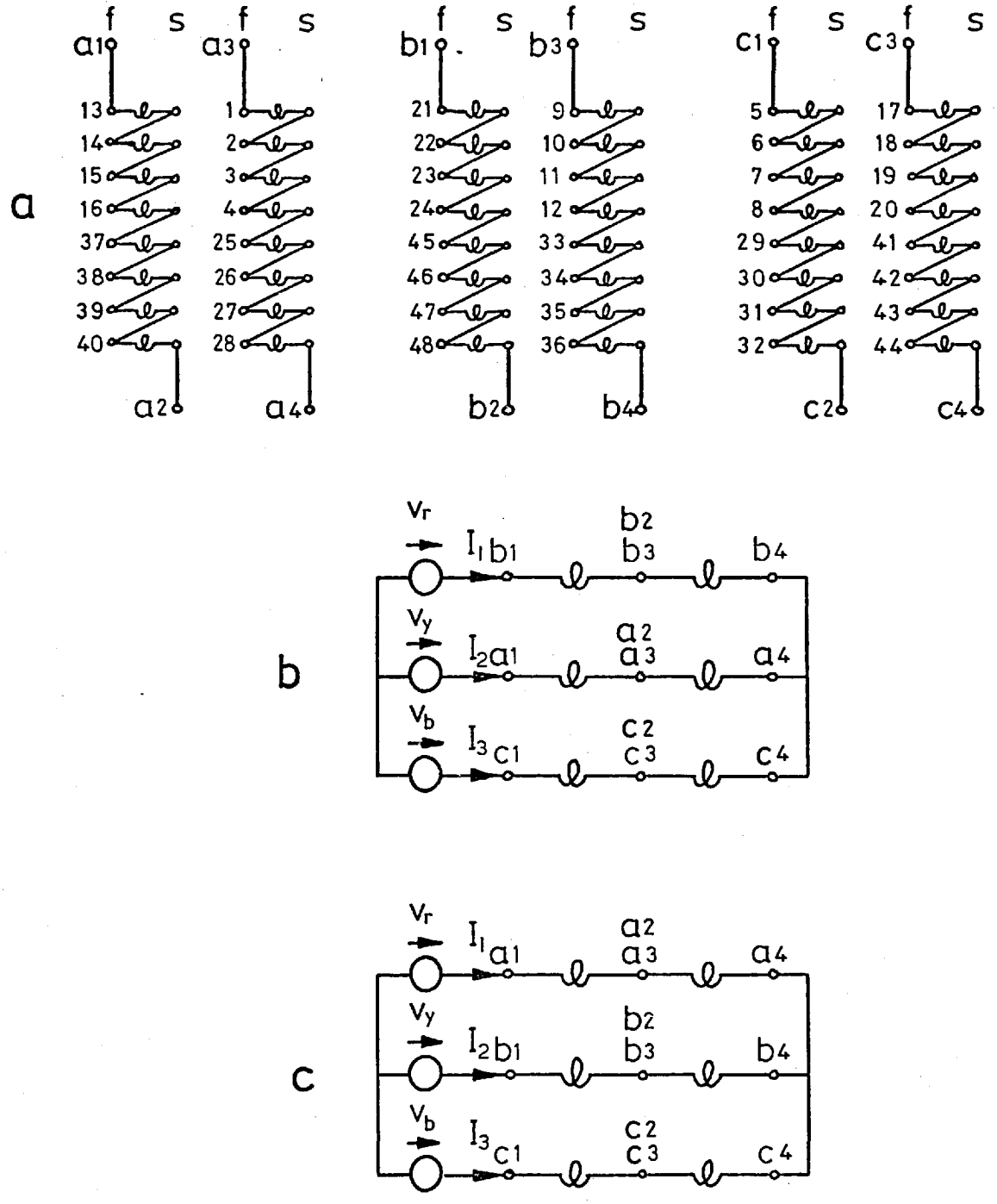

Fig. 2.24 Series connections for the experimental machine

a) coil groups
b) 8-pole connection
c) 4-pole connection

(and overall machine) performance to be fully tested. This section amplifies the previous discussion and illustrates some of the processes involved in the design of windings giving speed ratios of other than two to one[2.1-2.3]. The basic technique, with some improvements, will be illustrated by considering the design of a six to eight pole winding.

Synthesis of a two-speed winding begins with an n-pole "carrier-wave" where n is the arithmetic mean of the two required pole-numbers (Figure 2.25(a)). The carrier wave is divided into a number of blocks, this number being the difference between the two required pole-numbers. A progressively increasing phase shift of m $\pi/2$ is applied to each block where m is the block number and m = 0 for the first block. This process yields the six-pole setting shown in Figure 2.25(b). Application of a similar modulation of - m $\pi/2$ to each block gives the eight-pole setting of Figure 2.25(c). The blocks required to form the two pole numbers can now be synthesised from two waves, one in phase (P) and one in quadrature (Q) with the carrier wave as Table 2.2 shows.

The P and Q waves are physically realisable with conventional three-phase windings. Fig. 2.26 shows the top layers of windings, each in 84 slots, that give two seven pole waves in space quadrature. If the number of slots per pole and phase is not an integer, then a fractional slot winding is required.

The appropriate sections of the windings in Figure 2.26 may be taken, according to Table 2.2, to give a basic six to eight pole arrangement. Distribution factors for these windings are given in Table 2.3.

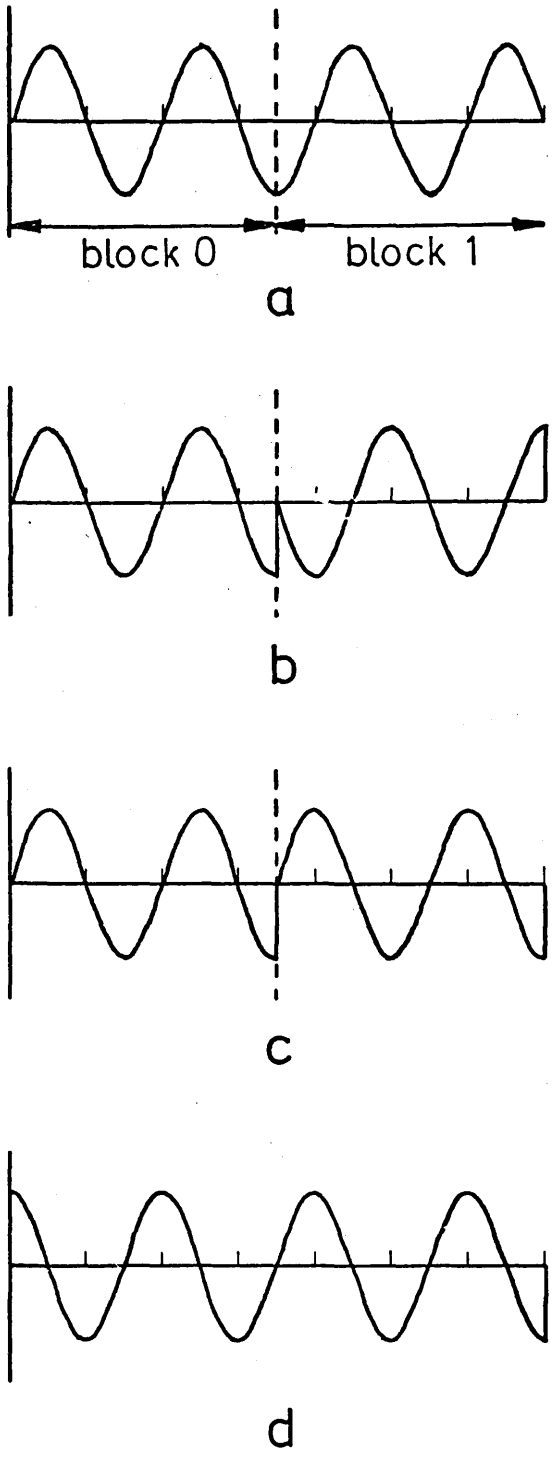

Fig. 2.25 Development of a 6 to 8-pole phase-modulated winding

a) carrier and space phase wave
b) 6-pole setting
c) 8-pole setting
d) space quadrature wave

POLES \ BLOCK NUMBER	0	1
8	P	Q
6	P	$\bar{Q}$

TABLE 2.2 Choice of winding blocks to give the 6 and 8 pole settings

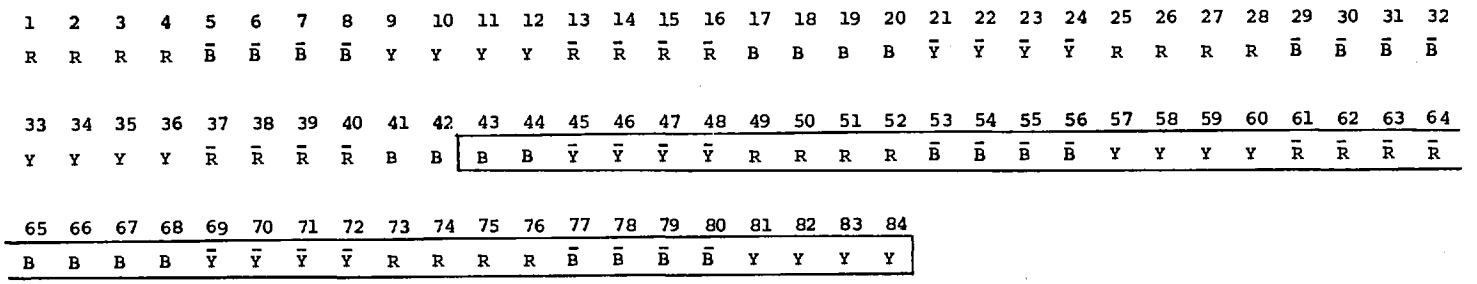

a) P-winding

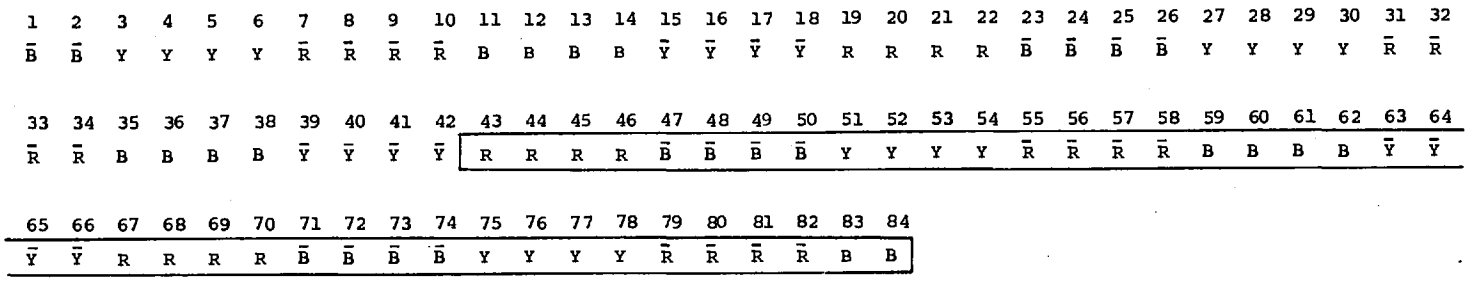

b) Q-winding

Fig. 2.26. P and Q windings for a basic 6 to 8-pole layout

6-pole setting				8-pole setting			
Poles	k_{df}	k_{db}	k_{dz}	Poles	k_{df}	k_{db}	k_{dz}
2	0.175	0.099	0.048	4	0.290	0.082	0.050
6	0.865	0.070	0.053	**8**	0.860	0.061	0.057
10	0.286	0.055	0.064	12	0.171	0.050	0.074
14	0.122	0.046	0.092	16	0.095	0.043	0.125
18	0.077	0.041	0.202	20	0.065	0.039	0.593

Table 2.3 Distribution factors for the 'basic' phase-modulated winding

Each winding produces high distribution factors on the required pole numbers but also large forward travelling harmonics at ten and twelve poles. These unwanted harmonics can be reduced by a judicious choice of coil-span. Table 2.4 shows the winding factors obtainable with different coil pitches. In the eight-pole case the harmonic content appears more favourable, but in the six-pole case there is still a large ten-pole component. Table 2.4 also shows the presence of backward and zero sequence components on the wanted pole numbers. This implies a supply current unbalance and the possibility that delta connections may be precluded.

The overall harmonic content of step phase-modulated windings may be further reduced by an "overlapping" technique first described in reference 2.3. A second identical winding is placed below the first with the edges of corresponding blocks displaced from each other. The effect of the second winding is analogous to that of the second conductor layer in a conventional winding. Abrupt changes between blocks are reduced and the result is a lower harmonic content for the complete winding. For the current example a displacement of 1.5 poles on the carrier wave (i.e. 18 slots) was chosen. In order to retain a two-layer construction, blocks must be interleaved where they overlap. Figure 2.27 shows the top layers of the overlapped six and eight-pole windings. The corresponding distribution and winding factors of Tables 2.5 and 2.6 show a significant drop in the overall harmonic content of the winding but only a small drop in the backward and zero components on the wanted pole number.

6-pole setting

Coil Pitch (slots)	9			10			11			12			13			14		
Poles	k_{wf}	k_{wb}	k_{wz}	k_{wf}	k_{wb}	k_{wz}	k_{wf}	k_{wb}	k_{wz}	k_{wf}	k_{wb}	k_{wz}	k_{wf}	k_{wb}	k_{wz}	k_{wf}	k_{wb}	k_{wz}
2	0.058	0.033	0.016	0.064	0.036	0.018	0.070	0.040	0.019	0.076	0.043	0.021	0.082	0.046	0.022	0.088	0.049	0.024
6	0.732	0.059	0.044	0.779	0.063	0.047	0.816	0.066	0.050	0.843	0.068	0.051	0.859	0.069	0.052	0.865	0.070	0.053
10	0.284	0.055	0.063	0.273	0.053	0.061	0.253	0.049	0.056	0.223	0.043	0.050	0.186	0.036	0.042	0.143	0.027	0.032
14	0.086	0.033	0.065	0.061	0.023	0.046	0.032	0.012	0.024	-	-	-	0.032	0.012	0.024	0.061	0.023	0.046
18	0.009	0.005	0.023	0.017	0.009	0.045	0.041	0.022	0.107	0.060	0.032	0.158	0.073	0.038	0.191	0.077	0.041	0.202

8-pole setting

Coil Pitch (slots)	9			10			11			12			13			14		
Poles	k_{wf}	k_{wb}	k_{wz}	k_{wf}	k_{wb}	k_{wz}	k_{wf}	k_{wb}	k_{wz}	k_{wf}	k_{wb}	k_{wz}	k_{wf}	k_{wb}	k_{wz}	k_{wf}	k_{wb}	k_{wz}
4	0.181	0.051	0.031	0.197	0.056	0.034	0.213	0.060	0.036	0.227	0.064	0.039	0.240	0.068	0.041	0.251	0.071	0.043
8	0.839	0.059	0.056	0.858	0.061	0.057	0.858	0.061	0.057	0.839	0.059	0.056	0.801	0.057	0.053	0.745	0.053	0.049
12	0.154	0.045	0.067	0.134	0.039	0.058	0.107	0.031	0.046	0.074	0.022	0.032	0.038	0.011	0.017	-	-	-
16	0.041	0.019	0.054	0.014	0.006	0.019	0.014	0.006	0.019	0.041	0.019	0.054	0.064	0.029	0.085	0.082	0.037	0.108
20	0.015	0.009	0.132	0.037	0.022	0.334	0.054	0.032	0.490	0.064	0.038	0.578	0.065	0.038	0.587	0.057	0.034	0.514

Table 2.4. Winding factors for the 'basic' phase-modulated winding

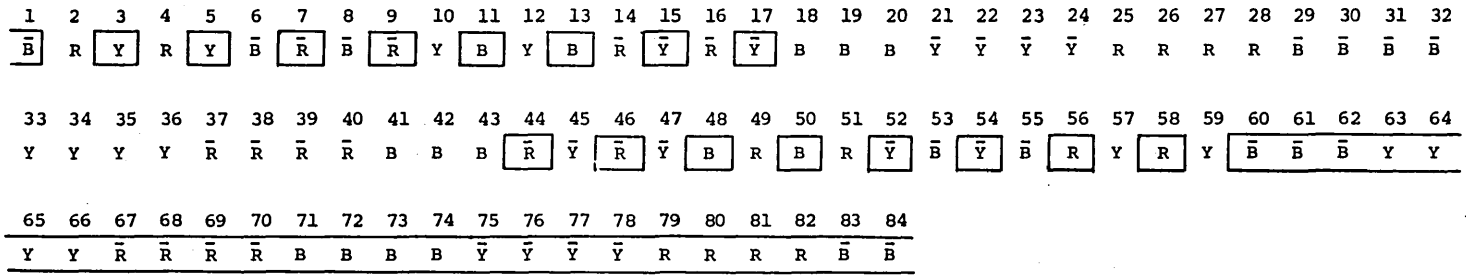

a) 6-pole setting

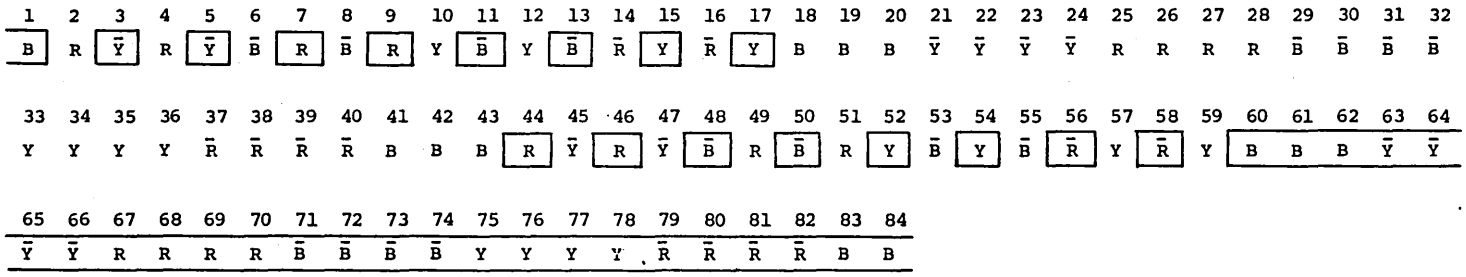

b) 8-pole setting

Fig.2.27. A 6 to 8-pole 'overlapped' winding

6-pole setting				8-pole setting			
Poles	k_{df}	k_{db}	k_{dz}	Poles	k_{df}	k_{db}	k_{dz}
2	0.017	0.096	0.031	4	0.128	0.067	0.022
6	0.788	0.039	0.045	**8**	0.853	0.021	0.036
10	0.204	0.033	0.026	12	0.011	0.051	0.074
14	0.055	0.046	0.092	16	0.094	0.005	0.029
18	0.081	0.005	0.024	20	0.038	0.040	0.498

Table 2.5 Distribution factors for the 'overlapped' phase-modulated winding

6-pole setting

Coil Pitch (slots)	9			10			11			12			13			14		
Poles	k_{wf}	k_{wb}	k_{wz}	k_{wf}	k_{wb}	k_{wz}	k_{wf}	k_{wb}	k_{wz}	k_{wf}	k_{wb}	k_{wz}	k_{wf}	k_{wb}	k_{wz}	k_{wf}	k_{wb}	k_{wz}
2	0.006	0.032	0.010	0.006	0.035	0.011	0.007	0.038	0.013	0.008	0.042	0.014	0.008	0.045	0.015	0.009	0.048	0.016
[6]	0.667	0.033	0.038	0.710	0.035	0.040	0.744	0.037	0.042	0.768	0.038	0.044	0.783	0.039	0.044	0.788	0.039	0.045
10	0.203	0.033	0.026	0.195	0.031	0.025	0.180	0.029	0.023	0.160	0.026	0.020	0.133	0.021	0.017	0.102	0.016	0.013
14	0.039	0.033	0.065	0.028	0.023	0.046	0.014	0.012	0.024	-	-	-	0.014	0.012	0.024	0.028	0.023	0.046
18	0.009	0.001	0.003	0.018	0.001	0.005	0.043	0.003	0.013	0.064	0.004	0.019	0.077	0.005	0.023	0.081	0.005	0.024

8-pole setting

Coil Pitch (slots)	9			10			11			12			13			14		
Poles	k_{wf}	k_{wb}	k_{wz}	k_{wf}	k_{wb}	k_{wz}	k_{wf}	k_{wb}	k_{wz}	k_{wf}	k_{wb}	k_{wz}	k_{wf}	k_{wb}	k_{wz}	k_{wf}	k_{wb}	k_{wz}
4	0.080	0.042	0.013	0.087	0.046	0.015	0.094	0.049	0.016	0.100	0.053	0.017	0.106	0.056	0.018	0.111	0.058	0.019
[8]	0.832	0.021	0.035	0.851	0.021	0.036	0.851	0.021	0.036	0.832	0.021	0.035	0.794	0.020	0.033	0.739	0.018	0.031
12	0.010	0.046	0.067	0.008	0.040	0.058	0.007	0.032	0.046	0.005	0.022	0.032	0.002	0.011	0.017	-	-	-
16	0.041	0.002	0.013	0.014	0.001	0.004	0.014	0.001	0.004	0.041	0.002	0.013	0.064	0.003	0.020	0.081	0.004	0.025
20	0.008	0.009	0.111	0.021	0.022	0.281	0.031	0.033	0.412	0.037	0.039	0.486	0.038	0.039	0.493	0.033	0.034	0.431

Table 2.6. Winding factors for the 'overlapped' phase-modulated winding

2.5.2 Machine performance

In the previous section the design of two six to eight pole windings was considered. Tables 2.4 and 2.6 show that the ten pole harmonic on the six pole setting is most likely to be detrimental to machine performance. The complete mathematical model of Section 2.3 is now used to determine the acceptability of these windings for a particular machine design.

An outline design was performed for a medium speed traction machine. This machine had an active area 2 m x 30 cm, a track clearance of 10 mm and an aluminium secondary 41.5 cm wide and 4 mm deep. The effects of the ten pole harmonic may be observed by first arranging a conventional winding for six poles in the slots of the machine. This winding is then connected in series with a conventional ten-pole winding located in the same slots, the whole being connected in star and supplied from a balanced three-phase constant voltage source. Being conventional arrangements, these windings have a very low harmonic content except at six and ten poles. The effective slot conductor ratio between these two windings was varied and the resulting force backward to forward sequence current ratio characteristics are shown in Figure 2.28. These curves show that it is desirable to reduce the amplitude of the ten-pole harmonic to something less than 20% of the principal component before the winding can be considered acceptable.

Machines with both "basic" and "overlap" versions of the six to eight-pole winding were tested using the complete mathematical model of the machine. The results of the calculations, using a coil pitch of twelve slots, are shown in Figure 2.29. Both windings give adequate

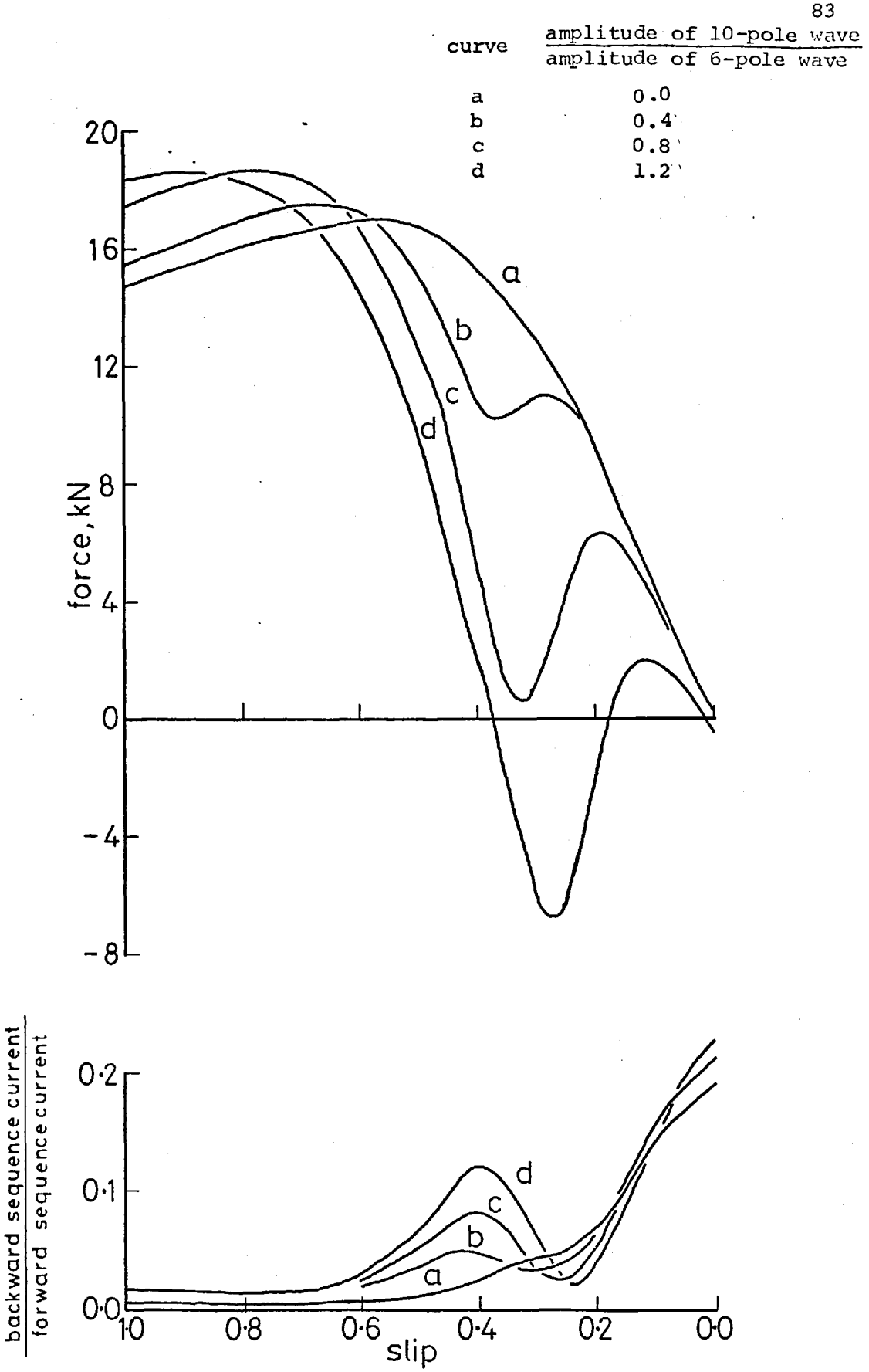

Fig. 2.28 Effect of a 10-pole sub-harmonic winding on a 6-pole principal

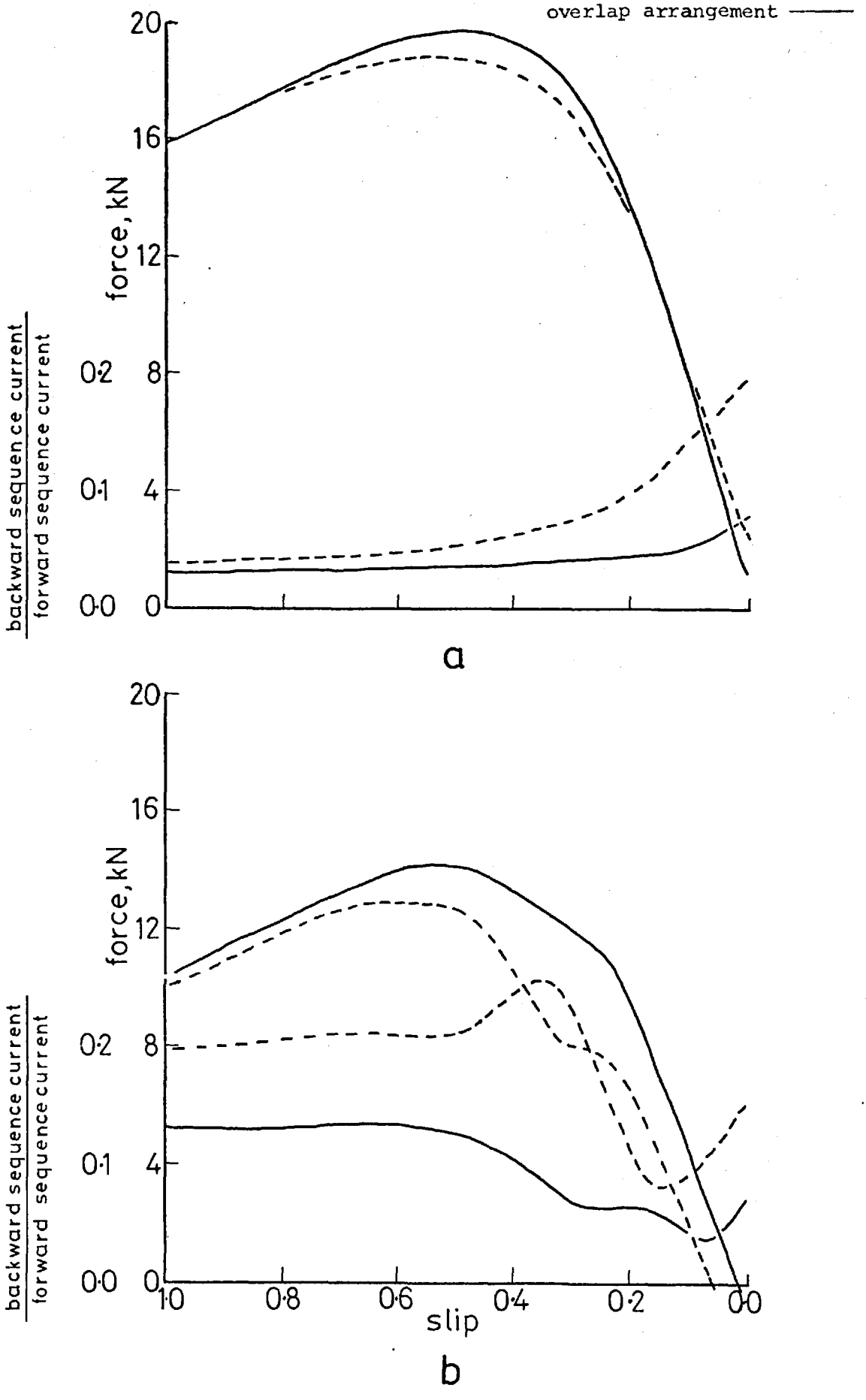

Fig. 2.29 Machine performance using basic and overlapped winding arrangements

a) 8-pole setting
b) 6-pole setting

performance on the eight-pole setting. On the six-pole setting the performance of the "overlap" winding is adequate. The performance of the basic arrangement is considerably degraded due to the presence of the ten-pole harmonic. This manifests itself by producing current unbalance and a considerable depression in the force/speed curve.

2.6 Conclusions

The induction machine is essentially a single speed device. Pole-change windings provide a means by which a number of efficient running speeds can be obtained when using a supply of fixed frequency.

Conventional forms of series connected winding can be employed without modification in low speed linear machine designs. Machines designed for high speed working present a large end-winding to core width ratio as a result of the longer pole-pitches required. The use of very short-pitched coils enables end-winding overhang (and hence stator leakage reactance) to be reduced at the expense of increasing the winding harmonic content. A simple analysis has been presented that gives the harmonic distribution of any winding. This enables identification of those winding harmonics that may adversely affect the machine performance.

Sole use of series connected windings restricts the number of choices open to the designer. Conventional machine designs employ a variety of coil groupings to enable changes in effective applied voltage and reduction of the number of control switch contacts to be made. Because of the non-uniform nature of the flux distribution in a linear machine, direct parallel connection of coil groups is not possible.

In this chapter a novel double winding has been described that makes possible parallel connections. The technique gives some reduction in the number of switch contacts required over equivalent series connections.

Incorporation of closed paths within a linear machine winding demands a more sophisticated model than those currently in use. A new machine winding model has been developed that is applicable to any general design and that makes no prior assumptions about current magnitudes or methods of connection. The currents flowing in linear machine windings are very dependent on leakage reactance, the calculation of which is always approximate. Other uncertainties are introduced by the curvature of the machine and finite width effects. However, even with these shortcomings the complete machine mathematical model has proved reasonably accurate in its predictions of phase and parallel path currents and also of forces and flux densities.

The new parallel connection technique was tested on a linear machine having a winding designed to produce either eight or four poles. It was found that despite considerable flux distortion on the four-pole setting, the circulating current component within the parallel paths was small at all speeds. Also, the overall performance was comparable to that of an equivalent series connected machine. Although the tests were performed on a relatively small machine, it is expected that similar results will be obtained for most designs intended for traction applications. It is unlikely that machines of this type will have fewer than four poles or a slot pitch greater than 3.0 $cm^{2.9}$. The difference in flux linked by two coil groups displaced by this amount will be small even at high speeds in a well coupled machine.

A design process for linear machine windings has been outlined. The harmonic content of trial designs may be examined using a simple analysis technique. When an acceptable layout is achieved the complete model may be used to check overall machine performance and that individual coil group currents are as required.

At present most linear machine development for traction applications is concerned with producing acceptable motoring characteristics. Since mechanical brakes are ineffective at high speeds and wasteful of energy, it is felt that the various braking regimes require some attention. The complete mathematical model developed in this chapter can be used directly for this work when alternating currents are applied to the machine windings. A simple coordinate transformation is required to adapt the model for direct current excitation.

The "network" approach chosen for the complete model makes it easily adaptable for simulating conditions when other electrical components (such as capacitors) are connected to machine windings. Also, since the model is applicable to any general conductor distribution, it is hoped to check the performance of machines employing graded windings and other entry-edge compensation techniques.

2.7 Appendices

2.7.1 Calculation of harmonic winding factors

(a) Surface conductor distribution

The periodic function representing the surface distribution of conductors on a stator surface may be expressed in Fourier Series form as:

$$n = \sum_{r=-\infty}^{\infty} C_r e^{jr\theta} \qquad \text{(A.2.1a)}$$

where θ is measured in radians and

$$C_r = \frac{1}{2\pi} \int_0^{2\pi} n\, e^{-jr\theta}\, d\theta \qquad \text{(A.2.1b)}$$

For the coil side shown in Figure 2.13 the coefficient of equation (A.2.1b) becomes

$$C'_r = \frac{N_s}{2\pi} \frac{\sin(r\delta')}{r\delta'} e^{-jr\theta_s} \qquad \text{(A.2.2)}$$

where θ_s is the slot angle and δ' is in radians.
Since the distribution of conductors across the slot opening is of no direct interest in this case it may be assumed that $\delta' \to 0$. Under this condition $\frac{\sin(r\delta')}{r\delta'} \to 1$.
An expression similar to (A.2.2) applies for all the coil sides of the red phase in the top layer of the winding. The Fourier coefficient representing all these coil sides is therefore

$$C_{rR} = \sum_{s=1}^{Q} \frac{N_{sR}}{2\pi} e^{-jr\theta_{SR}}$$

which may be written as

$$C_{rR} = \frac{N_{rR}}{2\pi} e^{j\phi_{rR}} \qquad (A.2.3)$$

where $N_{rR} = \left| \sum_{s=1}^{Q} N_{sR} e^{-jr\theta_{sR}} \right|$

The corresponding red phase conductor distribution is given from (A.2.1a) as

$$n_R = \sum_{r=-\infty}^{\infty} C_{rR} e^{jr\theta} \qquad (A.2.4)$$

Since the machine is coil wound n_R is symmetrical about the θ axis so that $C_{OR} = 0$. Equation (A.2.4) may therefore be written as

$$n_R = \sum_{r=1}^{\infty} (C_{rR} e^{jr\theta} + C^{*}_{rR} e^{-jr\theta})$$

or as $$n_{rR} = Re\left[\frac{N_{rR}}{\pi} e^{j(r\theta+\phi_{rR})}\right] \qquad (A.2.5)$$

for the rth harmonic only.

Similar arguments apply to the yellow and blue phases giving

$$n_{rY} = Re\left[\frac{N_{rY}}{\pi} e^{j(r\theta+\phi_{rY})}\right] \qquad (A.2.6)$$

$$n_{rB} = Re\left[\frac{N_{rB}}{\pi} e^{j(r\theta+\phi_{rB})}\right] \qquad (A.2.7)$$

(b) Distribution factors

Using symmetrical components, the three phase windings represented by equations (A.2.5 to A.2.7) may be resolved into balanced "forward", "backward" and "zero" sequence sets of windings. For the forward sequence winding

$$n_{rf} = Re\left[\frac{N_{rf}}{3\pi} e^{j(r\theta+\phi_{rf})}\right] \qquad (A.2.8)$$

where $N_{rf} = |N_{rR} + hN_{rY} + h^2N_{rB}|$

and $h = e^{j\,2\pi/3}$

Similarly for the backward and zero sequence windings

$$n_{rb} = Re\left[\frac{N_{rb}}{3\pi} e^{j(r\theta+\phi_{rb})}\right]$$

$$n_{rz} = Re\left[\frac{N_{rz}}{3\pi} e^{j(r\theta+\phi_{rz})}\right]$$

where

$$N_{rb} = |N_{rR} + h^2N_{rY} + hN_{rB}|$$

$$N_{rz} = |N_{rR} + N_{rY} + N_{rB}|$$

If N is the total number of conductors in the top layer of the winding, the maximum conductor amplitude possible is $N/3\pi$ cond/rad. The amplitude of the forward sequence winding is less than this since the conductors are distributed over a number of spatially separated slots. For the forward sequence then, the harmonic distribution factor may be defined as

$$k_{dfr} = \frac{N_{rf}}{N}$$

and for the backward and zero sequence windings as

$$k_{dbr} = \frac{N_{rb}}{N}$$

$$k_{dzr} = \frac{N_{rz}}{N}$$

(c) Winding factors

The top layer of the winding produces the forward sequence distribution given by equation (A.2.8). A corresponding distribution is produced by the bottom layer that is of opposite sign and displaced by the harmonic coil pitch (i.e. $r\pi\beta$). The nett rth harmonic forward sequence winding is thus given by

$$n_{rfT} = \frac{2N_{rf}}{3\pi} \sin(\frac{r\pi\beta}{2}) j\, e^{-j\, r\pi\beta/2}\, e^{j(r\theta+\phi_{rf})}$$

In this case the maximum possible conductor amplitude is $\frac{2N}{3\pi}$ cond/rad, hence the harmonic winding factor for the forward sequence winding may be defined as

$$k_{wfr} = \frac{N_{rf}}{N} \sin(\frac{r\pi\beta}{2})$$

Similarly for the backward and zero sequence windings

$$k_{wbr} = \frac{N_{rb}}{N} \sin(\frac{r\pi\beta}{2})$$

$$k_{wzr} = \frac{N_{rz}}{N} \sin(\frac{r\pi\beta}{2})$$

2.7.2 Solution of Maxwell's Equations in a moving layer

A reference frame is fixed to the layer of Figure 2.12(a) so that its y-axis coincides with that of the stationary frame shown. Corresponding x and z-axes remain parallel with the origin coinciding at t = 0. A point (x', y', z') in the moving frame appears in the rest frame at (x, y, z), where

$$\begin{aligned} x &= x' \\ y &= y' + vt \\ z &= z' \end{aligned} \qquad \text{(A.2.9)}$$

Using the transformations of equations (A.2.9) a travelling wave $a = A\, e^{j(\omega t - k_r y)}$ in the rest frame becomes $a = A\, e^{j[\omega t - k_r (y' + vt)]}$ in the moving frame assuming that the amplitude is invariant. If the speed of the wave in the fixed frame is $v_{sr} = \frac{\omega}{k_r}$ then "slip" is defined as $s = \frac{v_{sr} - v}{v_{sr}}$ and the wave may be represented by $a = A\, e^{j(s\omega t - k_r y')}$.

Each of the field components shown within the layer in Figure 2.12(a) varies sinusoidally both in time and space, i.e.

$$k = \sqrt{2}\, K\, e^{j(s\omega t - k_r y')}$$

$$e' = \sqrt{2}\, E'\, e^{j(s\omega t - k_r y')}$$

$$b = \sqrt{2}\, B\, e^{j(s\omega t - k_r y')}$$

$$h = \sqrt{2}\, H\, e^{j(s\omega t - k_r y')}$$

The wavelength of each along the y' axis corresponds to that of the rth winding harmonic. Since the layer model is assumed to be infinitely wide in the x' direction variations along this axis are ignored.

In the y'-z' plane (neglecting displacement currents) the condition curl h = k together with $b = \mu_o \mu_z\, h_z$ and $k = \sigma e'$ gives

$$\frac{dH}{dz'} + j \frac{k_r}{\mu_o \mu_z} B = - \sigma E' \qquad \text{(A.2.10)}$$

In the x'-y' plane curl e' $= - \frac{\partial b}{\partial t}$ gives

$$- k_r E' = s\omega B \qquad \text{(A.2.11)}$$

For continuity of flux, div b = 0, and this together with $b_y = \mu_o \mu_y\, h$ gives

$$\frac{dB}{dz'} - j\, k_r\, \mu_o \mu_y\, H = 0 \qquad \text{(A.2.12)}$$

Solving equations (A.2.10-12) for E' gives

$$\frac{d^2E'}{(dz')^2} = \gamma^2 E' \qquad \text{(A.2.13)}$$

where $\gamma^2 = k_r^2 \frac{\mu_y}{\mu_z} + js\omega\mu_o\mu_y\sigma$

The solution of equation (A.2.13) is

$$E' = P \cosh(\gamma z') + Q \sinh(\gamma z') \qquad \text{(A.2.14a)}$$

where P and Q are arbitrary constants.

A corresponding solution for H may be obtained from (A.2.10 and A.2.11) as

$$H = \frac{-\gamma}{js\omega\mu_o\mu_y} [P \sinh(\gamma z') + Q \cosh(\gamma z')] \qquad \text{(A.2.14b)}$$

In order to apply boundary conditions to equations (A.2.14) they must first be transformed to the stationary frame. As H is assumed to be invariant the required relationships are

$$z' = z$$

and $E' = E + vB$

The transformation for E' reduces to

$$E' = sE$$

after substituting from (A.2.11) for B and relating v to the slip.

On the under side of the layer, z = 0, $E = E_L$ and $H = H_L$ so that the transformed versions of equations (A.2.14) become

$$E_L = \frac{P}{s}$$

$$H_L = \frac{-\gamma}{js\omega\mu_o\mu_y} Q$$

At the upper surface $z = S$, $E = E_u$ and $H = H_u$ so that

$$E_u = \frac{1}{s} [P \cosh(\gamma S) + Q \sinh(\gamma S)]$$

$$H_u = \frac{-\gamma}{js\omega\mu_o\mu_y} [P \sinh(\gamma S) + Q \cosh(\gamma S)]$$

Eliminating P and Q gives the final result

$$E_u = E_L \cosh(\gamma S) - Z_o H_L \sinh(\gamma S)$$

$$H_u = -\frac{1}{Z_o} E_L \sinh(\gamma S) + H_L \cosh(\gamma S) \qquad \text{(A.2.15)}$$

where $Z_o = \frac{j\omega\mu_o\mu_y}{\gamma}$

Equations (A.2.15) may be represented by the network model of Figure 2.16(b). A corresponding result for backward travelling fields may be obtained by replacing r with -r in the above analysis.

2.7.3 Calculation of the induced emf in a coil group

The rth harmonic component of the electric field at the winding surface (represented by equation 2.14) is

$$e_r = \sqrt{2} \{ E_{Fr} e^{j(\omega t - k_r y)} + E_{Br} e^{j(\omega t + K_r y)} \}$$

This field excites an instantaneous voltage in the rth harmonic of the νth winding given by

$$n_{r\nu} = C^*_{r\nu} e^{-jk_r y} + C_{r\nu} e^{jk_r y}$$

such that $e'_{T\nu r} = w \int_o^{2k_B P_B} n_{r\nu} e_r \, dy$

When the integral is performed it is found that

$$e'_{T\nu r} = \sqrt{2}\, e_{T\nu r}\, e^{j\omega t}$$

where $e_{T\nu r}$ is given in equation (2.15).

2.7.4 Network solution using the connection matrix technique

When equation (2.17) is abbreviated to

$$[e_T] = -[Z_M][I]$$

equation (2.18) may be written as

$$[e] + [E] = ([Z] + [Z_M])[I] \qquad \text{(A.2.16)}$$

In order to be able to solve equation (A.2.16), a set of independent currents (I') is first chosen. Each of these currents flows on one closed path in the network. The independent currents are related to all the winding currents by:

$$[I] = [S][I'] \qquad \text{(A.2.17)}$$

where [S] is the connection matrix[2.18]. The terminal voltages across each network element sum to zero around each closed path and it is found that

$$[S]^T[E] = [O] \qquad \text{(A.2.18)}$$

Premultiplication of (A.2.16) by $[S]^T$ and substitution of (A.2.17 and 18) gives

$$[S]^T[e] = \{[S]^T([Z] + [Z_M])[S]\}\,[I']$$

Inverting, premultiplying by [S] and applying (A.2.17) yields the solution for all the winding currents given by equation (2.19).

CHAPTER THREE

PERFORMANCE OF LINEAR INDUCTION MACHINES WITH AIR-GAP WINDINGS

3.1 Introduction

In a recent paper[3.1], a method for improving the performance of axial flux linear induction motors was outlined. The essence of the scheme was to incorporate as much as possible of the primary end-windings into the main magnetic circuit of the machine thus reducing the primary leakage reactance.

The simplest way to make use of the coil end-turns is to continue the stator iron and secondary member out over the end-windings of a conventionally wound motor. The thrust developed by a set of parallel conductors lying on a plane iron surface and energised with poly-phase alternating current is normal to the conductor direction and lies in their plane. This means that the resultant thrust due to the two layers of an end-winding will be in the same direction as that developed by the conventionally used centre portion as Figure 3.1 shows.

Other coil geometries are seen to be possible, bearing in mind that conventional end-windings produce thrust in the required direction. The central portion of parallel conductors may be omitted to leave a winding formed of "diamond-shaped" coils in which the conductors are skewed with respect to the direction of motion.

The two arrangements so far described may be laid in slots as usual although the use of non-standard punchings of several different types may be necessary in a single stator block. When a linear motor is correctly designed for high-speed working, it is found that the air-gap flux-density is low. This leads to the use of thin teeth when a slotted construction is used. Also, because of the reduced tooth space available between skewed conductors, it may become impossible

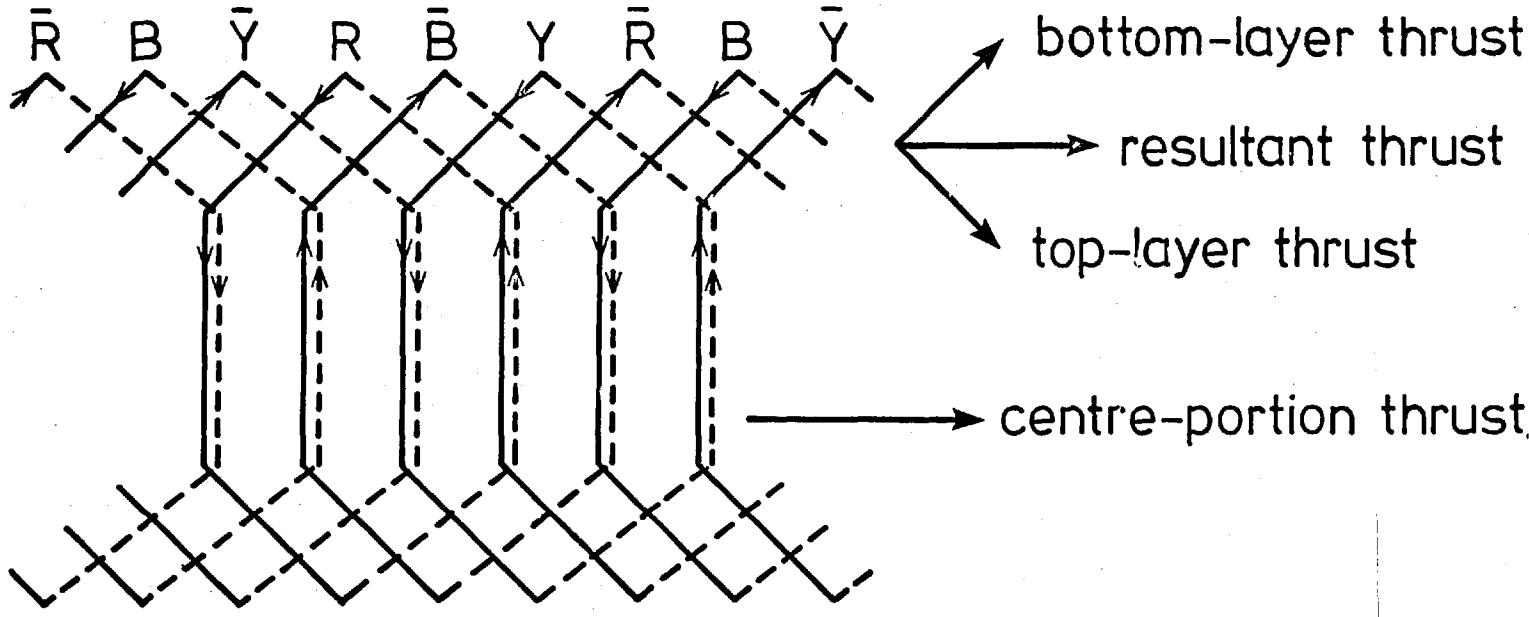

Fig. 3.1 Direction of thrust produced by skewed windings

to incorporate any iron between them. It is therefore of interest to examine the possibilities of eliminating the teeth altogether to produce a winding of the air-gap type.

The effective air-gap seen by an unslotted winding is greater than that seen by conventional types. An increased magnetising current may therefore be the price to be paid for a reduction in leakage reactance in these machines. For the long pole-pitches required on high speed motors fed from the usual 50 Hz mains supply, it is considered likely that the reduction in stator leakage reactance will more than compensate for the increased magnetising current. This implies a higher input power factor than could be obtained with a conventional design.

In this chapter linear machines with both air-gap and conventional windings are examined on the same analytical basis. A common mathematical model is developed that allows competing designs of both types to be compared.

3.2 A model for machines with skewed windings

3.2.1 Introduction

Figure 3.1 shows the most general coil shape for the machines under consideration. The skewed end-winding portions produce two perpendicular components of current density so that a 2-dimensional analysis is required.

A number of 2-dimensional analyses of conventional axial-flux machines have been performed[3.2-3.6] for studying the 'transverse edge-effect'. Bolton's paper[3.2] was addressed to this problem alone.

He modelled the machine windings with a thin sheet of current sinusoidally distributed in the direction of motion and ignored field variations in this direction and in a direction normal to the secondary surface.

A multi-layer model was used in references 3.3-3.6 so that thickness effects could be included. This model consisted of parallel layers of material of uniform thickness and infinite extent. Each layer corresponded to a region in the real machine such as the secondary plate or the air-gap. The machine windings in these models were also represented by current sheets sinusoidally distributed in the direction of motion. These were repeated, alternately positive and negative, in the transverse direction at intervals corresponding to the secondary width thus simulating a number of oppositely connected machines laid side by side. The periodicity introduced in the transverse direction by this device allowed the chosen transverse distributions of current density to be expressed in Fourier Series form in this direction.

Variation of fields in the direction of motion was also examined in reference 3.6 by a similar technique. In this case the total length of the model consisted of an excited portion, corresponding to the machine winding, plus an unexcited portion. The length of the unexcited portion was such that all fields could decay substantially to zero within one model section. Periodicity was introduced by arranging a number of similar sections end to end thus allowing a longitudinal Fourier representation of the current sheet.

The analyses in references 3.2-3.6 were mainly concerned with the prediction of thrust and flux density under the stator block of a conventionally wound linear motor. As a result of this, little attention was paid to the distribution of the current density components in the end-winding region. Also, a sinusoidal distribution of current density in the direction of motion was assumed in each case. This representation is only valid in "current-forced" situations where a balanced series connected winding, with no half-filled end slots, carries a set of balanced phase currents, a situation which is rarely true. The majority of linear motors are operated from constant voltage supplies and may require a number of more complex connections in each phase.

As only conventionally slotted windings have been considered for linear motors, the use of the thin current sheet for representing the winding is adequate. However, in cases where a high degree of tooth saturation is present or there are no teeth at all, any thickness effects due to the winding must be taken into account.

The analysis to be presented in this chapter will be based on the multi-layer model of references 3.3-3.6 using the surface impedance boundary matching technique[3.4,3.6] to simplify the solution. The model excitation will be provided by a double Fourier series winding representation similar to that used in reference 3.6 but suitably modified to take account of the distribution of separate conductor groups and excitation layer thickness effects.

3.2.2 Surface conductor density distribution produced by slotted skewed windings

The machine windings to be considered are formed of a number of series connected coil groups. All the coils have the same pitch 2β. In this section, for the sake of convenience, it is also assumed that the coils are laid in a uniformly slotted iron stator so that the usual current sheet approximation [3.7,3.8] may be used.

Figure 3.2 shows the cth coil of the νth coil group together with its oppositely connected complements required for periodicity along the x-axis. This coil has $N_{c\nu}$ turns. For $-\frac{w}{2} \leq x \leq \frac{w}{2}$ the surface conductor density produced by its two sides may be represented by a Fourier series along the y-axis using the techniques developed in Chapter 2. The amplitude of the rth component of this series is:

$$C''_r = \frac{1}{2k_B P_B} \frac{\sin(k_r\delta)}{k_r\delta} N_{c\nu} \left\{ e^{-jk_r(y_{c\nu}-\beta)} - e^{-jk_r(y_{c\nu}+\beta)} \right\}$$

A similar harmonic amplitude may be obtained for each coil of the νth group. When these are summed over all the coils in the machine the net rth harmonic amplitude of the surface conductor density of the νth coil group is found to be:

$$C_{r\nu} = A_{r\nu} \sin(k_r\beta)$$

where

$$A_{r\nu} = \frac{j}{k_B P_B} \frac{\sin(k_r\delta)}{k_r\delta} \sum_{c=1}^{C} N_{c\nu} e^{-jk_r y_{c\nu}}$$

The same conductor distribution is seen in the region for which $\frac{w}{2} \leq x \leq (\frac{w}{2} + f)$ as was seen in the previous case, but here the coil half-pitch is shortened to

$$\beta' = \frac{\beta}{f}(f + \frac{w}{2} - x)$$

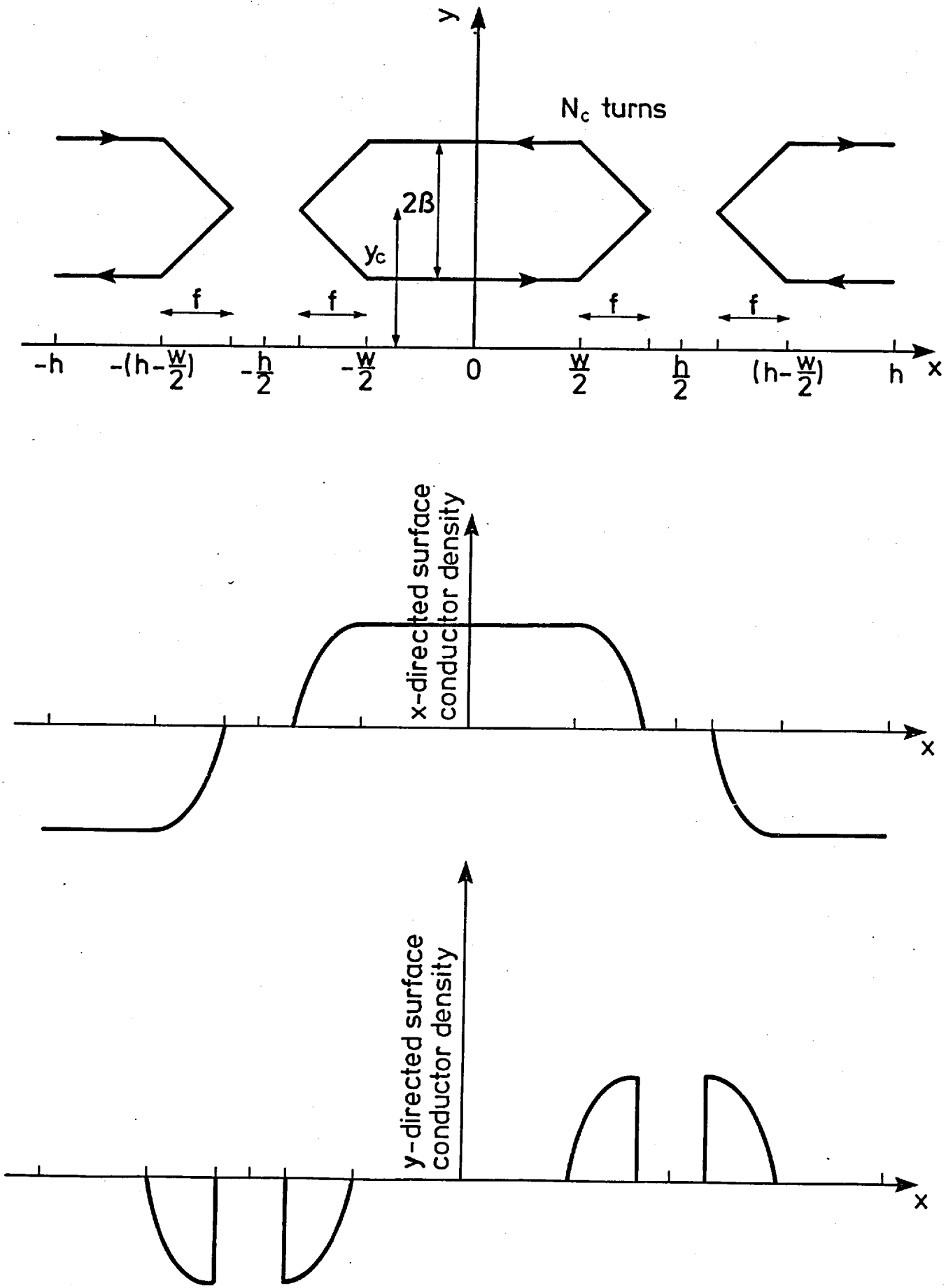

Fig. 3.2 Two-dimensional winding representation

In this case the surface conductor density harmonic amplitude is given by

$$C_{r\nu} = A_{r\nu} \sin(k_r \beta')$$

Similar arguments apply to the corresponding coil sections shown in Figure 3.2. The piecewise function representing $C_{r\nu}$ may be expressed in a Fourier Series along the x-axis such that

$$C_{r\nu} = \sum_{m=1}^{\infty} C_{rm\nu} \cos(k_m x) \qquad (3.1)$$

where the coefficient is given in Appendix 3.6.1.

The complex amplitude $C_{r\nu}$ is contained within the longitudinal Fourier series for the x-directed surface conductor density given by equation (2.10), i.e.

$$n_{\nu x} = \sum_{r=1}^{\infty} \{C^*_{r\nu} e^{-jk_r y} + C_{r\nu} e^{jk_r y}\} \qquad (3.2)$$

When $C_{r\nu}$ is expressed in the transverse series given by equation (3.1) and all the coil groups are considered, the conductor density of equation (3.2) becomes

$$[n_x] = \sum_{r=1}^{\infty} \sum_{m=1}^{\infty} \{[C^*_{rm}]\cos(k_m x) e^{-jk_r y} + [C_{rm}]\cos(k_m x) e^{jk_r y}\} \qquad (3.3)$$

where the column vectors are of length ρ.

A set of currents $[i] = \mathrm{Re}\{\sqrt{2}[I]e^{j\omega t}\}$ applied to the coil groups produces a total surface current density distribution of

$$j_x = [n_x]^T [i] \qquad (3.4)$$

Substitution of equation (3.3) into (3.4) allows forward and backward travelling waves of current density to be identified with complex harmonic RMS amplitudes of

$$J_{xFrm} = [C^{*}_{rm}]^{T}[I] \qquad J_{xBrm} = [C_{rm}]^{T}[I] \qquad (3.5a)$$

Continuity of current within a surface winding is expressed in field form by div k = 0. To satisfy this condition the y-directed components of surface current density must be

$$J_{yFrm} = j\frac{k_m}{k_r}J_{xFrm} \qquad J_{yBrm} = -j\frac{k_m}{k_r}J_{xBrm} \qquad (3.5b)$$

3.2.3 Current density in a skewed air-gap winding

Many field-type analyses of electrical machine structures assume that windings may be represented by infinitely thin sheets of current. This assumption is valid only if the coils are placed in slots in iron, since most of the mmf of the coil sides appears across the slot openings[3.7,3.8]. The mmf distribution may then be considered as having been produced by a surface current at the level of the slot tops and resting on smooth iron. When machines possess air-gap windings the conditions for analysis using a thin current sheet are not directly applicable. In this section a model is developed that is used to represent windings in which thickness effects are apparent.

The windings considered are assumed to be stationary, of uniform depth and formed of many transposed thin conductors connected in series. These conditions imply an absence of skin-effect and define a layer in which a uniform constant current density exists over the whole of its depth.

When depth ℓ of the winding is considered the current density may be defined such that

$$k_x = j_x/\ell$$

where j_x is given by equation (3.4). The layer is of infinite extent in the x-y plane and of constant permeability. It is also assumed that the effects of displacement currents are negligible and that div k = 0 applies. As in the previous section, harmonic forward and backward travelling waves of current density may be identified such that

$$k_{xFrm} = \sqrt{2}\, K_{xFrm} \cos(k_m x)\, e^{j(\omega t - k_r y)} \qquad (3.6a)$$

$$k_{xBrm} = \sqrt{2}\, K_{xBrm} \cos(k_m x)\, e^{j(\omega t - k_r y)} \qquad (3.6b)$$

where $K_{xFrm} = \frac{1}{\ell} [C^*_{rm}]^T [I]$ $\qquad$ $K_{xBrm} = \frac{1}{\ell} [C_{rm}]^T [I]$

Figure 3.3(a) shows the field components considered for the analysis outlined in Appendix 3.6.2. A solution of Maxwell's equations is obtained that relates the electric and magnetic field strengths at the upper surface of the layer (E_{xyu},H_{yu}) to the corresponding quantities at the lower surface. The equations may be represented by a "T" section of transmission line with an added current source as shown in Figure 3.3(b) where

$$J'_x \text{ corresponds to } J'_{xFrm} = K_{xFrm} \frac{\sinh(\gamma_{rm}\ell)}{\gamma_{rm}}$$

$$\text{or } J'_{xBrm} = K_{xBrm} \frac{\sinh(\gamma_{rm}\ell)}{\gamma_{rm}}$$

This result is interesting for it shows that the current density distribution may be replaced by a surface current sheet of the type described in the previous section lying at an appropriate level within the layer. The surface conductor distribution of equation (3.3) is modified to become

$$[n_x] = \sum_{r=1}^{\infty} \sum_{m=1}^{\infty} \left\{ [C'^*_{rm}] \cos(k_m x)\, e^{-jk_r y} + [C'_{rm}] \cos(k_m x)\, e^{jk_r y} \right\}$$

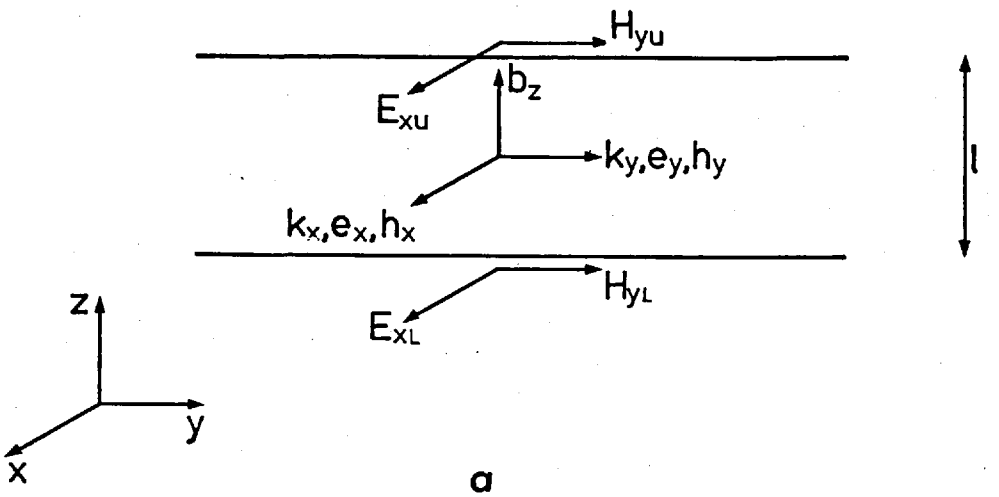

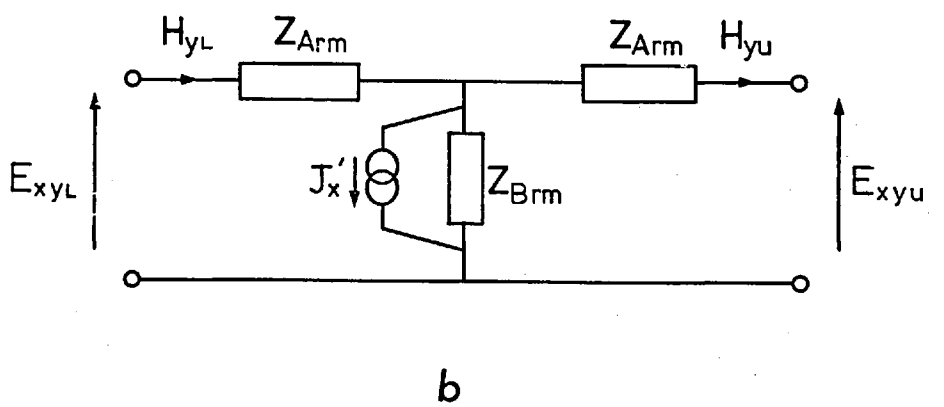

Fig. 3.3 Winding layer mathematical model

a) Field components

b) Network representation

where the harmonic conductor density is now multiplied by a "winding depth factor" such that

$$[C'_{rm}] = \frac{\sinh(\gamma_{rm}\ell)}{\gamma_{rm}\ell}\,[C_{rm}]$$

3.2.4 Calculation of machine terminal quantities

So far only the representation of the machine windings has been considered. The rest of the machine is modelled using layers as shown in Figure 3.4. Each of the layers is represented by the network model[3.4,3.6] described in Appendix 3.6.3. Provision has been made to accommodate slotted regions in the model by the use of different permeabilities in each coordinate direction. The layer considered in the Appendix is of uniform depth in the z-direction, infinite extent in the x-y plane and travels with constant velocity parallel to the y-axis. It is assumed that displacement currents may be neglected and that the material forming the layer may be adequately described by constant values of permeability and resistivity. Values of permeability for slotted regions may be obtained from the simple magnetic circuits employed by Greig and Freeman[3.9]. In order to simplify the solution of the field equations it is also assumed that no currents flow in the z-direction, i.e. $\sigma_z = 0$.

The complete layer model network is excited either by a current sheet or the winding layer model of Appendix 3.6.2. Both winding models possess sources that represent currents flowing in a surface conductor sheet. This means that the evaluation of terminal quantities for a "thick layer" winding is the same as for the more usual "current sheet" winding except that use must be made of the depth factor of Section 3.2.3.

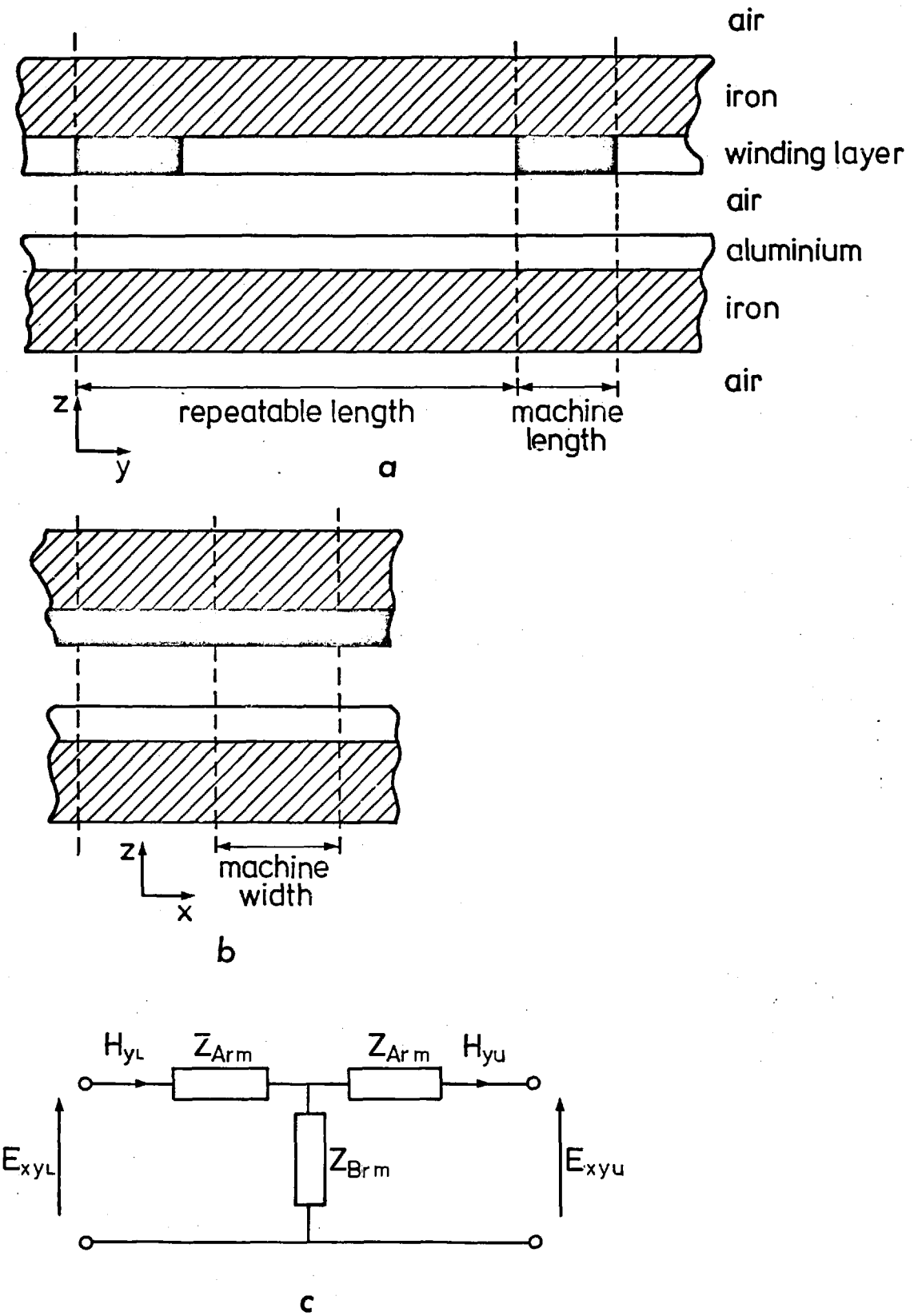

Fig. 3.4 Machine mathematical model

a) View in z-y plane

b) View in z-x plane

c) Network representation for one layer

In Appendix 3.6.4 the flow of VA into the layer model is used to derive equation (A.3.4) which gives the induced emf in each coil group. These emf sources are included in network branches together with the winding resistances and leakage reactances. The entire network is then solved for the coil group currents given the supply voltages and inter-connections in the manner described in Chapter 2.

Once the winding currents are known, the thrust is calculated by evaluating the loss in the layer model as is shown in Appendix 3.6.5.

Appendix 3.6.5 also shows how the z-directed component of the flux density distribution on the rotor surface is calculated. The flux density is also evaluated at the exit edge and the retarding force given in formula (2.20) is numerically integrated over this distribution to give the force required for "exit-edge correction" in the 2-dimensional case.

3.3 Experimental verification of the machine model

3.3.1 Air-gap flux density due to a skewed winding

In order to verify the 2-dimensional winding model, a static test was performed using a machine with no conducting material in the secondary member.

The stator of the test machine was constructed with 60 diamond shaped coils of the type shown in Fig. 3.5. Each coil had a pitch of 30.5 cm at the centre and was bonded to a laminated iron core 30.5 cm wide so forming a 2 cm thick air-gap winding. The coils were connected to form a conventional 3-phase winding with 4 poles of 30.5 cm pitch.

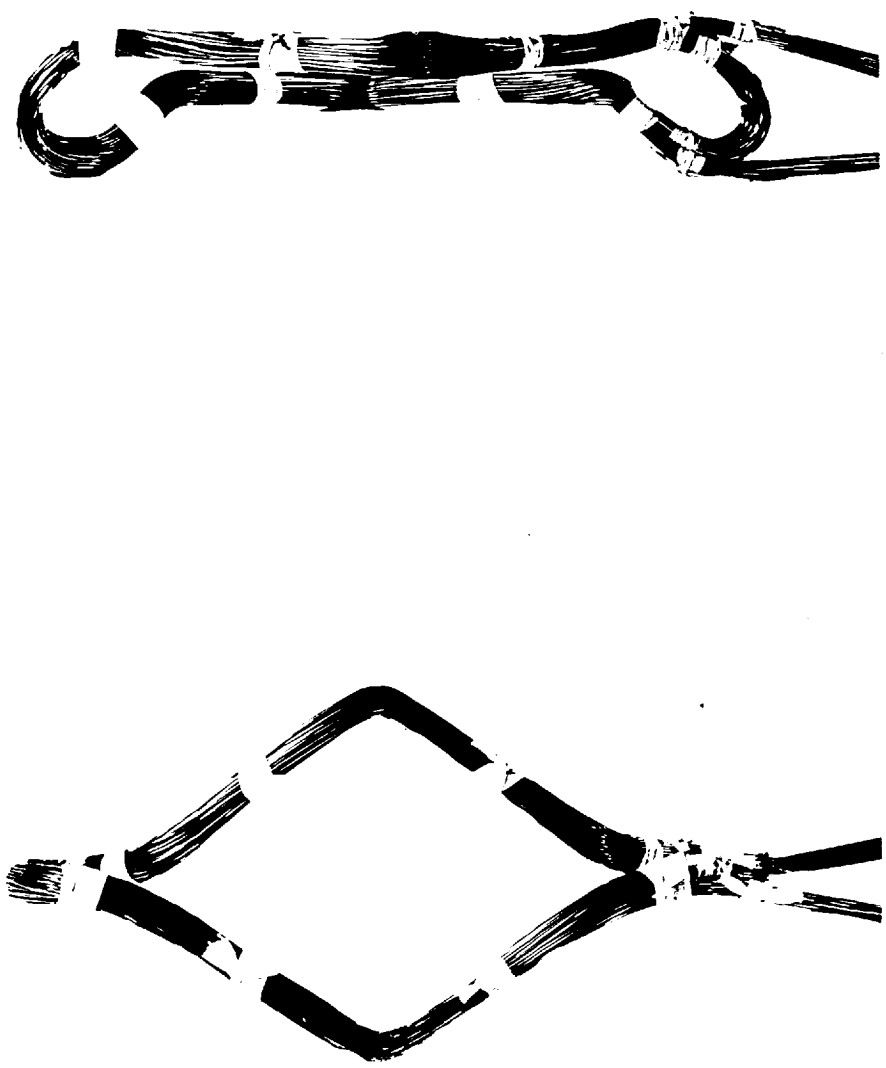

Fig.3.5. Coil used in skewed windings

The magnetic circuit was completed with a similar laminated core being fixed above the first leaving a 2.2 cm clearance to the surface of the winding layer.

Search-coil measurements of the flux-density normal to the air-gap surfaces were made on a plane lying at 0.95 cm from the winding. Figure 3.6 shows the measured and calculated distributions of the flux-density along the longitudinal and transverse centre-lines of the machine with a supply of 20 V phase at 50 Hz.

The calculated distributions were obtained after setting the conductor regions in Figure 3.2 corresponding to $-\frac{w}{2} \leqslant x \leqslant \frac{w}{2}$ to zero. Measured values of winding resistance were used and any leakage reactance due to the circular parts of the coils lying outside the primary stack (i.e. the coil "noses") was ignored.

3.3.2 Dynamic tests

To verify the complete model, a set of dynamic tests were performed using the disc apparatus described in Chapter 2. A test motor (shown in Figure 3.7) was constructed with the following dimensions:

Mean core length	1.46 m
Core width	15.9 cm
Core depth	6.0 cm
Winding layer depth	2.5 cm
Number of full coils	96
Coil pitch (at centre)	11.5 cm
Turns/coil	8

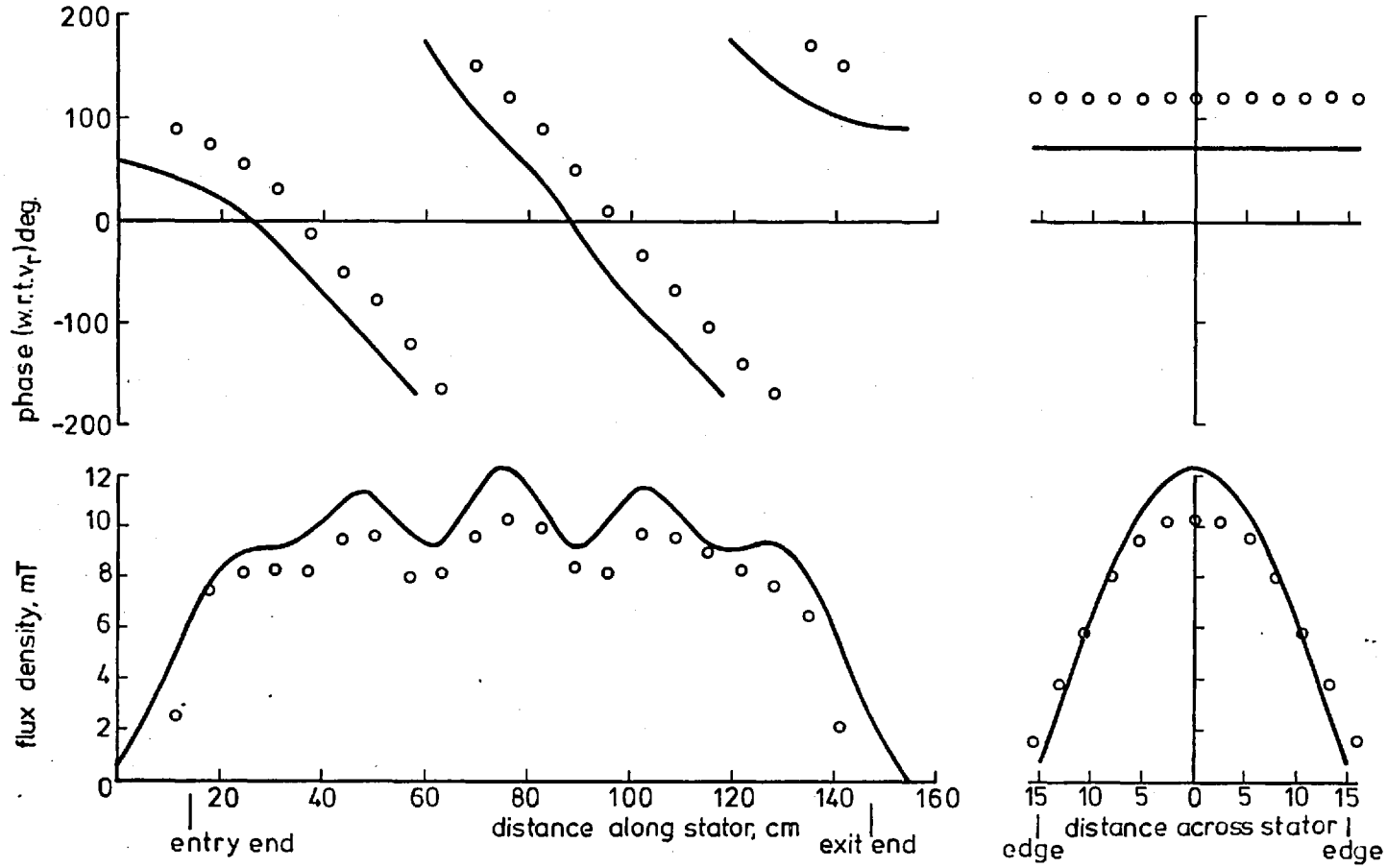

Fig.3.6. Air-gap flux density produced by a skewed winding

o o o measured
—— calculated

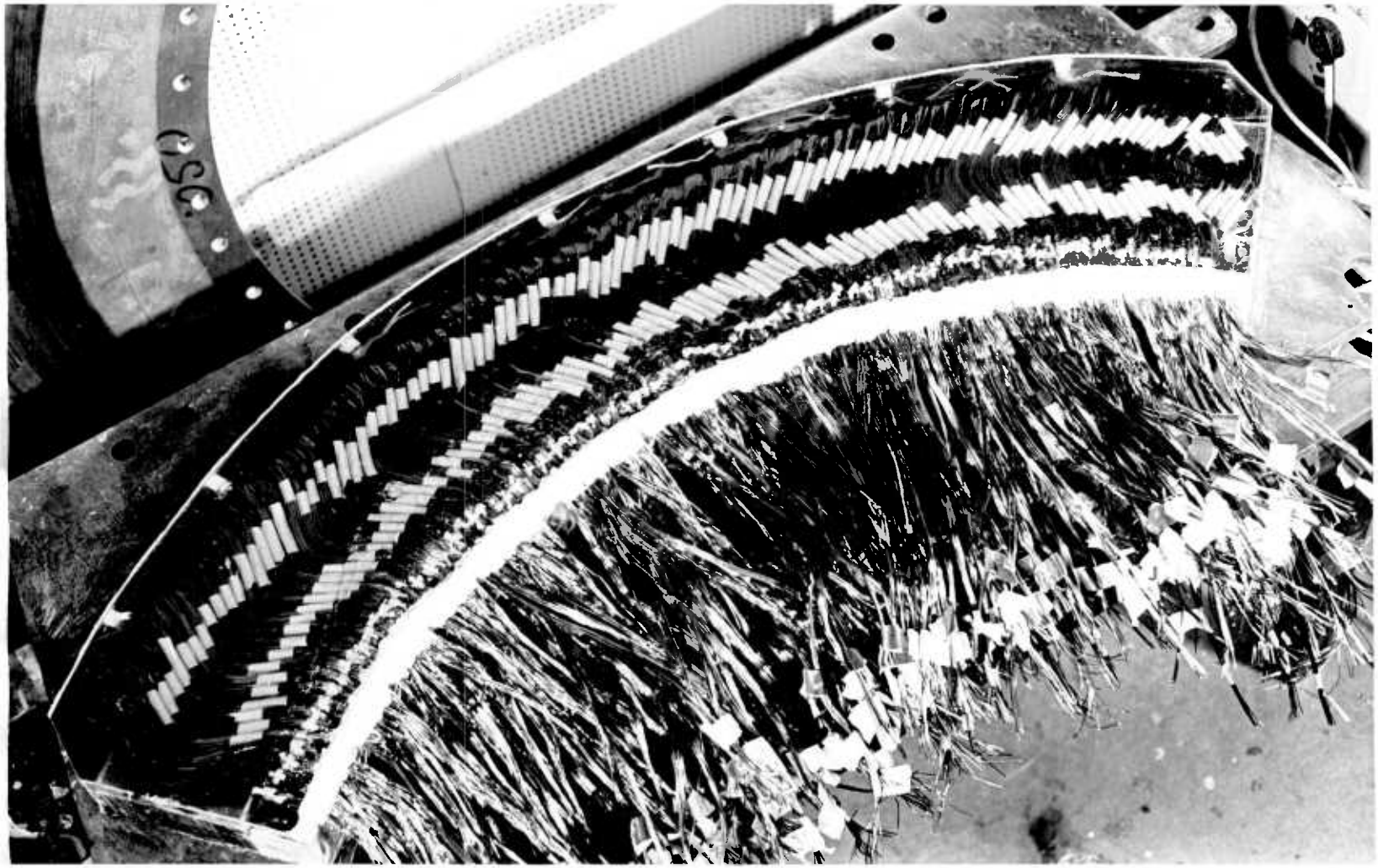

Fig.3.7. Stator with skewed air-gap winding

The coils were connected as shown in Figure 3.8 to form a three-phase star connected winding with twelve poles of pitch 11.1 cm. Each phase contained two parallel paths and was designed using the technique detailed in Section 2.2.4. Being a fractional slot winding, a number of "half coils" were required in order to arrange each parallel group with the same number of conductors.

The secondary member consisted of an unlaminated mild steel annulus 2 cm thick faced with a 1.6 mm layer of aluminium giving an effective width of 22.9 cm.

Figure 3.9 shows the measured and predicted curves of phase currents and power factors, parallel path currents and the thrust force with a supply of 20 V phase at 100 Hz. Figure 3.10 shows corresponding curves of normal flux density on the rotor surfaces at points along the longitudinal and transverse centre-lines of the stator at slips of 1.0 and 0.2.

As in the static tests, the calculations were performed after setting the regions corresponding to $-\frac{w}{2} \leqslant x \leqslant \frac{w}{2}$ in Figure 3.2 to zero. Measured values for the coil group resistances were used and the coil "nose" leakage was ignored.

To check the analysis against a conventional slotted structure, the performance of the 4-pole series connected machine of Section 2.4.2 was recalculated. Figures 3.11, 3.12 and 3.13 show the phase currents and power factors, thrust and flux density together with the predictions from the 1-dimensional analysis. A considerable increase in accuracy is apparent over the 1-dimensional calculations with the transverse edge effect[3.2,3.3,3.6] also being displayed.

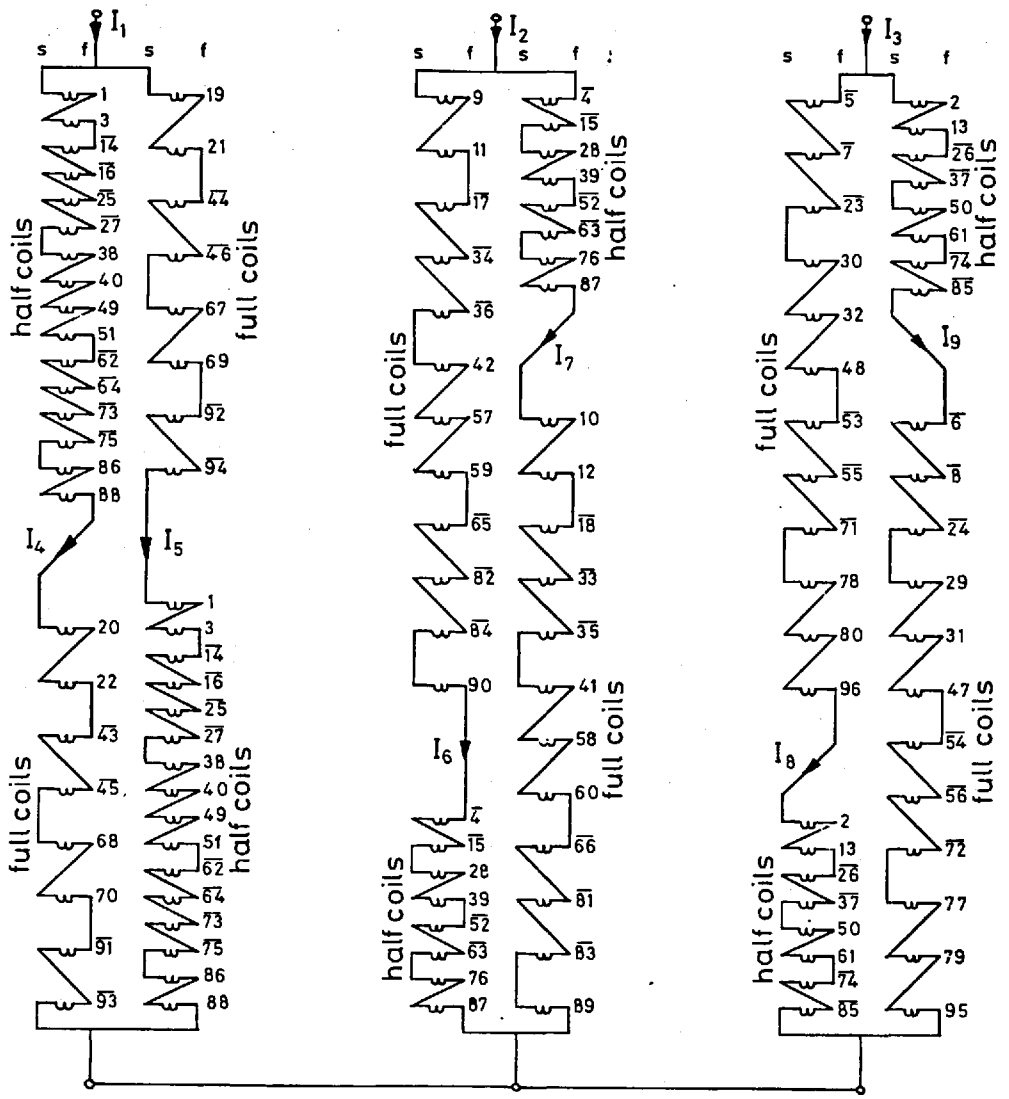

Fig.3.8. Winding connections for dynamic tests

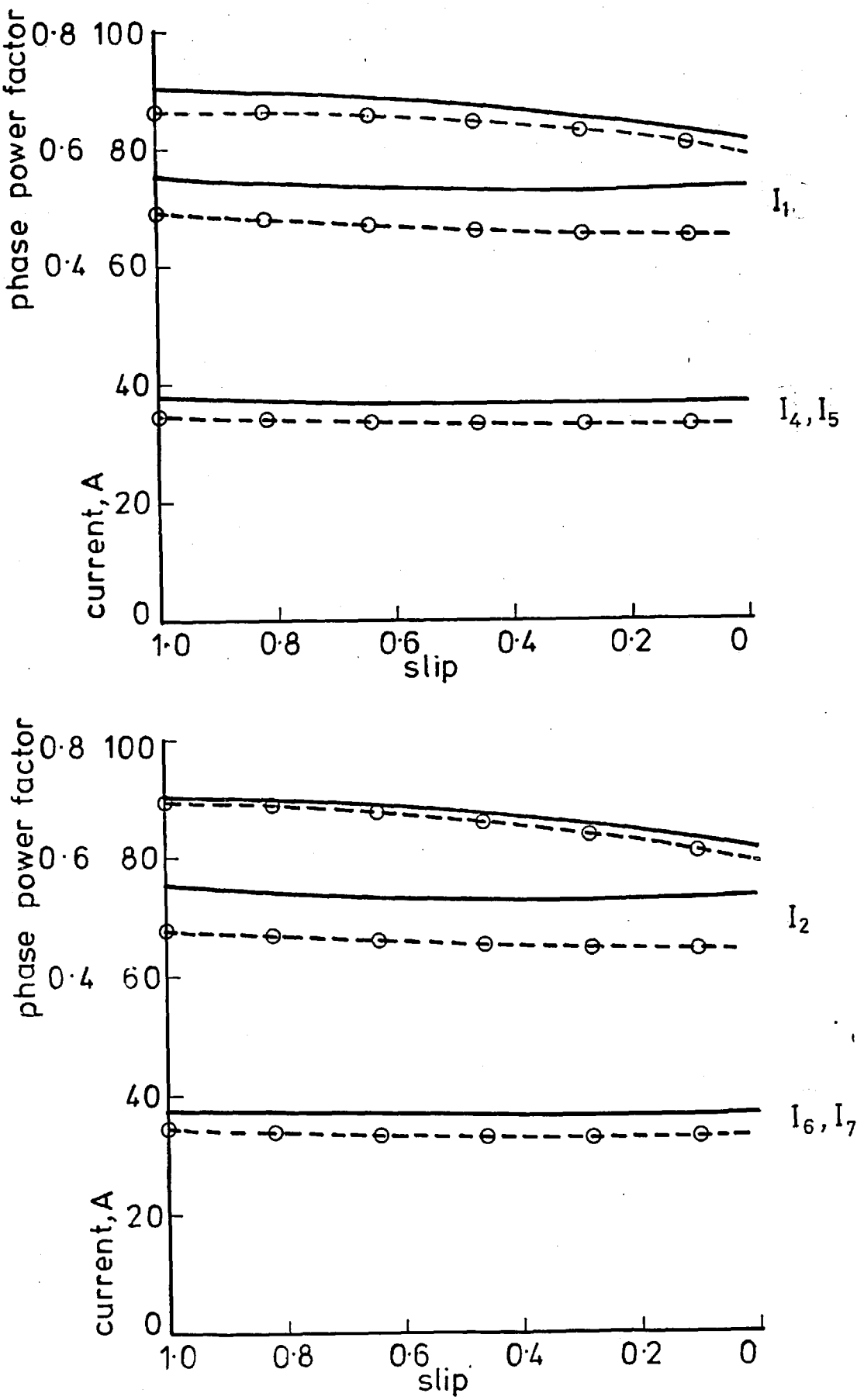

Fig. 3.9a Dynamic test machine terminal characteristics

- o - measured

—— calculated

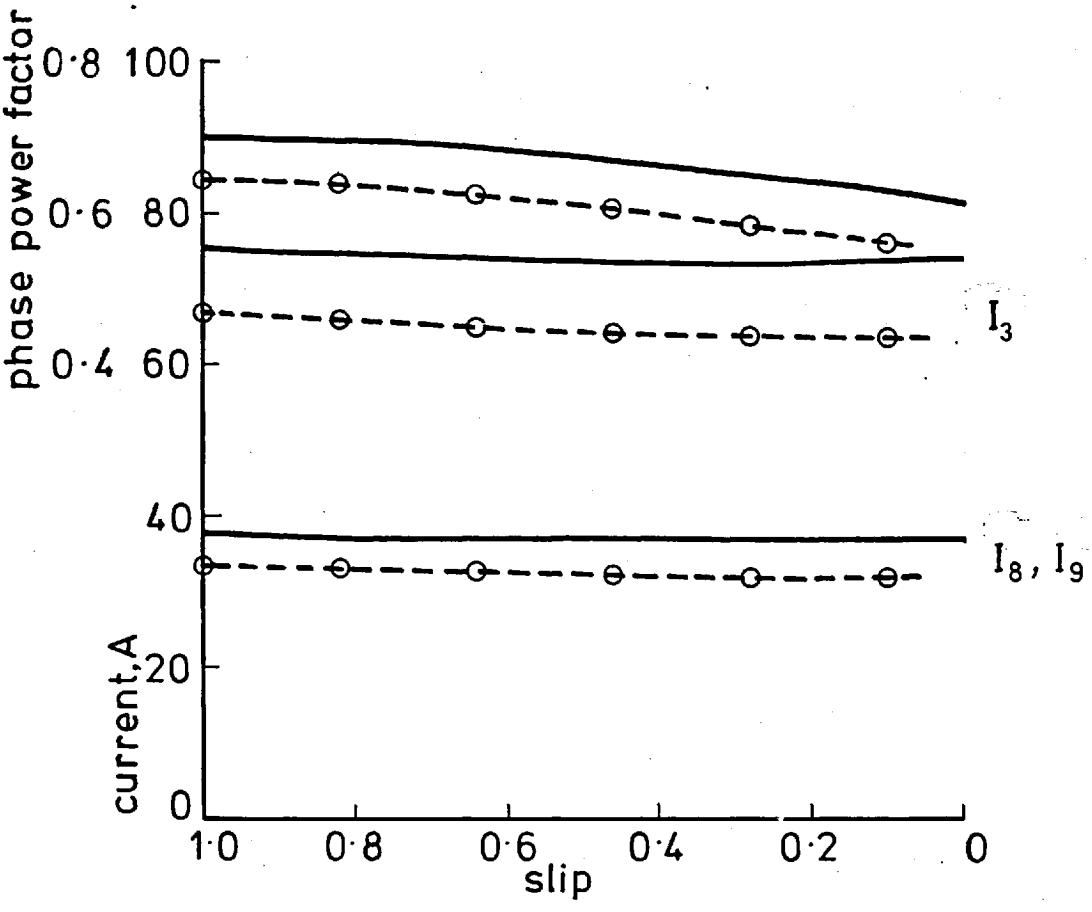

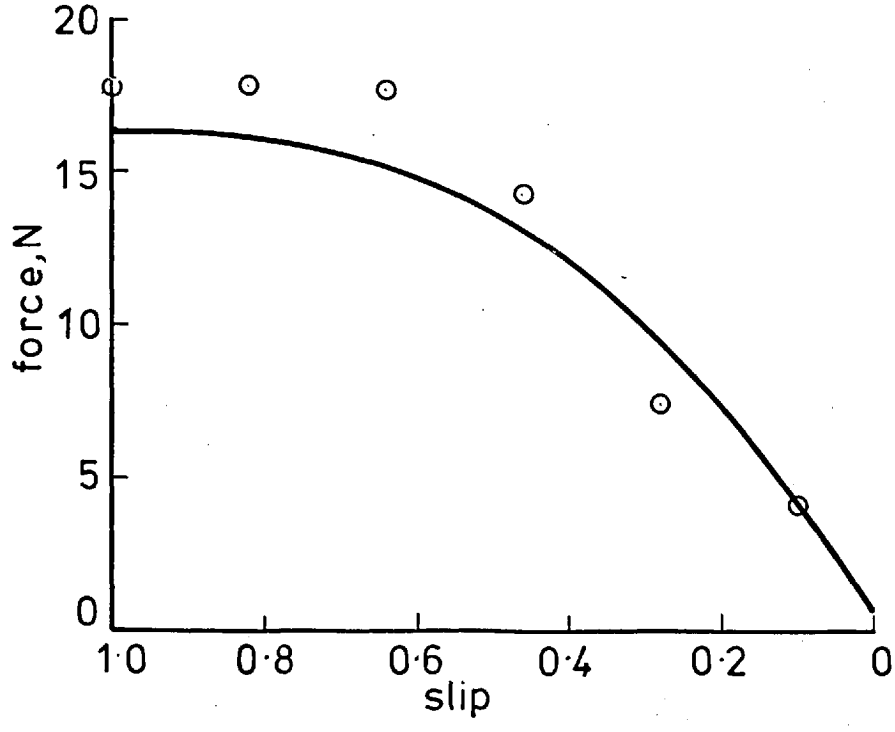

Fig. 3.9b Dynamic test machine terminal characteristics

- o - measured

——— calculated

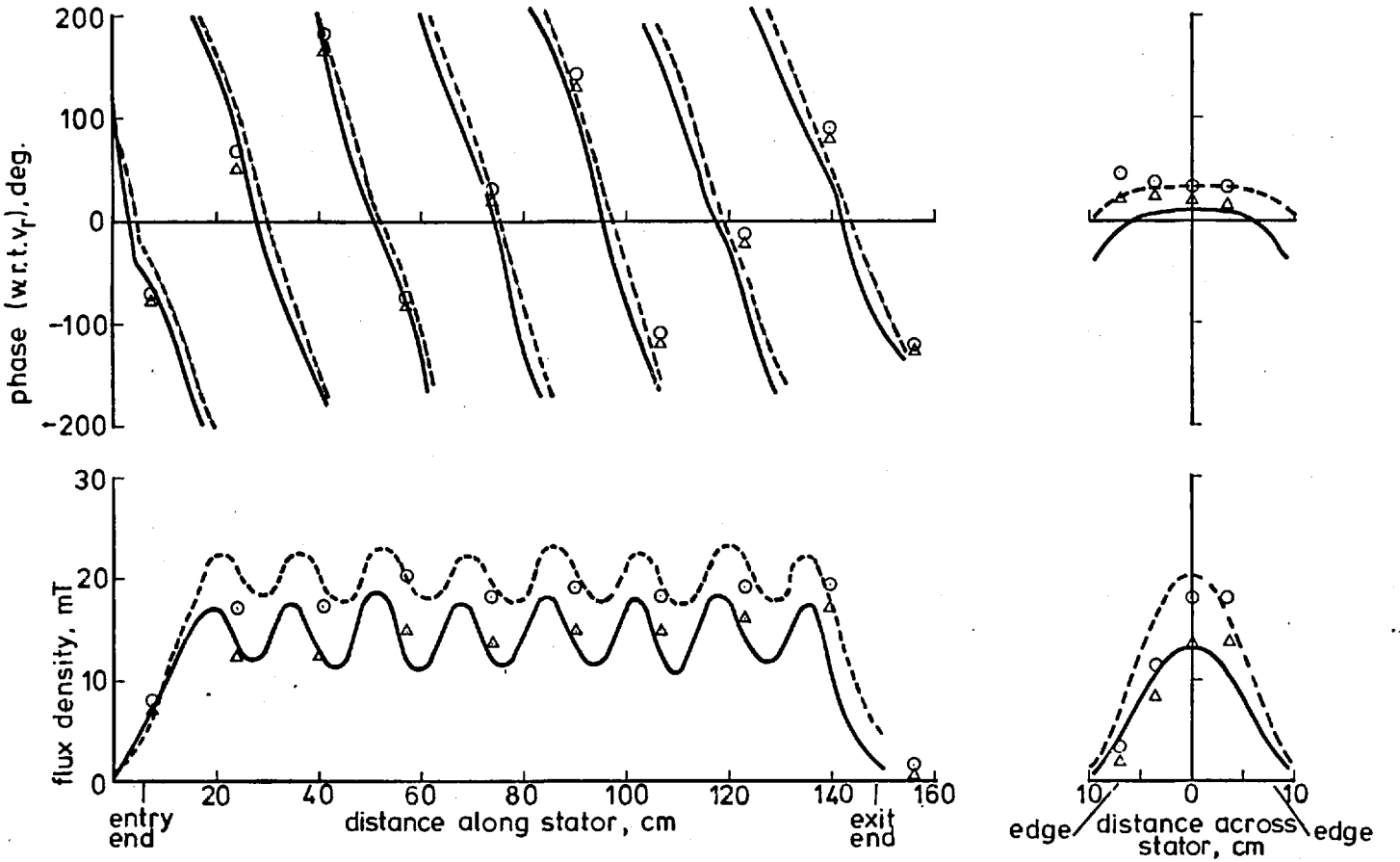

Fig.3.10. Dynamic test flux density

△ △ △ measured } slip 1·0
——— calculated }

o o o measured } slip 0·2
----- calculated }

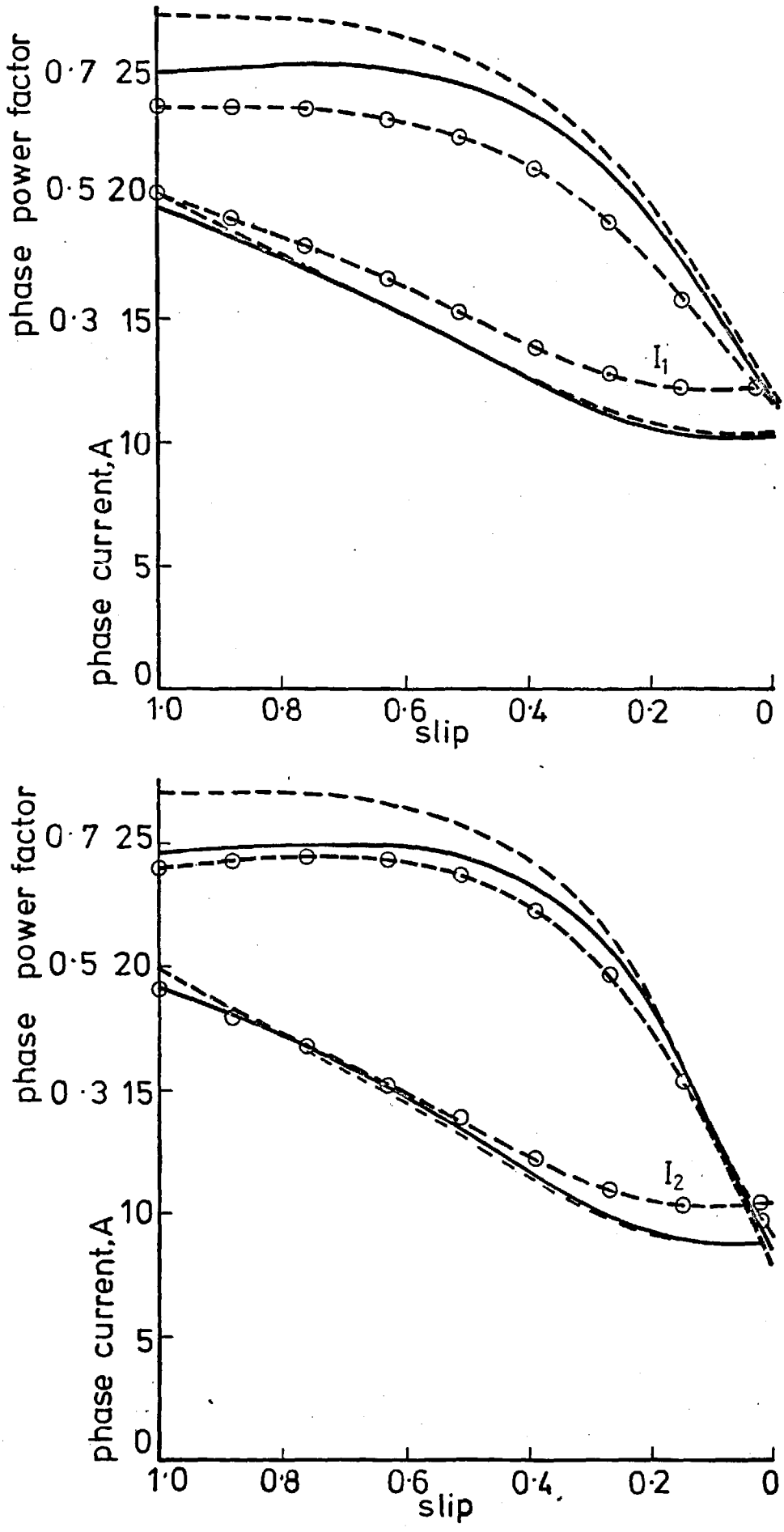

Fig. 3.11a Conventional 4-pole machine terminal characteristics
- o - measured - - - calculated using 1-dimensional model
_____ calculated

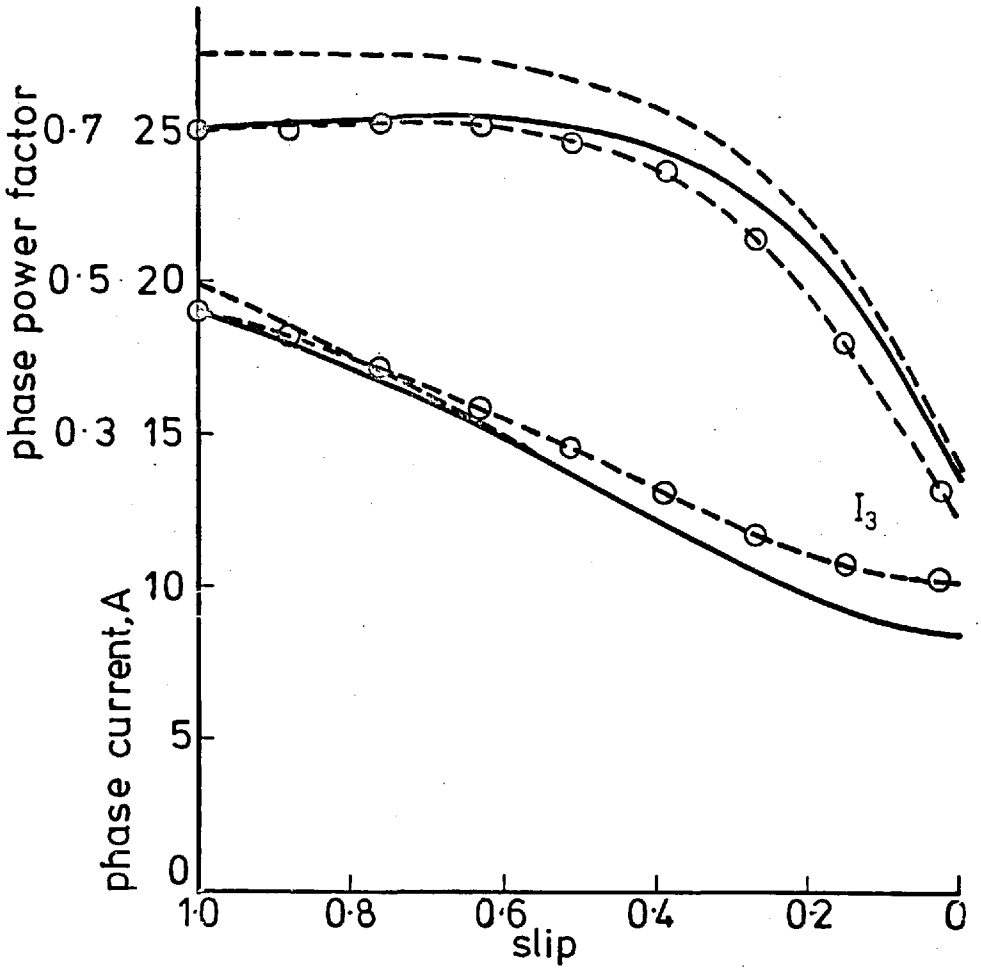

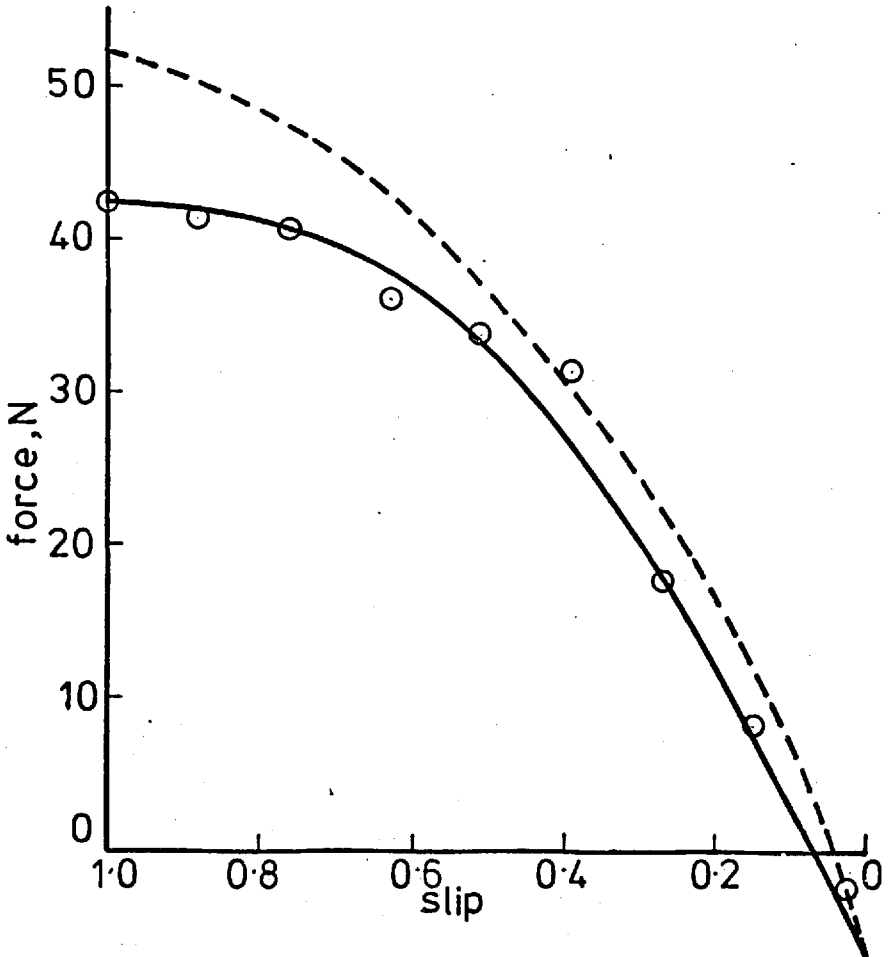

Fig. 3.11b Conventional 4-pole machine terminal characteristics

- o - measured - - - calculated using 1-dimensional model

——— calculated

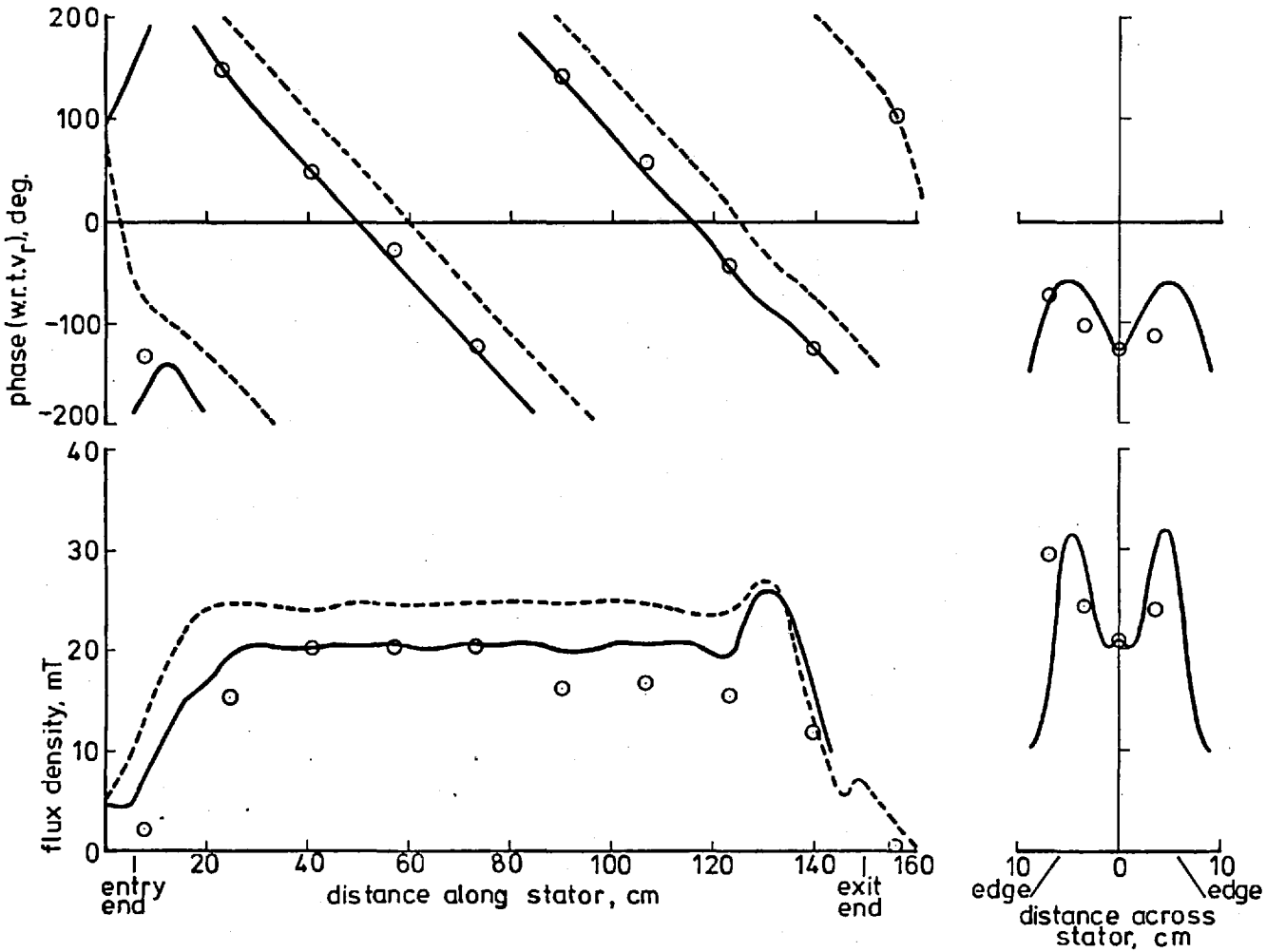

Fig.3.12. Conventional 4-pole machine flux density at 1·0 slip

o o o measured

—— calculated

---- calculated using 1-dimensional model

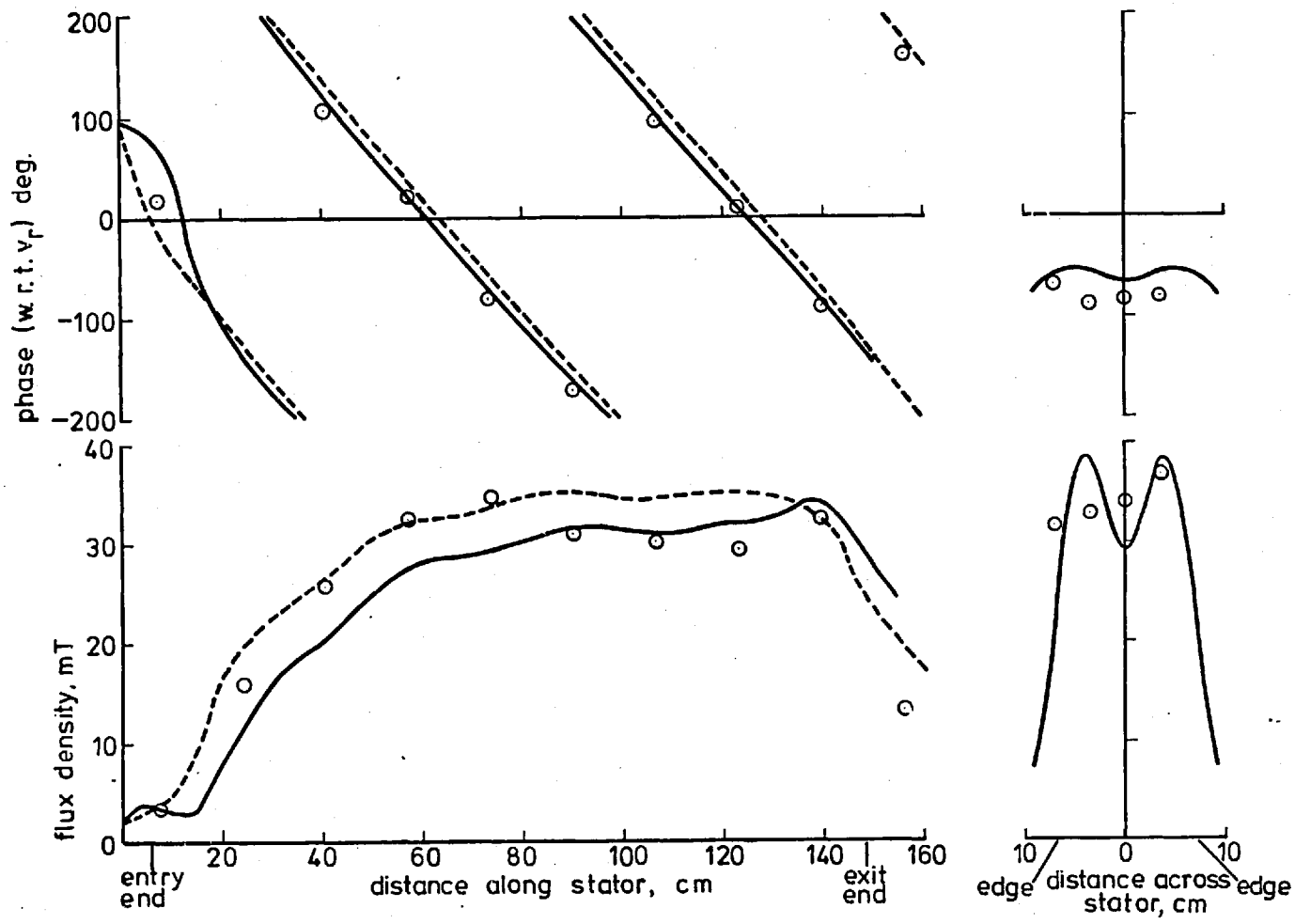

Fig.3.13. Conventional 4-pole machine flux density at 0·2 slip

o o o measured
—— calculated
---- calculated using 1-dimensional model

A disadvantage of the 2-dimensional analysis is that the primary and secondary iron cores must project over the stator end-windings and the rotor conducting plate. This extra iron causes the stator and rotor end-winding leakages to be modified. To reduce the effects of this, the end-winding regions (of width f) in Figure 3.2 were set to zero. The previously estimated values of winding resistance and leakage reactance were used in the calculations together with a thin layer winding representation. Constant values of permeability and resistivity were again assumed for the solid iron of the rotor.

Even with the limitations imposed on the model, the calculated performance showed favourable agreement with the measured results for the variety of machines tested. This gave some confidence that performance estimates from the model could be extrapolated to larger machines.

3.4 A theoretical performance comparison between a conventional and an air-gap wound machine

The previous section showed that the 2-dimensional mathematical model developed in Section 3.2 is capable of predicting, with reasonable accuracy, the performance of both conventional and air-gap wound axial flux linear induction machines. Two typical high speed designs are considered in this section and their electrical performances estimated using this model.

Equivalent conventional and air-gap wound machines were designed to operate from a 50 Hz supply with 4 poles of 1.2 m pitch. The secondary conducting plate in each case was formed of aluminium sheet 0.8 m wide and 1 cm thick with a 2 cm clearance to the stator surface.

The conventional machine (Figure 3.14) had primary and secondary core widths of 0.6 m and a slot pitch to slot width ratio of 25:17. A coil pitch of $\frac{1}{3}$ of a pole-pitch was chosen in this case as representing a reasonable compromise between reducing the coil end turn (and hence leakage reactance) and excessive reduction of the winding factor.

The core required for the air-gap wound machine of Figure 3.15 was 0.8 m for both the primary and secondary members. Diamond shaped coils of the type shown in Figure 3.5 were used. Each coil had the same number of turns and the same copper cross-section as those used in the conventional design. The coil pitch in this case was $\frac{2}{3}$ of a pole pitch at the coil centre. This allowed the full secondary width to be used whilst leaving no space between adjacent coil-sides.

In order to use the 2-dimensional model to predict the conventional machine performance, the winding resistances and leakage reactances (as estimated by the method described in Section 2.3.4) were added to each phase. The winding layer in the model was placed at the level of the tooth tops and its thickness set to a small value. Also, the end-winding overhang was set to zero.

In the case of the air-gap wound machine, the winding resistance was estimated from the mean coil turn and any leakage due to the coil "noses" was ignored.

The same constant current was applied to the windings in each case and Figure 3.16 shows the predicted performance characteristics of the two designs. As can be seen, the two machines have similar efficiencies over the whole speed range. However, the air-gap machine has a

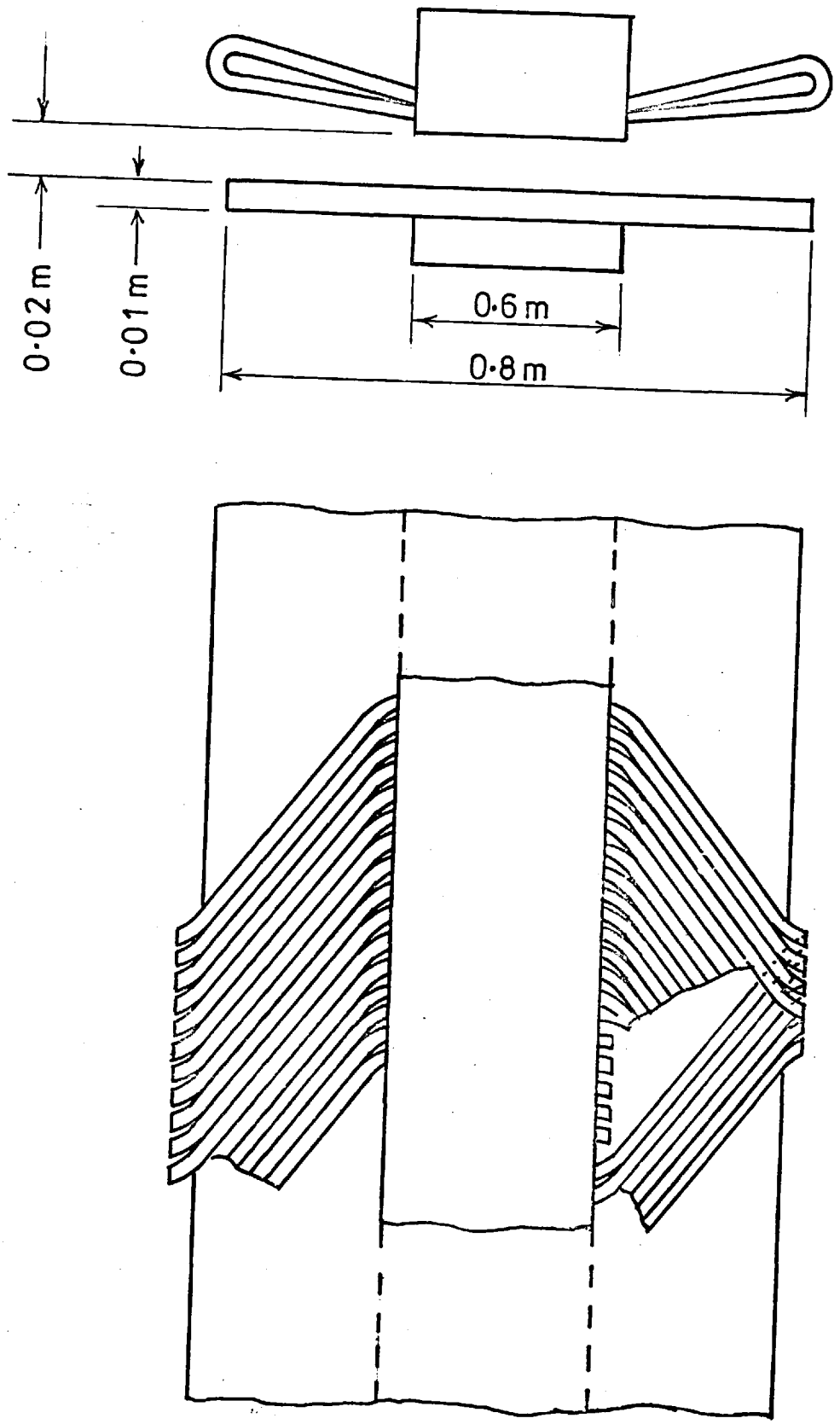

Fig. 3.14 Arrangement of conventional machine

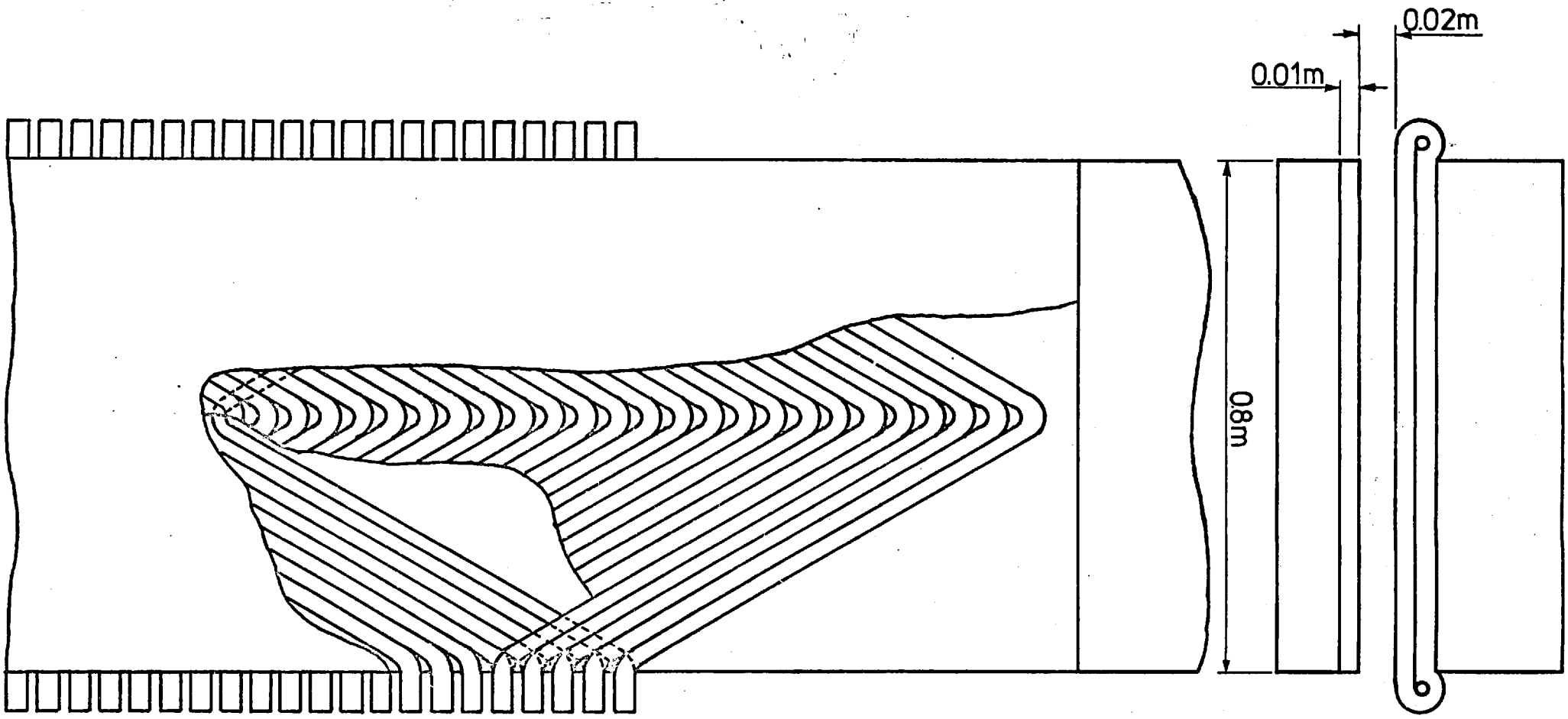

Fig. 3.15 Arrangement of machine with skewed air-gap winding

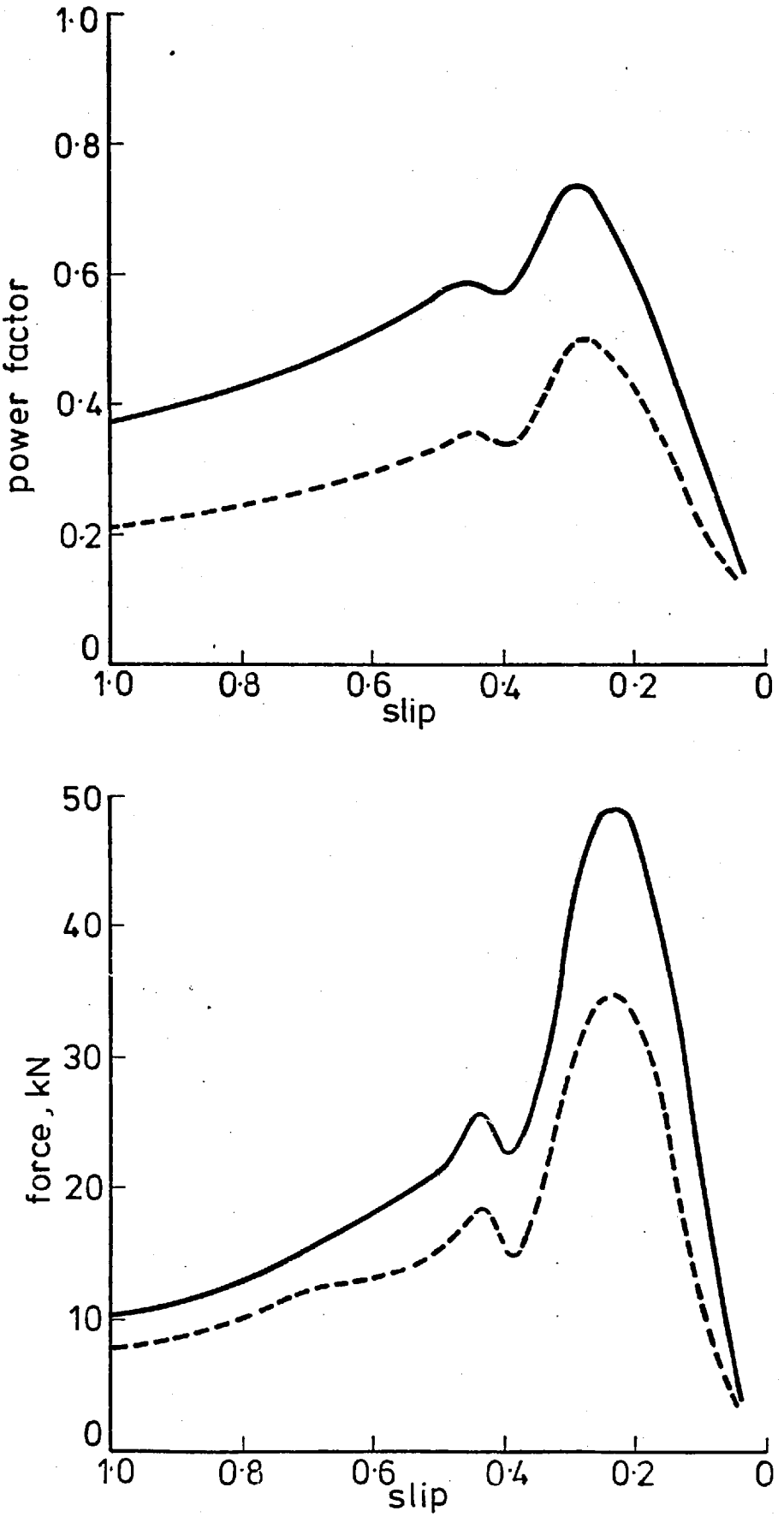

Fig. 3.16a Calculated performance of equivalent 4-pole machines

——— skewed air-gap winding

- - - conventional design

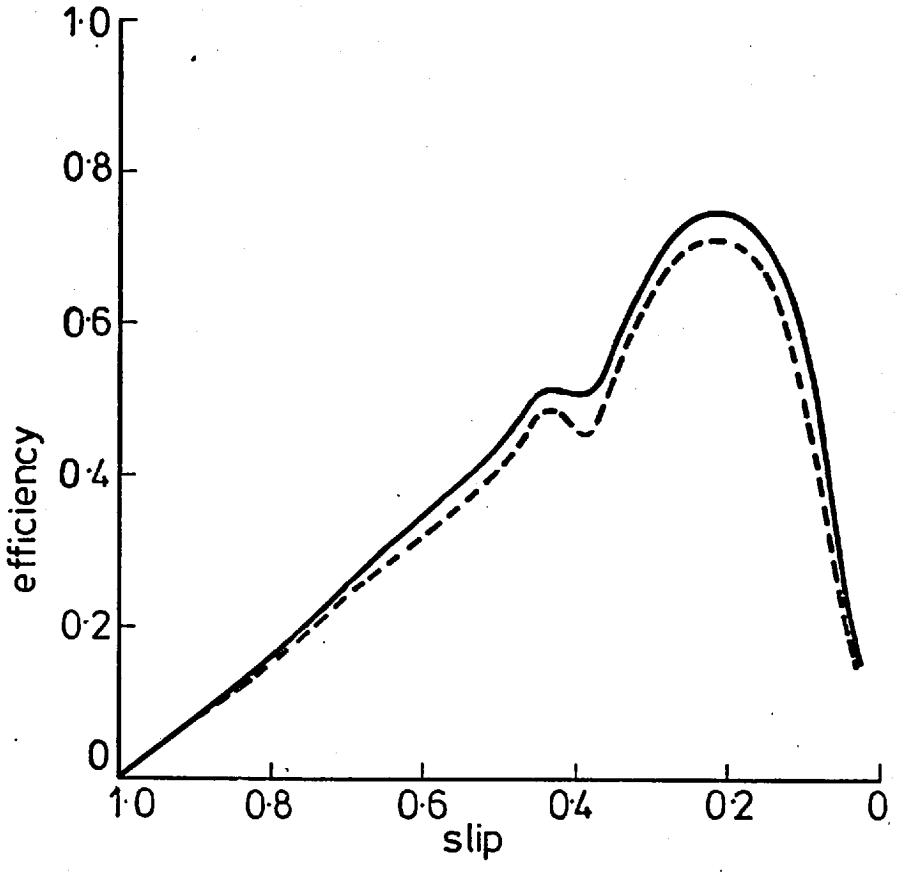

Fig. 3.16b Calculated performance of equivalent 4-pole machine

——— skewed air-gap winding

- - - conventional design

superior power factor characteristic and this is reflected in the increased thrust which is developed.

3.5 Conclusions

A two-dimensional mathematical model has been developed for linear induction machines capable of representing winding depth effects and separate conductor groups. The analysis is especially suited to machines with air-gap windings and with windings whose conductors are not normal to the direction of thrust. The validity of the model has been established by favourable comparison with results from a variety of practical tests.

Using this model, it has been shown that an air-gap wound axial flux machine with skewed windings has a better power factor than an equivalent slotted version for typical high-speed designs.

In future work it is hoped to perform the straight-forward modifications required in the analysis to allow comparisons with other machine types. These include certain "transverse-flux" designs[3.1,3.10] and machines with other coil geometries derivable from sections of parallel and skewed conductor.

An air-gap winding may disproportionately increase the magnetising current of low and medium speed machines. For these designs the use of a slotted structure is envisaged. As has already been indicated, the model is applicable to slotted windings by using either a "current sheet" or different values of permeability along each coordinate axis. Further experimental work is required in order to estimate leakage reactances when using the "current sheet" model and to verify the

"thick layer" winding model when using different permeabilities.

It is also hoped to use the model to estimate flux densities in the iron parts of linear machines. This will give a valuable guide to estimating the minimum sizes of stator and rotor cores.

3.6 Appendices

3.6.1 Transverse Fourier Series

In Figure 3.2 the rth harmonic amplitude of the surface conductor density of the νth coil group ($C_{r\nu}$) for positions on the x-axis such that $0 \leqslant x \leqslant h$ is given by

$$C_{r\nu} = \begin{cases} A_{r\nu} \sin(k_r\beta) & \text{for } 0 \leqslant x \leqslant \frac{w}{2} \\ A_{r\nu} \sin[\frac{k_r\beta}{f}(\frac{w}{2} + f - x)] & \frac{w}{2} \leqslant x \leqslant (\frac{w}{2} + f) \\ - A_{r\nu} \sin[\frac{k_r\beta}{f}(h - \frac{w}{2} - f - x)] & (h - \frac{w}{2} - f) \leqslant x \leqslant (h - \frac{w}{2}) \\ - A_{r\nu} \sin(k_r\beta) & (h - \frac{w}{2}) \leqslant x \leqslant h \end{cases}$$

For all other x values $C_{r\nu} = 0$. The function representing $C_{r\nu}$ may be expressed in series form by equation (3.1) in which

$$C_{rm\nu} = \frac{2}{h}\int_o^h C_{r\nu} \cos(k_m x)\,dx$$

When the integral is performed it is found that

$$C_{rm\nu} = \frac{2}{h} A_{r\nu} w_{rm} \qquad \text{for } m = 1,3,5, \ldots\ldots$$

where

$$w_{rm} = w \sin(k_r\beta) \frac{\sin \alpha_{3rm}}{\alpha_{3rm}} + f \sin(\alpha_{2rm} - \alpha_{3rm}) \frac{\sin \alpha_{1rm}}{\alpha_{1rm}} + f \sin(\alpha_{1rm} + \alpha_{3rm}) \frac{\sin \alpha_{2rm}}{\alpha_{2rm}}$$

and

$$\alpha_{1rm} = \tfrac{1}{2}(k_r\beta + k_m f)$$

$$\alpha_{2rm} = \tfrac{1}{2}(k_r\beta - k_m f)$$

$$\alpha_{3rm} = \tfrac{1}{2} k_m w$$

3.6.2 Winding layer model

With the assumptions given in Section 3.2.3 and a current density defined by equation (3.6a), the field equations

$$\text{curl } h = k \qquad \text{curl } e = -\frac{\partial b}{\partial t}$$

$$\text{div } b = 0$$

together with $b = \mu h$ may be solved to give the following field quantities (with subscripts suppressed for convenience):

$$h_x = \sqrt{2}\, H_x \sin(k_m x) e^{j(\omega t - k_r y)} \qquad e_x = \sqrt{2}\, E_x \cos(k_m x) e^{j(\omega t - k_r y)}$$

$$h_y = \sqrt{2}\, H_y \cos(k_m x) e^{j(\omega t - k_r y)} \qquad e_y = \sqrt{2}\, E_y \sin(k_m x) e^{j(\omega t - k_r y)}$$

where

$$E_x - j\frac{k_m}{k_r} E_y = E_{xy}$$

$$E_{xy} = -\frac{j\omega\mu_o\mu_z}{k_r^2}\{\gamma_{rm} P \sinh(\gamma_{rm} z) + \gamma_{rm} Q \cosh(\gamma_{rm} z) + K_x\}$$

$$H_y = P \cosh(\gamma_{rm} z) + Q \sinh(\gamma_{rm} z)$$

$$H_x = -j\frac{k_m}{k_r} H_y$$

$$\gamma_{rm}^2 = k_m^2 \frac{\mu_x}{\mu_z} + k_r^2 \frac{\mu_y}{\mu_z}$$

Application of the boundary conditions

$$E_{xy} = E_{xyL} \quad \text{and} \quad H_y = H_{yL} \quad \text{at} \quad z = 0$$

$$\text{and} \quad E_{xy} = E_{xyu} \quad \text{and} \quad H_y = H_{yu} \quad \text{at} \quad z = \ell$$

enables the constants P and Q to be eliminated. The resulting expressions can be represented by the network model of Figure 3.3(b) in which

$$Z_{Arm} = Z_{orm} \tanh(\tfrac{1}{2}\gamma_{rm}\ell)$$

$$Z_{Brm} = Z_{orm}/\sinh(\gamma_{rm}\ell)$$

and $Z_{orm} = \dfrac{j\omega\mu_o(k_m^2\mu_x + k_r^2\mu_y)}{\gamma_{rm} k_r^2}$

The corresponding result for the backward travelling fields is obtained by replacing r with -r.

3.6.3 Machine layer model and equivalent network

The field equations, together with the material relations $b = \mu h$ and $k = \sigma e$, may be solved in a frame of reference attached to the layer described in Section 3.2.4. Assuming a model excitation of the form given by equation (3.6a), the following results are obtained for the rmth forward travelling harmonic:

$$h_x = \sqrt{2}\, H_x \sin(k_m x')\, e^{j(s\omega t - k_r y')} \qquad e_x = \sqrt{2}\, E_x \cos(k_m x')\, e^{j(s\omega t - k_r y')}$$

$$h_y = \sqrt{2}\, H_y \cos(k_m x')\, e^{j(s\omega t - k_r y')} \qquad e_y = \sqrt{2}\, E_y \sin(k_m x')\, e^{j(s\omega t - k_r y')}$$

where s is the fractional slip of the layer with respect to the rth harmonic waves and

$$E_x - j\frac{k_m}{k_r} E_y = E_{xy}$$

$$E_{xy} = -\frac{s\omega}{k_r}\left[P\cosh(\gamma_{rm} z') + Q\sinh(\gamma_{rm} z')\right]$$

$$H_y = \frac{\gamma_{rm} k_r}{j\mu_o(k_r^2\mu_y + k_m^2\mu_x)}\left[P\sinh(\gamma_{rm} z') + Q\cosh(\gamma_{rm} z')\right]$$

$$H_x = -j\frac{k_m}{k_r} H_y$$

$$\gamma_{rm}^2 = k_m^2\frac{\mu_x}{\mu_z} + k_r^2\frac{\mu_y}{\mu_z} + js\omega\mu_o\sigma\frac{(k_m^2\mu_x + k_r^2\mu_y)}{(k_m^2 + k_r^2)}$$

When similar boundary conditions to those of Appendix 3.6.2 are applied in a stationary frame of reference, the constants P and Q can be eliminated. The resulting expressions can be represented by the network model of Figure 3.4(c) in which

$$Z_{Arm} = Z_{orm} \tanh(\tfrac{1}{2} \gamma_{rm} S)$$

$$Z_{Brm} = Z_{orm} / \sinh(\gamma_{rm} S)$$

where S is the layer thickness and

$$Z_{orm} = \frac{j\omega\mu_o (k_m^2 \mu_x + k_r^2 \mu_y)}{\gamma_{rm} k_r^2}$$

The corresponding result for the backward travelling fields is obtained by replacing r with -r.

When the layer depth is large, as is the case with the air spaces behind the iron cores, it may be assumed that at one boundary E_{xy} and H_y are small. In this case $z_{Arm} \to 0$ and $z_{Brm} \to z_{orm}$.

3.6.4 Winding induced voltages

The time average flow of VA into the winding layer due to the forward travelling fields is given by:

$$S_{Frm} = -\int_{-h/2}^{h/2} \int_{o}^{2k_B P_B} \{ [J_{xF} \cos(k_m x) e^{-jk_r y}]^* [E_{yF} \cos(k_m x) e^{-jk_r y}] + [J_{yF} \sin(k_m x) e^{-jk_r y}]^* [E_{yF} \sin(k_m x) e^{-jk_r y}] \} dy dx$$

This expression reduces to:

$$S_{Frm} = h\, k_B P_B\, J_{xF}^*\, z_{inF}\, J_{xF} \qquad \text{(A.3.1a)}$$

after applying equation (3.5b) together with

$$E_{xF} - j \frac{k_m}{k_r} E_{yF} = - z_{inF} J_{xF} .$$

z_{inF} is the input impedance seen at the current sheet.

The corresponding result for backward travelling fields is

$$S_{Brm} = h\, k_B P_B\, J^*_{xB}\, z_{inB}\, J_{xB} \qquad \text{(A.3.1b)}$$

When equations (A.3.1a) and (A.3.1b) are added and J_{xF} and J_{xB} are replaced by equations (3.5), it is found that

$$S_{rm} = [I^*]^T[C_{rm}]z_{inF}[C^*_{rm}]^T[I] + [I^*]^T[C^*_{rm}]z_{inB}[C_{rm}]^T[I] \qquad \text{(A.3.2)}$$

The total VA into the winding is

$$S = -[I^*]^T[e_T] \qquad \text{(A.3.3)}$$

Comparing equation (A.3.2), summed over all the harmonics, and equation (A.3.3) gives

$$[e_T] = -h\, k_B P_B \sum_{r=1}^{\infty}\sum_{m=1}^{\infty} \left\{[C_{rm}]z_{inF}[C^*_{rm}]^T + [C^*_{rm}]z_{inB}[C_{rm}]^T\right\}[I] \qquad \text{(A.3.4)}$$

3.6.5 Thrust and flux density

The power inputs to the layer model on the rmth harmonic (i.e. P_{Frm} and P_{Brm}) are given by the real parts of equation (A.3.1). Assuming all the loss in the layer model to be in the moving secondary, the net forward thrust on the rth longitudinal harmonic is

$$F_r = \frac{1}{v_{sr}} \sum_{m=1}^{\infty} \{P_{Frm} - P_{Brm}\}$$

where $v_{sr} = \frac{\omega}{k_r}$ and is the synchronous speed of the rth harmonic waves. The total thrust is then given by

$$F = \sum_{r=1}^{\infty} F_r$$

The flux density on the rmth harmonic is given from the electric field strength at the appropriate surface in the layer model, i.e. E'_{xyFrm} and E'_{xyBrm}. The total flux density at coordinates x' and y' is then given by

$$B = \sum_{r=1}^{\infty} \sum_{m=1}^{\infty} \left\{ \frac{k_r}{\omega} \cos(k_m x') \left[E'_{xyBrm} e^{jk_r y'} - E'_{xy'Frm} e^{-jk_r y'} \right] \right\}$$

CHAPTER FOUR

REFERENCES

1.1 LAITHWAITE, E.R. and BARWELL, F.T.:

'Application of linear induction motors to high-speed transport systems', Proc.I.E.E., 1969, 116, (5), pp.713-724.

1.2 LAITHWAITE, E.R.:

'Linear induction motors', Proc.I.E.E., 1957, 104(A), (12), pp.461-470.

1.3 BLAKE, L.R.:

'Conduction and induction pumps for liquid metals', Proc.I.E.E., 1957, 104(A), (7), pp.49-63.

1.4 WILLIAMS, F.C., LAITHWAITE, E.R. and PIGGOTT, L.S.:

'Brushless variable-speed induction motors', Proc.I.E.E., 1957, 104(A), (6), pp.102-118.

1.5 WILLIAMS, F.C., LAITHWAITE, E.R. and EASTHAM, J.F.:

'Development and design of spherical induction motors', Proc.I.E.E., 1959, 106A, pp.471-484.

1.6 LAITHWAITE, E.R.:

'Induction machines for special purposes' (Newnes, 1966).

1.7 BOLTON, H.:

'Transverse edge effect in sheet-rotor induction motors', Proc.I.E.E., 1969, 116, (5), pp.725-731.

1.8 MAZDA, F.F.:

'An investigation of invertor circuits for variable speed single-phase induction motors', M.Phil. Thesis, London University, 1971.

1.9 EASTHAM, J.F. and BALCHIN, M.J.:

'Pole-change linear induction motors', I.E.E. Conference Publication No. 120 (Linear electric machines), October 1974, pp.9-14.

1.10 EASTHAM, J.F. and BALCHIN, M.J.:

'Pole-change windings for linear induction motors', Proc.I.E.E., 1975, 122, (2), pp.154-160.

1.11 BALCHIN, M.J. and EASTHAM, M.J.:

'Performance of linear induction motors with air-gap windings', Proc.I.E.E. (to be published).

2.1 EASTHAM, J.F.:

'Close-ratio phase modulated change-pole machines with improved winding balance', Proc.I.E.E., 1968, 115, (11), pp.1641-1648.

2.2 EASTHAM, J.F. and LAITHWAITE, E.R.:

'Pole-change motors using phase-mixing techniques', Proc.I.E.E., 1967, 109A, pp. 397-409.

2.3 WILLIAMS, F.C. EASTHAM, J.F. and PIGGOTT, L.S.:

'Analysis and design of pole-change motors using phase-mixing techniques', Proc.I.E.E., 1964, 111, (1), pp. 80-94.

2.4 RAWCLIFFE, G.H., BURBRIDGE, R.F. and FONG, W.:

'Induction motor speed changing by pole-amplitude modulation', Proc.I.E.E., 1958, 105A, pp.411-419.

2.5 RAWCLIFFE, G.H. and FONG,W.:

'Speed changing induction motors: further developments in pole-amplitude modulation', Proc.I.E.E., 1960, 107A, pp.513-528.

2.6 LAITHWAITE, E.R. and BARWELL, F.T.:

'Application of linear induction motors to high-speed transport systems', Proc.I.E.E., 1969, 116, (5), pp.713-724.

2.7 WILLIAMS, F.C. LAITHWAITE, E.R. and EASTHAM, J.F.:

'Development and design of spherical induction motors', Proc.I.E.E., 1959, 106A, pp.471-484.

2.8 LAITHWAITE, E.R.:

'Induction machines for special purposes' (Newnes, 1966).

2.9 LAITHWAITE, E.R., EASTHAM, J.F., BOLTON, H.R. and FELLOWS, T.G.:
'Linear motors with transverse flux', Proc.I.E.E., 1971, 118, (12), pp.1761-1767.

2.10 GREIG, J. and FREEMAN, E.M.:
'Travelling wave problem in electrical machines', Proc.I.E.E., 1967, 114, (11), pp.1681-1683.

2.11 FREEMAN, E.M.:
'Travelling waves in induction machines: input impedance and equivalent circuits', Proc.I.E.E., 1968, 115, (12), pp.1772-1776.

2.12 CULLEN, A.L. and BARTON, T.H.:
'A simplified electromagnetic theory of the induction motor, using the concept of wave impedance', Proc.I.E.E., 1958, 105C, pp.331-336.

2.13 HESMONDHALGH, D.E. and TIPPING, D.:
'General method for prediction of the characteristics of induction motors with discontinuous exciting windings', Proc.I.E.E., 1965, 112, (9), pp.1721-1735.

2.14 ALWASH, J.H.H.:
'Analysis and design of linear induction motors', Ph.D. Thesis, London University (Imperial College), 1972.

2.15 HAGUE, B.:
'Electromagnetic problems in electrical engineering' (Oxford University Press, 1929).

2.16 SAUNDERS, R.M.:

'Electromechanical energy conversion in double cylindrical structures', Trans.Am.Inst.Elec.Eng., 1963, 82, pp.631-638.

2.17 BROWN, J.E. and JHA, C.S.:

'Generalised rotating-field theory of polyphase induction motors and its relationship to symmetrical component theory', Proc.I.E.E., 1962, 109A, pp.59-69.

2.18 KRON, G.:

'Tensor analysis of networks', (Macdonald, 1965).

2.19 RUSSELL, R.L. and NORSWORTHY, K.H.:

'Eddy currents and wall losses in screened rotor induction motors', Proc.I.E.E., 1958, 105A, pp.163-175.

2.20 TIPPING, D.:

'The analysis of some special-purpose electrical machines', Ph.D. Thesis, Manchester University, 1964.

2.21 LIWSCHITZ-GARIK, M. and WHIPPLE, C.C.:

'Electric machinery', Vol.I, (D. Van Nostrand, 1948).

3.1 EASTHAM, J.F. and LAITHWAITE, E.R.:

'Linear motor topology', Proc.I.E.E., 1973, 120, (3), pp.337-343.

3.2 BOLTON, H.:

'Transverse edge effect in sheet-rotor induction motors', Proc.I.E.E., 1969, 116, (5), pp.725-731.

3.3 PRESTON, T.W. and REECE, A.B.J.:

'Transverse edge effects in linear induction motors', Proc.I.E.E., 1969, 116, (6), pp.973-979, corrigend. 1970, 117, (9), p.1808.

3.4 FREEMAN, E.M. and LOWTHER, D.A.:

'Transverse edge effects in linear induction motors', correspondence on above item, Proc.I.E.E., 1971, 118, (12), pp.1820-1821.

3.5 VESKE, T.A.:

'Solution of the electromagnetic field equations for a plane linear induction machine with secondary boundary effects, Magnetohydrodynamics, 1965, 1, (1), pp.64-71.

3.6 ALWASH, J.H.H.:

'Analysis and design of linear induction motors', Ph.D. Thesis, London University (Imperial College), 1972.

3.7 SAUNDERS, R.M.:

'Electromechanical energy conversion in double cylindrical structures', Trans.Am.Inst.Elec.Eng., 1963, 82, pp.631-638.

3.8 HAGUE, B.:

'Electromagnetic problems in electrical engineering' (Oxford University Press, 1929).

3.9 GREIG, J. and FREEMAN, E.M.:

'Travelling wave problem in electrical machines', Proc.I.E.E., 1967, 114, (11), pp.1681-1683.

3.10 LAITHWAITE, E.R., EASTHAM, J.F. BOLTON, H.R. and FELLOWS, T.G.:

'Linear motors with transverse flux', Proc.I.E.E., 1971, 118, (12), pp.1761-1767.

POLE-CHANGE LINEAR INDUCTION MOTORS*

J.F. Eastham and M.J. Balchin

1. Introduction

Pole-change techniques have been in common use over many years as one method for controlling the speed of rotary induction motors. This method can give only discrete changes in speed but does have the advantage of providing efficient running at those speeds with a minimum of control gear. It is thought likely that these advantages will make pole-change methods useful for the speed control of linear induction motors used in transport systems.

Series connected multi-speed windings are directly applicable to linear machines. However, as is the case with rotary machines, it is found that these windings are inflexible insofar as switching arrangements and changes of voltage are concerned. In a rotary machine, where the flux wave is always sinusoidally distributed in space, extra flexibility is introduced by designing windings which contain parallel groups.

In linear machines the flux wave is far from sinusoidally distributed and this contribution discusses the particular difficulties this presents to the design of windings containing parallel groups.

2. The Basic Consequent Pole Technique

The simplest form of change-pole arrangement is the two-speed consequent-pole winding. Fig. 1 illustrates the layout of the electric and magnetic circuits for one phase of a linear machine using this type of winding, which, for the sake of clarity shows only single coils. As can be seen, reversal of current in alternate coils yields the higher pole number. Three similar sets of circuits, displaced by 120° in space and excited with three-phase currents, will produce a travelling wave of flux.

In rotary pole-change machines, parallel connections are normally used on one of the settings so that the number of switch contacts which are necessary is reduced. Parallel path working is not possible in the linear case because of the non-uniform nature of the air-gap flux density. Essentially, this increases from a small value at the leading edge of the machine to larger values along its length. Thus, considering the coils of Fig. 1, it is not possible to parallel a series combination of coils 1 and 3 with a series combination of coils 2 and 4 because each series path would have a different induced emf. On each setting, all the coils of a phase must be in series and Fig. 2 shows how this may be achieved in the three-phase case for a series star/series star arrangement using 12 switch contacts.

In the case of the primitive machine of Fig. 1, R1 represents a series connection of coils such as 1 and 3 and R2 a similar connection of such coils as 2 and 4. It will be appreciated that whilst the system has been

The authors are with the University of Aberdeen Engineering Department, Broad Street, Aberdeen.

* I.E.E. Conference Publication No. 120 (Linear electric machines), October 1974.

described in terms of the simplest possible case, the statements about series working being necessary and the switching system of Fig. 2 will apply to all consequent pole windings whatever their complexity. Many other two-speed change-pole systems apart from the consequent pole scheme have been devised. Detailed examination reveals that most of them reverse half the winding with respect to the other half to provide a change in pole number, and that a series/series switching arrangement is necessary in the linear case.

3. The Use of Double Winding Sections

The number of switch contacts used may be reduced by using a double winding arrangement which allows parallel connections to be made.

The basic principle of the double winding section may be explained by referring again to the single phase diagram of Fig. 1. Each coil in this figure is replaced by two coils as shown in Fig. 3. The coils labelled "A" are connected in series forming an identical winding with a series connection of the "B" coils. The voltage across each of these windings is obviously the same and so these two sections can be paralleled to give one phase of an eight pole setting as shown in Fig. 3d.

To form the four pole setting of Fig. 3b, it may be seen that the voltage across a series combination of coils 1A, 3A, 2B and 4B is also equal to that across a series combination of coils 2A, 4A, 1B and 3B. This allows the coil group connections to remain as in Fig. 3d, but now the current feed has to be moved so that the currents in coils 2B, 4B, 2A and 4A are reversed.

As with the series connected layouts, these arrangements may also be realised with surface windings. The obvious way of achieving this is to use two separate double layer windings and to make the connections between them.

Four layer construction can be avoided by placing the two windings one slot-pitch apart. This results in sections which are not strictly capable of being paralleled, but the difference in induced emf will be small and may be tolerable. The small difference in induced emf may be reduced further by placing one winding in the even numbered slots in one section, and in odd numbered slots in the following section.

Fig. 4 shows a three-phase arrangement using this system in which the winding is connected in star on each pole setting. A total of only 10 switch contacts is required compared with the 12 shown previously in Fig. 2.

It will be appreciated that only an outline of the use of the technique has been given. If it is required, for example, to change the effective winding voltage between settings then it can be shown that again advantages can be obtained using the double winding system[1].

4. Analysis and Experimental Results

Most of the analytical techniques available consider only 'current sheet' forms of excitation such as would be produced by polyphase windings taking balanced supply currents. These analyses are not apt

where parallel path working in asymmetrically wound machines is being considered, since here it is the balance of the input currents and the current sharing between parallel paths that is of interest.

A new form of analysis has recently been developed[1] which deals with the problem. It allows the complete performance of a linear motor with ρ serially connected sets of coils energised from ρ independent voltage sources to be found. The technique is based on a surface impedance approach[2] combined with a method for resolving groups of coils into equivalent sinusoidally disposed conductor distribution[3]. This allows the terminal quantities of the coil groups to be directly related to the surface impedance model. Standard network techniques are then used to relate the coil voltages and currents to the known supply quantities.

This theory has been tested against experimental results taken on a disc rig. The curved linear motor tested used a 4/8 pole winding in 54 slots. The double winding technique using odd and even slot numbers was employed. The machine had a mean length of 1.46 m, and a stack length of 0.16 m Many sets of results were taken, some of which are shown in Figs. 5,6,and 7. They refer to two different rotor resistivities with series and parallel stator connections. The results of Figs. 6 and 7 are for the high resistivity case whilst Fig. 5 refers to a low resistivity rotor. It will be observed that good correlation between theory and practice is obtained. It will also be noticed from Figs. 5 and 6 that the currents in the two parallels are reasonably equal. This confirms that the philosophy of the new change pole connections is valid.

5. Conclusions

A novel connection method for linear motor change-pole windings has been described. This method saves some switch contacts. A new form of analysis has been discussed and supported by experimental results from a test machine of substantial size. It is thought that this analysis has more general application than the particular use to which it has been put in this work. The experiments and winding designs described use the well known consequent pole technique. It will, however, be understood that the double winding technique can be applied with equal benefit to other change pole systems and for pole ratios different to the simple 2:1 case.

6. References

1. EASTHAM, J.F. and BALCHIN, M.J., 'Pole change winding for linear motors', Submitted to the I.E.E. Proceedings, 1974.

2. FREEMAN, E.M., 'Travelling waves in induction machines: input impedance and equivalent circuits', Proc.I.E.E., 1968, (12), pp. 1772-1776.

3. WILLIAMS, F.C., EASTHAM, J.F. and PIGGOTT, L.S., 'Analysis and design of pole-change motors using phase-mixing technique', Proc.I.E.E., 1964, 111, (1), pp. 80-94.

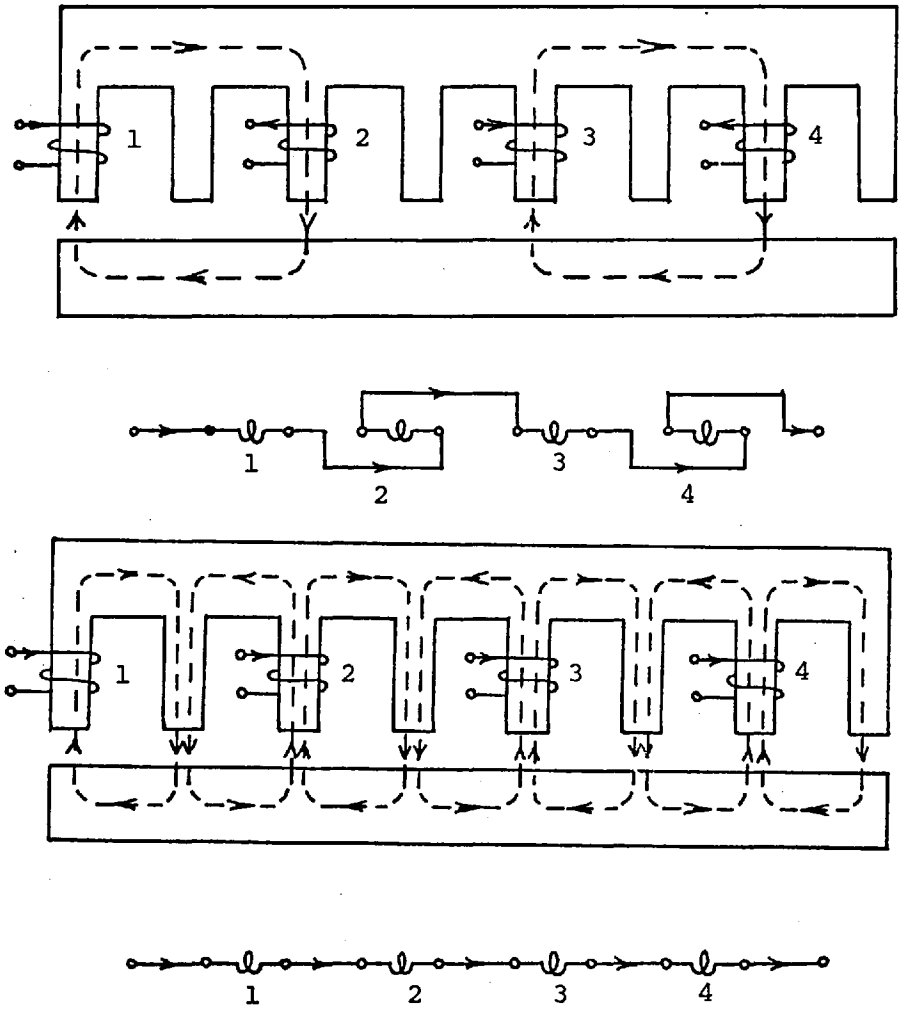

Fig. 1 PRINCIPLE OF SERIES CONNECTED CONSEQUENT POLE-CHANGE WINDINGS

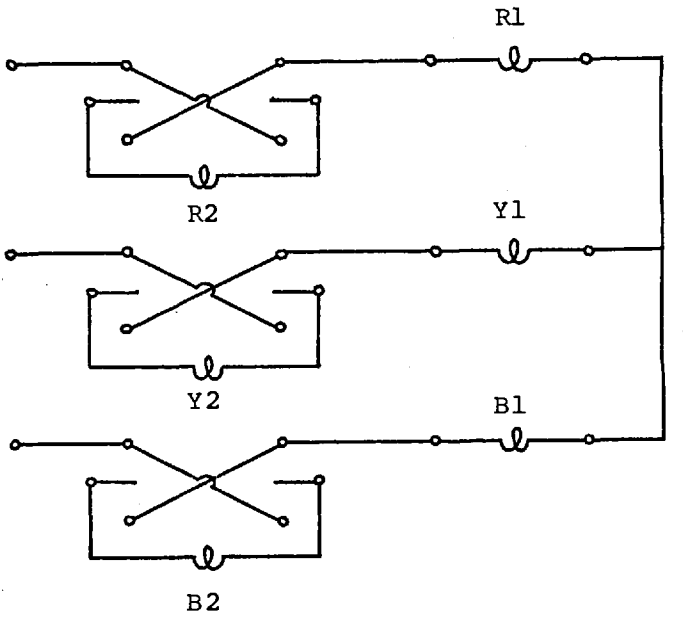

Fig. 2 SWITCHING ARRANGEMENT FOR SERIES STAR/SERIES STAR CONNECTIONS

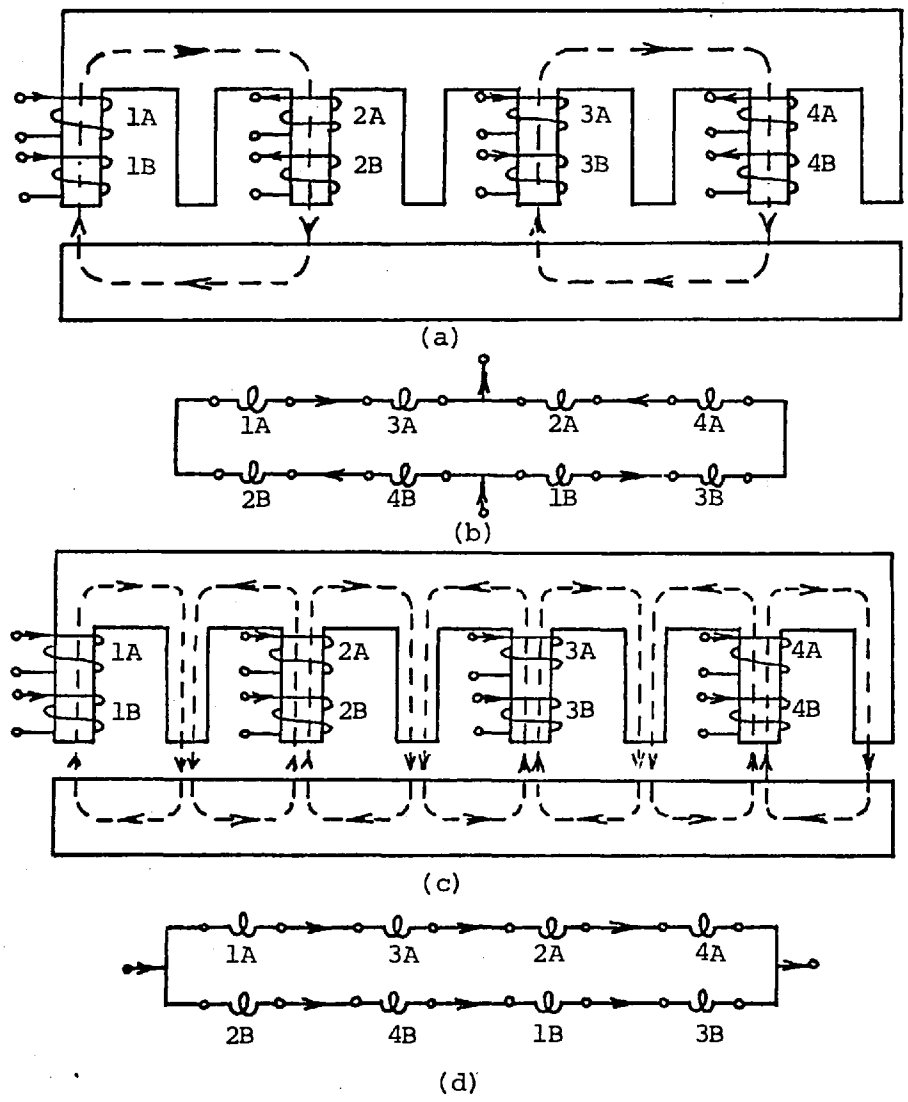

FIG. 3 PRINCIPLE OF PARALLEL CONNECTED CONSEQUENT POLE-CHANGE WINDINGS

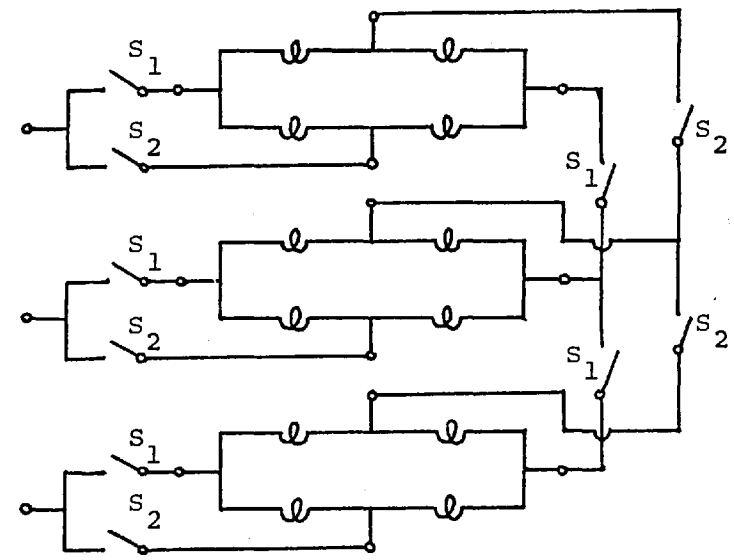

FIG. 4 SWITCHING ARRANGEMENT FOR PARALLEL STAR/PARALLEL STAR CONNECTIONS

Switches S_1 closed for first pole setting

Switches S_2 closed for second pole setting

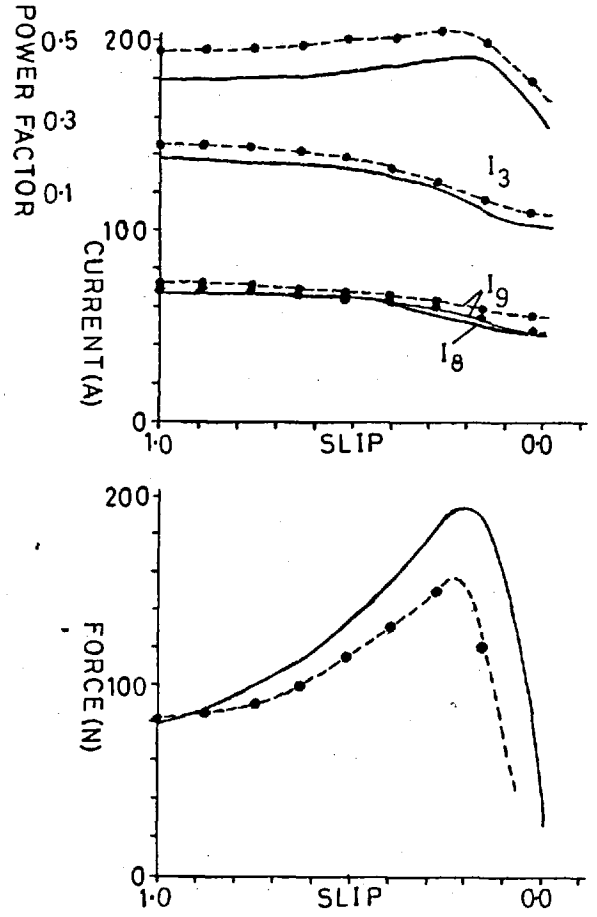

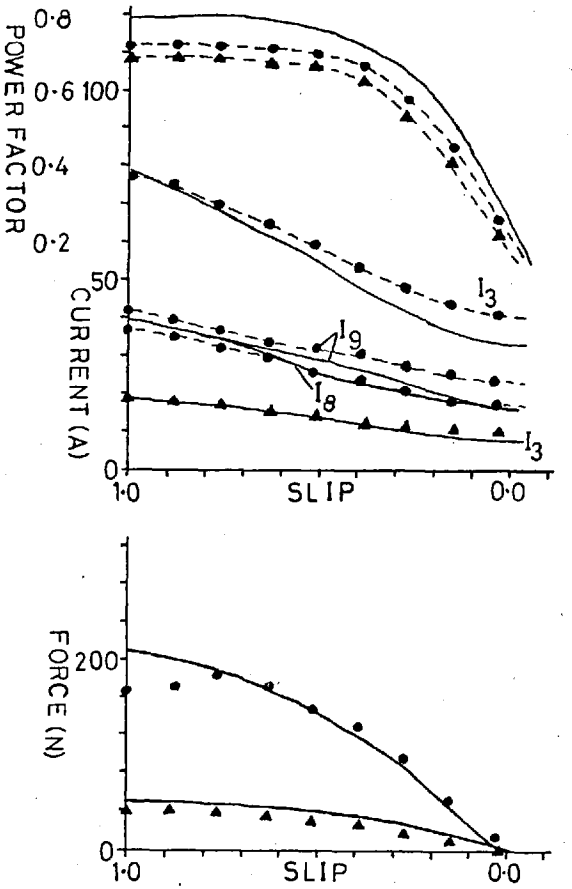

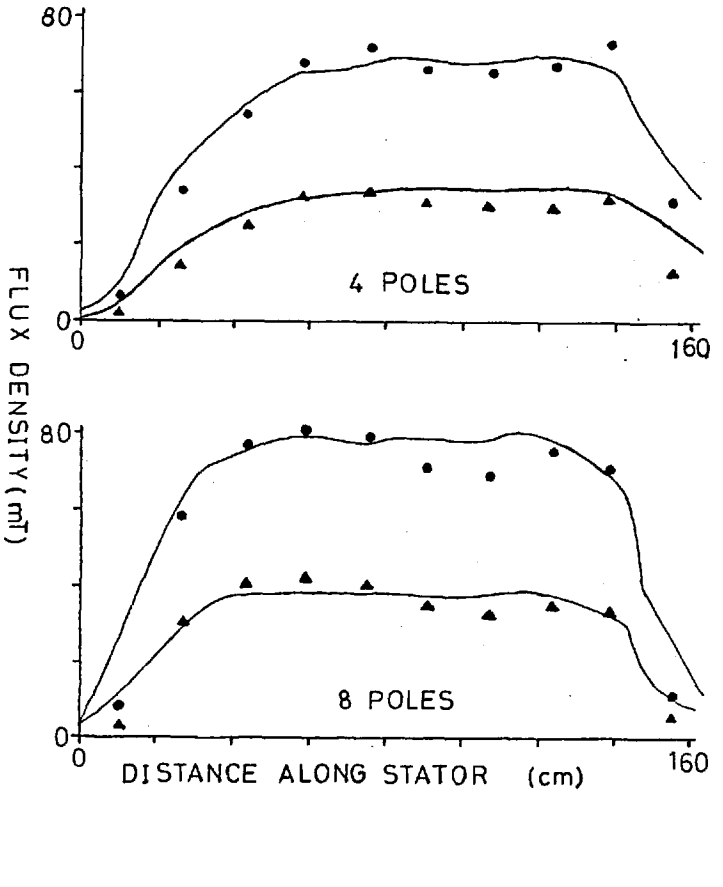

CALCULATED ——— MEASURED (PARALLEL CONNECTION) --- ● --- MEASURED (SERIES CONNECTION) --- ▲ ---

FIG. 5 PHASE CURRENT AND FORCE ON 8-POLE SETTING WITH PARALLEL CONNECTED STATOR AND LOW RESISTIVITY ROTOR.

FIG. 6 PHASE CURRENT AND FORCE ON 4-POLE SETTING WITH SERIES AND PARALLEL CONNECTED STATORS AND HIGH RESISTIVITY ROTOR.

FIG. 7 FLUX DENSITY AT 0.2 SLIP WITH SERIES AND PARALLEL CONNECTED STATORS AND HIGH RESISTIVITY ROTOR.

Pole-change windings for linear induction motors

Prof. J. F. Eastham, M.Sc., Ph.D., C.Eng., F.I.E.E., and M. J. Balchin, B.Sc.(Eng.), A.C.G.I.

Indexing terms: Induction motors, Linear motors, Machine windings

Abstract

Pole-change techniques are potentially valuable for the speed control of linear induction motors. However, they are more difficult to apply in the linear case because of the nonuniform nature of the airgap flux. This precludes the use of parallel paths which are normally employed to reduce the complexity of the switching. The paper describes a new winding connection technique, and shows how it can reduce the number of switch contacts required. The method requires the series connection of alternate coils to form one winding; the remaining coils form a second. Parallel connections are then made between these two windings. An analysis is presented that gives the currents in any general set of serially connected coil groups connected to independent voltage sources. From this, the complete electrical and mechanical performance of the machine can be calculated. The technique can deal with any asymmetric windings having parallel paths, and, while it is ideally suited to the machines under consideration, it has other potential applications. The work is supported by a selection of experimental results that were taken from a pole-change linear motor driving a disc secondary.

List of principal symbols

B = magnetic-flux density, T
C = complex-Fourier-series conductor amplitude, conductors/m
F = force, N
i = instantaneous winding current, A
I = complex r.m.s. winding current, A
J = complex r.m.s. surface current density, A/m
n = surface-conductor density, conductors/m
N = winding slot conductors
P_w = winding pole pitch, m
Q = total number of stator slots
r = harmonic number
t = time, s
v = rotor speed, m/s
w = stator width, m
z_{in} = layer-model input impedance, Ω
$2k_BP_B$ = length of machine section, m
$k_r = r\pi/k_BP_B$ = wave number
2δ = slot opening, m
ω = angular frequency, rad/s
$[A]$ = matrix or vector
T indicates matrix transpose
$*$ indicates complex conjugate
Re indicates complex real part

1 Introduction

Pole-change techniques have been in common use over many years as one method for controlling the speed of rotary induction motors. This method can give only discrete changes in speed, but does have the advantage of providing efficient running at those speeds. It is thought likely that this advantage will make pole-change methods useful for the speed control of linear induction motors used in transport systems.

Series connected multispeed windings are directly applicable to linear induction motors. However, as is the case with rotary machines, it is found that these windings are inflexible in so far as switching arrangements and changes of effective applied voltage are concerned. In a rotary machine, where the flux wave is always sinusoidally distributed in space, these difficulties are removed by designing windings that contain parallel groups. In linear machines, the flux wave is far from sinusoidally distributed,[1] and it is the purpose of this paper to discuss the difficulties this presents to the design of windings.

A new form of winding is described in which parallel connections are possible. An analysis is presented that allows coil-group currents to be found, given known supply voltages. This technique allows the mechanical and winding performances to be predicted for machines that are wound and connected in any fashion.

2 Change-pole windings

The simplest form of change-pole arrangement is the 2-speed consequent-pole winding. Figs. 1(i) and 1(iii) (with coil pairs 1*a*, 1*b* etc. connected in series) illustrate the layout of the electric and magnetic circuits for one phase of a linear machine using this type of winding. For the sake of clarity, only single coils are shown on the primary and there is no conducting member on the secondary. In practice, of course, the stator would be surface-wound in three phases with many coils, and the secondary would include some form of conducting plate.

As can be seen from the diagram, reversal of current in half of the coils yields the higher pole number. This is also true for the more general types of pole-change winding that have recently become available.[2-4,17,18] Therefore the new connection techniques in the following Sections will be described in terms of the simple consequent-pole arrangement, but it will be appreciated that the same methods can be directly applied to all 2-speed change-pole windings.

3 Switching arrangements for change-pole machines

3.1 The basic requirements

In rotary pole-change machines, parallel-path working is normally used on one of the settings in order that the number of switch

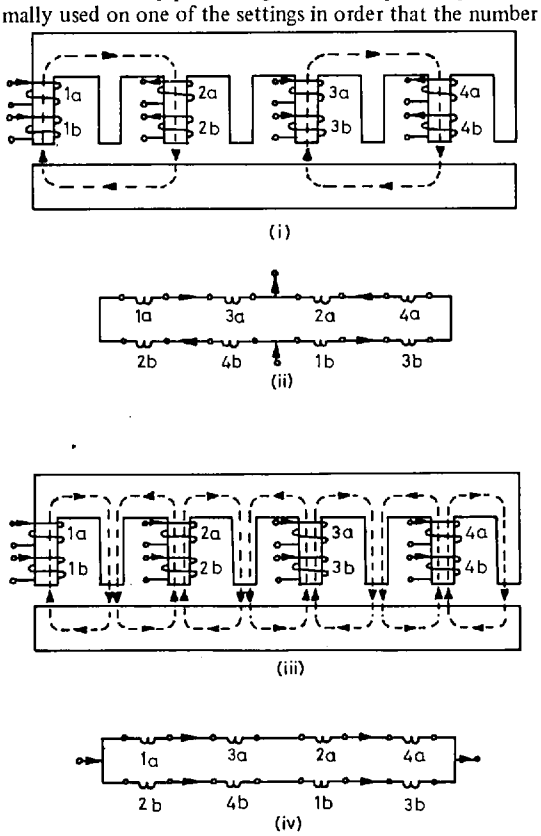

Fig. 1
Principle of consequent-pole windings for linear machines

(*i*) Circuits for the 4-pole connection
(*ii*) 4-pole coil connections
(*iii*) Circuits for the 8-pole connection
(*iv*) 8-pole coil connections

Paper 7357 P, first received 8th May and in revised form 3rd October 1974
Prof. Eastham and Mr. Balchin are with the Department of Engineering, University of Aberdeen, Marischal College, Aberdeen AB9 1AS, Scotland

contacts that are necessary is reduced. This is not possible in the linear case because of the nonuniform nature of the airgap flux density.[1] Essentially, this increases from a small value at the leading edge of the machine to larger values along its length. Therefore, if the coils of Figs. 1(i) and (iii) are connected conventionally with 1*a* and 1*b* in series etc., it is not possible to parallel a series combination of groups 1 and 3 with a series combination of groups 2 and 4, because each path would have a different induced e.m.f. On each setting, all the coils of a phase must be in series, and Fig. 2 shows how this may be achieved in a series-star/series-star arrangement using 12 switch contacts. The single coil r_1 in this Figure is used to indicate a series combination of half of the coils in the red phase, and r_2 the other half. Similar considerations apply to the other phase groups.

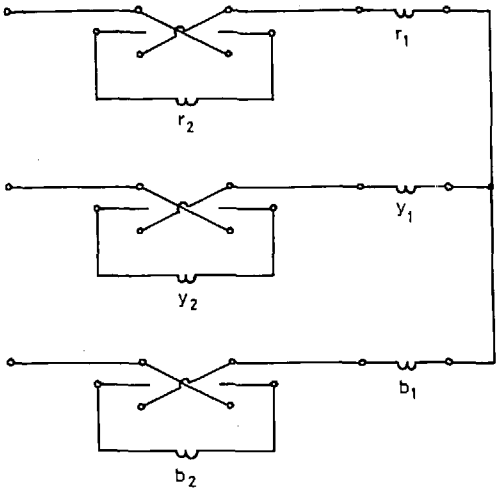

Fig. 2
Switching arrangement for series-star/series-star connections

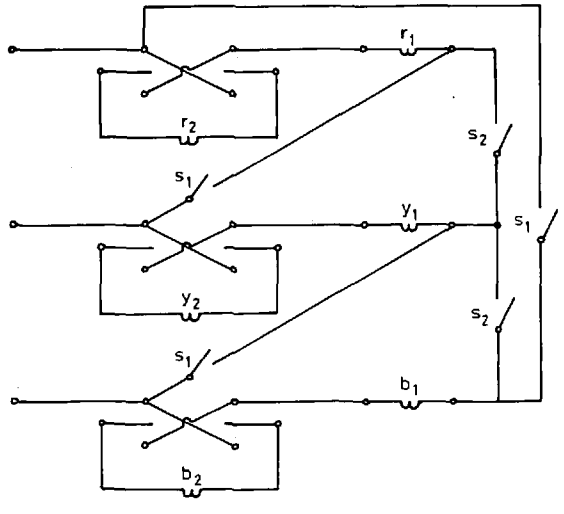

Fig. 3
Switching arrangement to provide series star or series delta on each pole setting

It is a frequent requirement in change-pole-machine design that the effective applied voltage can be changed between settings. This is to provide particular ratios of airgap flux density. In the case of linear-motor windings, with parallel-path working excluded, the only possibility to meet this requirement is a series in star/series-delta switch. When this is combined with a direction change in the winding groups, a considerable number of switch contacts is required. Fig. 3 shows an arrangement that will give star or delta connection on either pole setting by closing either switches s_1 or s_2. This arrangement uses 17 switch contacts compared with the 12 used in the series–series only switch of Fig. 2.

The connection of Fig. 3 allows for either star or delta on each pole setting. This is only needed if two effective voltages are required at the same pole number. The normal switching requirement is for a change of voltage with a change of pole number. Fig. 4 shows a connection that will accomplish this, the s_1 switches being closed to provide a series-star arrangement for one pole number and the s_2 switches being closed to give a series-delta arrangement for the second pole number. In this case, the main control function uses only 11 contacts, but the machine would not be isolated with both sets of switches open. Hence the three isolating switches I_1, I_2 and I_3 are required, making 14 switch contacts in all.

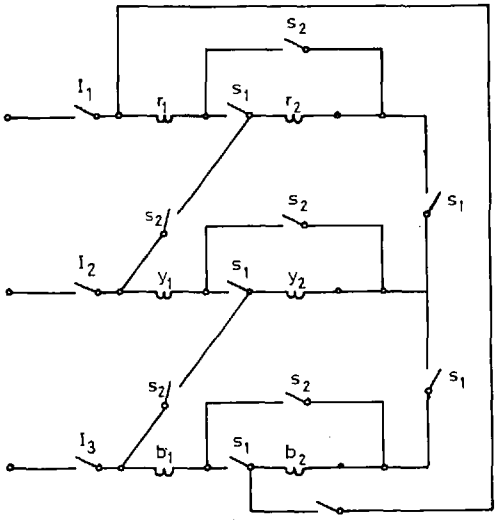

Fig. 4
Switching arrangement to provide series star to series delta

3.2 The use of double winding sections

The number of switch contacts used so far may be reduced by using a double-winding arrangement that allows parallel connections to be made.

The basic principle of the double-winding section may be explained by referring again to the single-phase diagram of Fig. 1. The coils labelled *a* are connected in series forming an identical winding with a series connection of the *b* coils. The voltage across each of these windings is obviously the same, and so these two sections can be paralleled to give one phase of an 8-pole setting as shown in Fig. 1(iv).

To form the 4-pole setting of Fig. 1(ii), it may be seen that the voltage across a series combination of coils 1*a*, 3*a*, 2*b* and 4*b* is also equal to that across a series combination of coils 2*a*, 4*a*, 1*b* and 3*b*.

This allows the coil-group connections to remain as in Fig. 1(iv), but now the current feed has to be moved so that the currents in coils 2*b*, 4*b*, 2*a* and 4*a* are reversed.

As with the series-connected layouts, these arrangements may also be realised with surface windings. The obvious way of achieving this is to use a 4-layer construction and to make the connections between

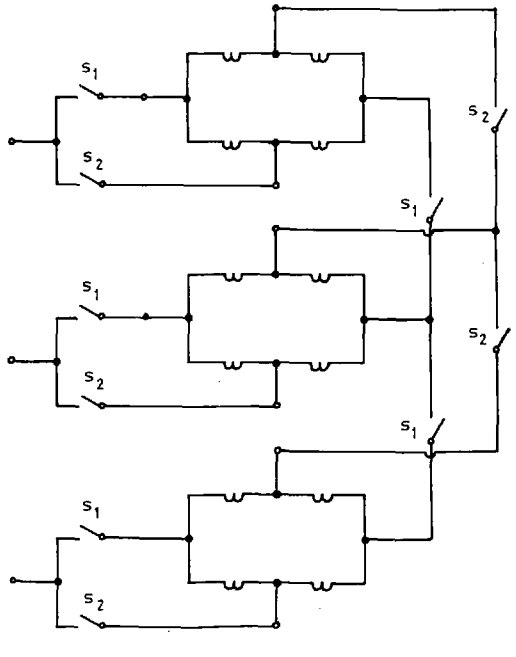

Fig. 5
Star–star connections using parallel groups

these two separate windings. This idea may also be extended to cover machines such as the U-core transverse-flux motor described in Reference 7, where there are already two distinct windings, one on each limb.

Four-layer construction can be avoided by placing the two windings one slot pitch apart. This results in sections that are not strictly capable of being paralleled, but the difference in induced e.m.f. will be small and may be tolerable. The small difference in induced e.m.f. may be reduced further by placing one winding in the even-numbered slots in one repeatable section, and in odd-numbered slots in the following.

Fig. 5 shows a 3-phase arrangement using this system in which the winding is connected in star on each pole setting. A total of only ten switch contacts is required compared with the 12 shown in Fig. 2. Fig. 6 shows a 3-phase arrangement in which star–delta switching between the two settings is provided. Here 11 contacts are required compared with the 14 required in Fig. 4. Again, in these last two Figures, either the s_1 or the s_2 switches are closed to provide the two settings.

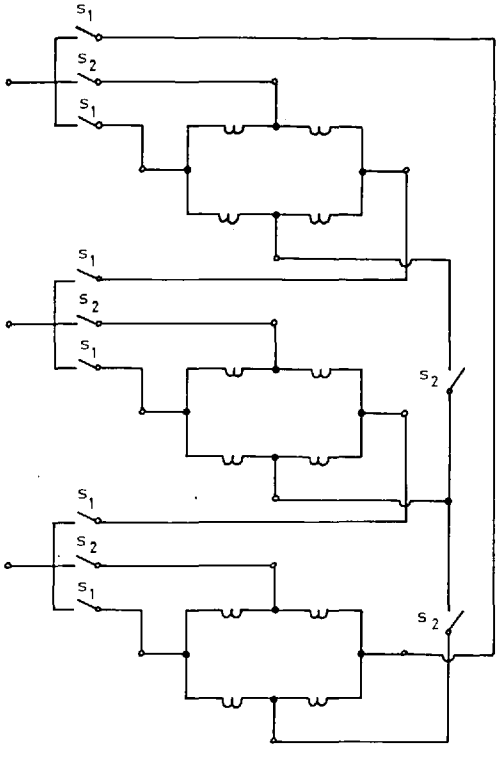

Fig. 6
Star–delta connections using parallel groups

4 Winding analysis

Section 3 discussed the connection arrangements for some change-pole windings for linear machines. This included a novel double-winding technique in which there is a possibility of circulating currents in its parallel paths. It is therefore the purpose of this Section to present an analysis that allows for the simple description of slot conductor layouts and winding connections. The analysis may be used to predict machine performance and winding currents in any arrangement, including those containing parallel paths.

Many practical tests have been performed on linear machines using drum or disc rigs. This type of apparatus provides a realistic simulation of actual operating conditions, provided that the rotor currents decay to zero, and its temperature to ambient, before re-entry to the stator. The ideas behind this type of apparatus may be used to form a corresponding mathematical model for the system, as shown in Fig. 7.

The model, in common with many employing field-type analyses,[5,6,8–11,15] consists of uniform layers of material. These are of the stator width w in the x direction, and stretch to infinity in the positive and negative y directions. The excitation is provided by infinitesimally thin layers of current flowing in the x direction. These layers correspond to the wound portion of the stator, and are repeated at periodic intervals in the y direction so that the secondary currents have time to decay between them. Since all the sections of the model are alike, only one of them is actually considered in the analysis.

The input impedance of the layers seen at the current sheets is found using established 1-dimensional methods,[8] except that the resistivity of the conducting parts of the secondary is modified by an appropriate Russell and Norsworthy factor.[9] This takes account of the restrictions placed on the current flow due to the finite width of the rotor.

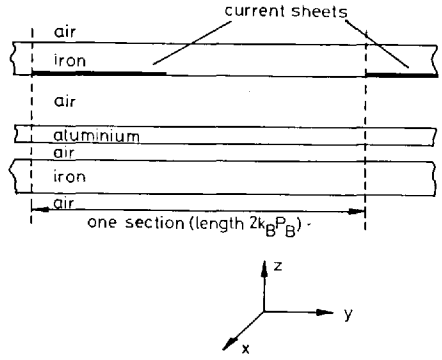

Fig. 7
Linear-machine mathematical model

Models of this type have been used previously by other workers,[10,11] but, in each of these cases, the excitation has been assumed to be a sinusoidally distributed current sheet appropriate to balanced winding currents. The purpose of this analysis is to calculate the winding currents, given the terminal conditions, and then use them for finding forces and flux densities. To this end, a winding analysis, based on the work of Eastham[4] and Brown and Jha,[12] is used, with each set of series-connected coil groups being considered as separate windings.

The windings are assumed to be laid in a uniformly slotted stator that has Q total slots, including those half filled at each end. Slotting allows the usual current-sheet approximation[13] to be used. Appendix 9.1 shows how each of the windings may be resolved into a Fourier surface-conductor distribution and then into a surface current sheet in the layer model. The total surface-current density for all the windings is simply related to the electric-field strength at the winding surface by the input impedance of the layer model. Induced voltages in each winding are then found by integrating the electric field over the appropriate conductor distribution. Each winding is finally included in a network branch consisting of a series connection of the above 'induced'-voltage source, an independent voltage source and the winding leakage impedance. These branches are then connected using standard network techniques to give the winding currents when the independent voltages are known.

Appendixes 9.2 and 9.3 show how the thrust-force and flux-density distribution may be obtained once the winding currents are known.

In a real linear machine, the stator iron usually only occupies the wound portion. The abrupt end of this iron causes a retarding force[1,15] whose approximate magnitude is given by

$$F_{ret} = \frac{|B_{ex}|^2 vw}{2\mu_0 v_s}\left(\frac{P_w}{\pi} - g_i\right)$$

where B_{ex} is the total flux density on the rotor surface at the exit edge, v_s is the synchronous speed on the winding pole pitch and g_i is the total airgap. This force must be subtracted from the total traction force.

In the solutions to the problem, represented by eqns. 7, 12 and 15, the summation is shown over an infinite number of harmonics. In a practical calculation, only a truncated solution is possible. This is found by increasing the number of harmonics considered until only small variations in the solution value appear.

It will be noted that the above analysis requires the leakage impedance of each winding. This consists of two parts, resistance and reactance. The winding resistance may easily be found by measurement or by calculation, knowing the usual geometric and material parameters. The winding reactance consists of those parts of its leakage reactance that are not taken into account by the layer model, namely the slot leakage and endturn leakage. Since the evaluation of these parameters forms an area of research in its own right, several frequently used methods were tried, the most consistent results being given by the Liwshitz–Garik[16] formulas. Each method tried is based on a balanced winding arrangement with a sinusoidal wave of the winding pole pitch. The reactance value given is per phase, and this was scaled to apply to individual windings. The use of this method was considered realistic, since the final machine design strives to achieve balance, and this was borne out by the experimental machines that were tried.

5 Experimental results

To verify the analysis of Section 4, a test machine was constructed to drive a 2·135 m diameter disc as the secondary member. The curved stator of this machine had a mean length of 1·46 m, a depth of 12 cm and a width of 15·9 cm. It had 54 open slots of depth 3·81 cm and width 1·43 cm, and was wound with 48 coils of 6-slots pitch. Each coil had 12 turns, and their ends were taken separately to a terminal board so that different winding arrangements could easily be connected.

The first type of secondary member tried consisted of a plain aluminium disc 2 cm thick, giving an effective secondary width of 39·3 cm.

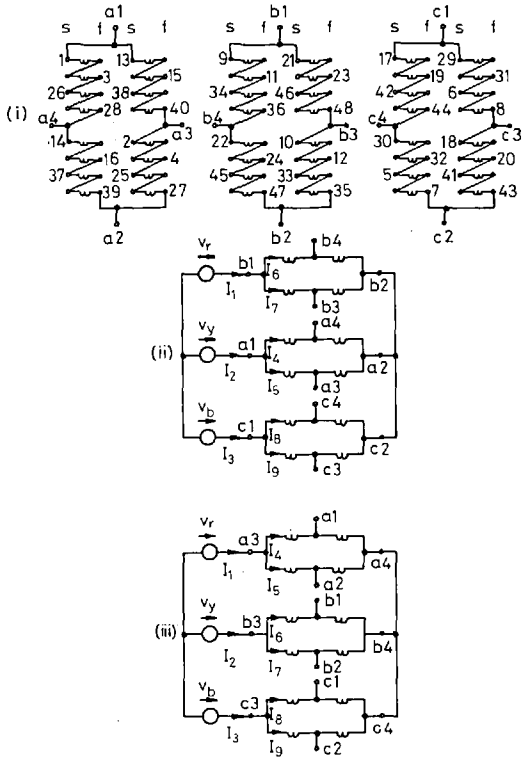

Fig. 8
Parallel connections for the experimental machine

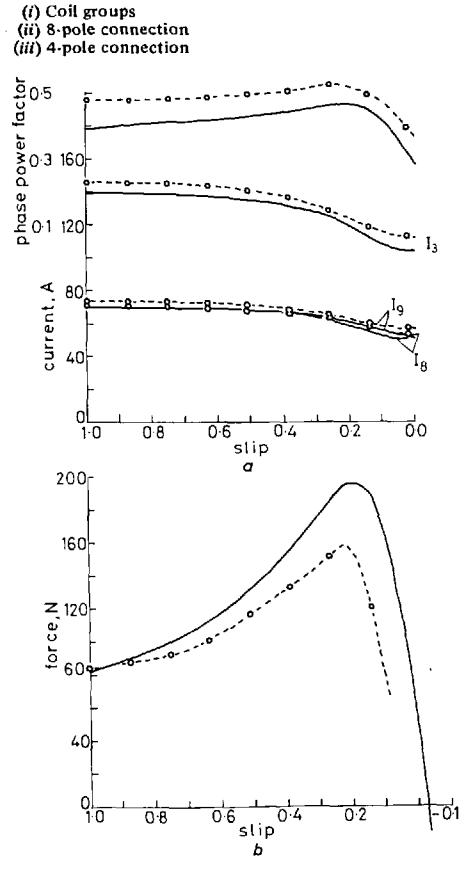

Fig. 9
Comparison of results for the 8-pole setting of the parallel-connected machine with plain aluminium secondary

—— calculated
- o - measured

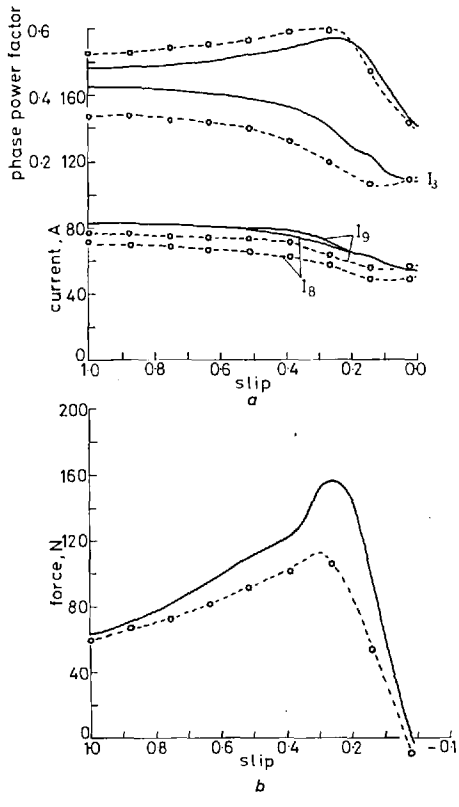

Fig. 10
Comparison of results for the 4-pole setting of the parallel-connected machine with plain aluminium secondary

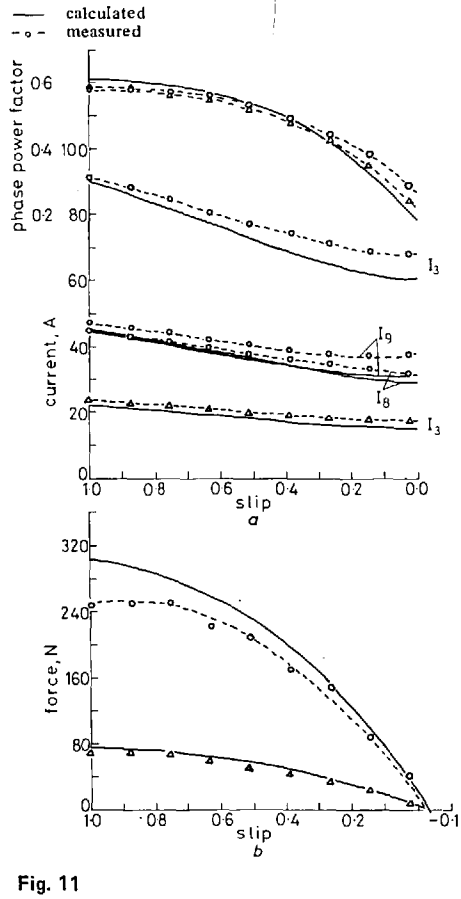

Fig. 11
Comparison of results for the 8-pole setting with the composite secondary

—— calculated
- o - measured (parallel)
- Δ - measured (series)

The magnetic circuit was completed by an unwound laminated block with the same dimensions as that of the stator, fixed behind the disc. This arrangement required two airgaps for the sake of disc clearance. The winding used in this case was an eight-to-four consequent pole arrangement with the coils connected according to the double-winding principle discussed in Section 3.2. The winding and connections are shown in Fig. 8, where the coil number is also the number of the slot in which its leading side falls. The calculated and experimental results for the *b* phase on the two pole settings, at a supply frequency of 50 Hz at 50 V, are shown in Figs. 9 and 10.

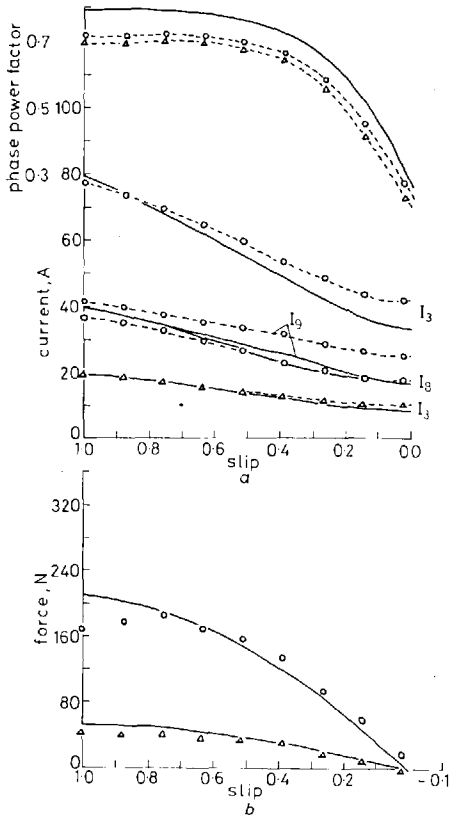

Fig. 12
Comparison of results for the 4-pole setting with the composite secondary

—— calculated
- ∘ - measured (parallel)
- Δ - measured (series)

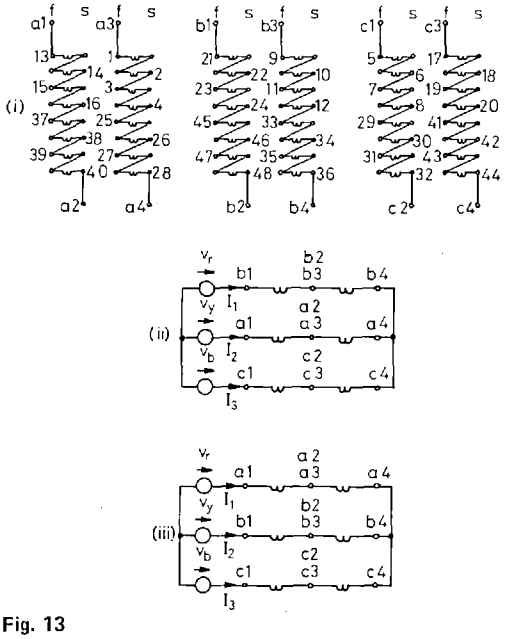

Fig. 13
Series connections for the experimental machine

(*i*) Coil groups
(*ii*) 8-pole connection
(*iii*) 4-pole connection

A different type of secondary, more in keeping with recent proposals for linear-machine-driven transport systems, was then tried. This consisted of an unlaminated mild-steel disc 2 cm thick, faced with a 1·6 mm thickness of aluminium, giving an effective secondary width of 22·9 cm.

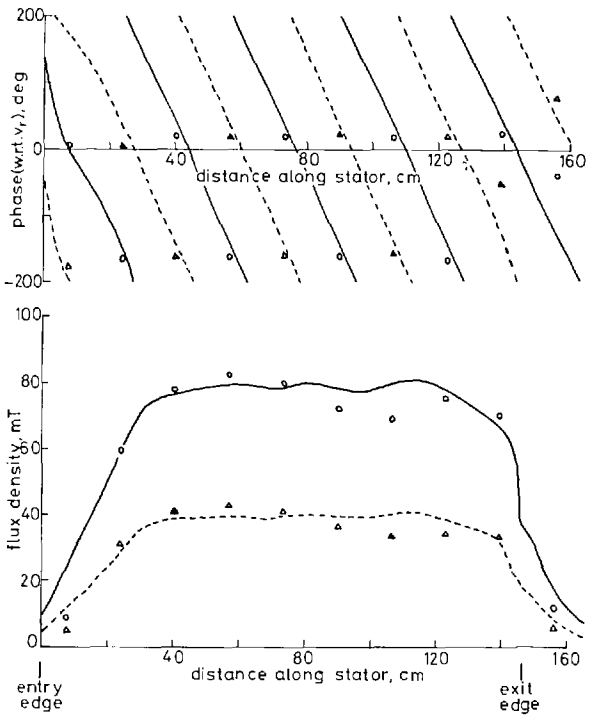

Fig. 14
Flux density for the composite-rotor machine with eight poles at 0·2 slip

—— calculated (parallel)
- - - calculated (series)
∘ measured (parallel)
Δ measured (series)

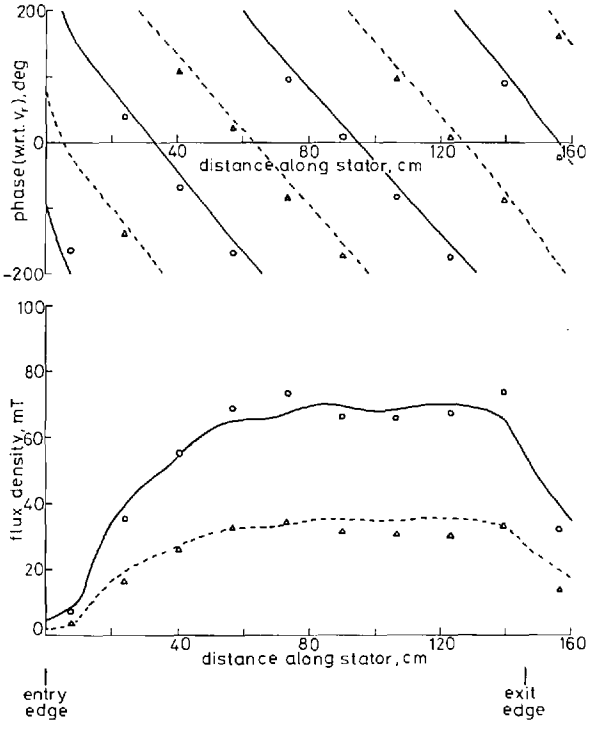

Fig. 15
Flux density for the composite-rotor machine with four poles at 0·2 slip

—— calculated (parallel)
- - - calculated (series)
∘ measured (parallel)
Δ measured (series)

The parallel-connected winding of Fig. 8 was again used, and curves corresponding to Figs. 9 and 10 are shown in Figs. 11 and 12. In the performance calculations for this case, the unlaminated steel was considered as a single layer in the model with constant values of resistivity and permeability. This is obviously a simplification, but one that appears to give reasonable results when the solid steel is faced with a conducting layer.

To compare the new parallel winding with the conventional series arrangement, the stator coils were connected as in Fig. 13. The experimental points for this case with a supply frequency of 50 Hz at 50 V are also shown in Figs. 11 and 12. Curves of flux density on the rotor surface for these two cases at a slip of 0·2 are shown in Figs. 14 and 15.

The experimental work on which this Section is based included a comprehensive series of tests in which measurements of all winding currents, fluxes and forces, at frequencies up to 200 Hz, were taken. For the sake of economy of presentation, however, only a representative selection of results is presented. It was found that the calculated levels of current in these machines is very dependent on the winding leakage reactance. As was mentioned before, the calculation of this component is very doubtful, and other uncertainties are introduced by the curvature of the rotor and secondary. However, the calculated results show favourable agreement over a wide range of conditions giving the correct general variations of currents and fluxes and the correct relative magnitudes.

6 Conclusions

A new connection method for change-pole linear motors has been described. This technique gives some reduction in the number of switch contacts required for control purposes. The underlying philosophy has been verified both theoretically and practically. The new analytical techniques developed specifically for this work are thought to be applicable to other situations.

7 Acknowledgments

The experimental work described in this paper was performed on the high-speed-disc test rig at Imperial College of Science & Technology, London. The authors would particularly like to thank D. H. Locke and D. A. Lowther for assistance with the experimental work, and P. J. McKeowan and B. Gingall for their assistance during the construction of the test machine. The authors would also like to thank Prof. E. R. Laithwaite, H. R. Bolton and E. M. Freeman for their interest and much useful discussion during the course of the work.

8 References

1 WILLIAMS, F.C., LAITHWAITE, E.R. and EASTHAM, J. F.: 'Development and design of spherical induction motors', *Proc. IEE*, 1959, **106**A, pp. 471–484
2 EASTHAM, J.F.: 'Close-ratio phase-modulated change-pole machines with improved winding balance', *ibid.*, 1968, **115**, (11), pp. 1641–1648
3 EASTHAM, J.F., and LAITHWAITE, E.R.: 'Pole-change motors using phase-mixing techniques', *ibid.*, 1962, **109**A, pp. 397–409
4 WILLIAMS, F.C., EASTHAM, J.F., and PIGGOTT, L.S.: 'Analysis and design of pole-change motors using phase-mixing techniques', *ibid.*, 1964, **111**, (1), pp. 80–94
5 CULLEN, A.L., and BARTON, T.H.: 'A simplified electromagnetic theory of the induction motor, using the concept of wave impedance', *ibid.*, 1958, **105**C, pp. 331–336
6 GRIEG, J., and FREEMAN, E.M.: 'Travelling-wave problem in electrical machines', *ibid.*, 1967, **114**, (11), pp. 1681–1683
7 LAITHWAITE, E.R., EASTHAM, J.F., BOLTON, H.R., and FELLOWS, T.G.: 'Linear motors with transverse flux', *ibid.*, 1971, **118**, (12), pp. 1761–1767
8 FREEMAN, E.M.: 'Travelling waves in induction machines: input impedance and equivalent circuits', *ibid.*, 1968, **115**, (12), pp. 1772–1776
9 RUSSELL, R.L., and NORSWORTHY, K.H.: 'Eddy currents and wall losses in screened rotor induction motors', *ibid.*, 1958, **105**A, pp. 163–175
10 HESMONDHALGH, D.E., and TIPPING, D.: 'General method for prediction of the characteristics of induction motors with discontinuous exciting windings', *ibid.*, 1965, **112**, (9), pp. 1721–1735
11 ALWASH, J.H.H.: 'Analysis and design of linear induction motors'. Ph.D. thesis, London University (Imperial College), 1972
12 BROWN, J.E., and JHA, C.S.: 'Generalised rotating-field theory of polyphase induction motors and its relationship to symmetrical component theory', *Proc. IEE*, 1962, **109**A, pp. 59–69
13 SAUNDERS, R.M.: 'Electromechanical energy conversion in double cylindrical structures', *Trans. Am. Inst. Elec. Eng.*, 1963, **82**, pp. 631–638
14 KRON, G.: 'Tensor analysis of networks' (Macdonald, 1965)
15 TIPPING, D.: 'The analysis of some special-purpose electrical machines'. Ph.D. thesis, Manchester University, 1964
16 LIWSCHITZ-GARIK, M., and WHIPPLE, C.C.: 'Electric machinery – Vol. 1' (D. Van Nostrand, 1948)
17 RAWCLIFFE, G.H., BURBRIDGE, R.F., and FONG, W.: 'Induction-motor speed changing by pole-amplitude modulation', *Proc. IEE*, 1958, **105**A, pp. 411–419
18 RAWCLIFFE, G.H., and FONG, W.: 'Speed changing induction motors: further developments in pole-amplitude modulation', *ibid.*, 1960, **107**A, pp. 513–528

9 Appendixes

9.1 Calculation of winding currents

The s th slot of the stator contains N conductors of the ν th winding (i.e. $N_{s\nu}$ conductors). These give a surface density of conductors at the tooth tips of

$$\frac{N_{s\nu}}{2\delta} \text{ conductors/m}$$

This conductor density may be resolved into a Fourier conductor distribution[4] whose r th harmonic amplitude is:

$$C'_{r\nu} = \frac{\sin(k_r\delta)}{k_r\delta}\frac{N_{s\nu}}{2k_BP_B}e^{-jk_ry_{s\nu}}$$

where $y_{s\nu}$ is the position of the centre of the slot. A similar harmonic amplitude may be obtained for each slot that contains conductors of the ν th winding. For each harmonic, these are summed, so that the r th harmonic amplitude of the surface-conductor density for the ν th winding is given by:

$$C_{r\nu} = \frac{\sin(k_r\delta)}{(k_r\delta)}\sum_{s=1}^{Q}\frac{N_{s\nu}}{2k_BP_B}e^{-jk_ry_{s\nu}}$$

The corresponding Fourier series for the winding is

$$n_\nu = \sum_{r=1}^{\infty}(C^*_{r\nu}e^{-jk_ry} + C_{r\nu}e^{jk_ry})$$

which assumes that $C_{0\nu} = 0$ since the machine is coil-wound.

If a current $i_\nu = \sqrt{2}I_\nu e^{j\omega t}$ flows in the winding, the instantaneous surface-current density is:

$$n_\nu i_\nu = \sqrt{2}\sum_{r=1}^{\infty}\{J_{Fr\nu}e^{j(\omega t-k_ry)} + J_{Br\nu}e^{j(\omega t+k_ry)}\}$$

where the amplitudes of the forward- and backward-travelling waves of current density are:

$$J_{Fr\nu} = C^*_{r\nu}I_\nu$$

$$J_{Br\nu} = C_{r\nu}I_\nu$$

The total r.m.s.-current density due to ρ windings may be expressed as the product of two vectors of length ρ; i.e.

$$J_{Fr} = [C^*_r]^T[I] \quad (1a)$$

$$J_{Br} = [C_r]^T[I] \quad (1b)$$

When these currents flow in the layer model, they excite corresponding electric fields

$$E_{Fr} = -z_{in\,Fr}J_{Fr} \quad (2a)$$

$$E_{Br} = -z_{in\,Br}J_{Br} \quad (2b)$$

which, when expressed in instantaneous form, may be integrated over each winding to give its terminal voltage. Thus, for the r th harmonic acting on the ν th winding, the induced voltage is

$$e_{Tr\nu} = 2k_BP_Bw(C_{r\nu}E_{Fr} + C^*_{r\nu}E_{Br})$$

When all ρ windings are considered, $e_{Tr\nu}$ becomes a column vector of length ρ so that:

$$[e_T] = 2k_BP_Bw([C_r]E_{Fr} + [C^*_r]E_{Br})$$

The total induced voltage for each winding is now found by substituting for E_r and J_r from eqns. 2 and 1 and summing over the r harmonics; hence

$$[e_T] = -[z_M][I] \quad (3)$$

where

$$[z_M] = 2k_BP_Bw\sum_{r=1}^{\infty}([C_r]z_{in\,Fr}[C^*_r]^T + [C^*_r]z_{in\,Br}[C_r]^T)$$

Now the network may be considered as ρ separate elements each consisting of a series connection of the winding leakage impedance z_ν, an independent voltage source e_ν and the 'induced' voltage source $e_{T\nu}$. For all the windings,

$$[e] + [e_T] + [E] = [z][I]$$

or, on substituting from eqn. 3,

$$[e] + [E] = ([z] + [z_M])[I] \quad (4)$$

where E_ν is the voltage across the network element.

To be able to solve eqn. 4, a set of independent winding currents

$[I']$ is chosen. Each of these currents flows on one closed path in the network. The independent currents are related to all the winding currents by

$$[I] = [S][I'] \tag{5}$$

where $[S]$ is the connection matrix.[14] The element terminal voltages around each of the closed paths must sum to zero, and it is found that

$$[S]^T[E] = [0] \tag{6}$$

Premultiplication of eqn. 4 by $[S]^T$ and substitution of eqns. 5 and 6 gives

$$[S]^T[e] = \{[S]^T([z] + [z_M])[S]\}[I']$$

Inverting, premultiplying by $[S]$ and applying eqn. 5 gives the solution for all the winding currents as

$$[I] = [S]\{[S]^T([z] + [z_M])[S]\}^{-1}[S]^T[e] \tag{7}$$

9.2 Calculation of thrust force

The power inputs to the layer model on the r th harmonic for the forward- and backward-travelling fields are:

$$P_{in\,Fr} = 2k_B P_B w |J_{Fr}|^2 \,\mathrm{Re}\,[z_{in\,Fr}] \tag{8a}$$

$$P_{in\,Br} = 2k_B P_B w |J_{Br}|^2 \,\mathrm{Re}\,[z_{in\,Br}] \tag{8b}$$

and the corresponding synchronous speeds are:

$$V_{sFr} = \frac{\omega}{k_r} \tag{9a}$$

$$V_{sBr} = -\frac{\omega}{k_r} \tag{9b}$$

The forces due to these two harmonic fields are thus:

$$F_{Fr} = \frac{P_{in\,Fr}}{V_{sFr}} \tag{10a}$$

$$F_{Br} = \frac{P_{in\,Br}}{V_{sBr}} \tag{10b}$$

and the net force in the y direction is

$$F = \sum_{r=1}^{\infty}(F_{Fr} + F_{Br}) \tag{11}$$

Substitution of eqns. 8, 9 and 10 in eqn. 11 gives the total traction force on the secondary as:

$$F = \sum_{r=1}^{\infty} \frac{2k_B P_B w k_r}{\omega}(|J_{Fr}|^2 \,\mathrm{Re}\,[z_{in\,Fr}] - |J_{Br}|^2 \,\mathrm{Re}\,[z_{in\,Br}]) \tag{12}$$

9.3 Calculation of flux densities

The flux density on the r th harmonic at the rotor surface is conveniently given from the electric-field strength at the appropriate surface in the layer model, i.e. E'_{Fr} and E'_{Br}. These may be summed to give the flux density at co-ordinate y' as

$$B = \sum_{r=1}^{\infty} \frac{k_r}{\omega}(E'_{Fr}e^{-jk_r y'} - E'_{Br}e^{jk_r y'}) \tag{13}$$